ABSTRACT

DOSS, SHOUBHIK RAVINDRANATH. Thermal Design and Optimization of Parasitics for High Power Converters. (Under the direction of Professor Alex Q. Huang).

Design of high power converters require deep insight into magnetic, thermal and mechanical parameters of the converter, besides the electrical parameters, for it to function in a desired manner.

The high power converters have losses proportional to their power rating; even a highly efficient converter (98%) could have losses as high as >100 kW. It is essential to extract this thermal energy form the system so that the components in the converter do not fail. Extraction of such large quantities of thermal energy is a formidable challenge and has been dealt with in detail in this work. Various options for this process have been discussed. Optimization of the interconnecting bus-bar network in the converter is another important aspect of the design. Minimization of stray inductances and loops lead to lower voltage stresses on the semiconductor devices and proper operation of the converter. Imperfect joints between interconnecting bus-bars form stray resistances which lead to localized heating of the bus-bars. This thermal cycling leads to faulty joints, causing inefficient operation of the converter. To maximize the efficiency of the converter, such interconnection issues have been addressed. Finally, the weight distribution, foot-print and volume of the converter play a key role in its manufacturability and marketability. Special attention has been given to the materials selected in the design process to maximize the life of the converter and ensure correct operation under different ambient temperatures and weather conditions.

A well built converter must follow the guidelines laid by the mechanical and thermal aspects of the design process.

Thermal Design and Optimization of Parasitics for High Power Converters

by
Shoubhik Ravindranath Doss

A thesis submitted to the Graduate Faculty of
North Carolina State University
in partial fulfillment of the
requirements for the Degree of
Master of Science

Electrical Engineering

Raleigh, North Carolina

2008

APPROVED BY:

Dr. Subhashish Bhattacharya
Co-chair of Advisory Committee

Dr. Mesut Baran

Dr. Alex Q. Huang
Chair of Advisory Committee

DEDICATION

To

My Mom and Dad

BIOGRAPHY

Shoubhik Ravindranath Doss was born on January 6th 1984, in Mumbai, India. He received the Bachelor of Engineering degree in Electronics Engineering from University of Mumbai in 2005. He was actively involved in intelligent robotics and basic embedded systems during the course of his undergraduate degree. His other hobbies include gaming, target practice and working with internal combustion engines.

Shoubhik has been a graduate student in the Electrical and Computer Engineering Department at North Carolina State University, Raleigh, NC since fall 2005. He completed two internships in Siemens and Eaton Corp in summer 2006 and 2007 respectively.

Shoubhik is currently working with Silicon Power Corporation, Malvern as a project lead engineer and his main focus is on the solid-state distribution transformer.

ACKNOWLEDGEMENTS

I would like to express my gratitude to my advisor Dr. Alex Q. Huang, for his astute and timely guidance throughout the length of my student career at NCSU. His deep insight into various fields of engineering both thermal and mechanical helped me see through the technicalities involved real converter.

I would also like to thank my co-advisor, Dr. Subhashish Bhattacharya for sharing his vast industrial experiences and providing timely guidance during the development of the thesis. His inputs during our one-to-one discussions have been valuable and have provided definitive direction to the thesis. Discussions with Dr. Mesut Baran provided the motivation and necessary direction to develop a FACTS building block for power systems.

I really appreciate our lab administrator Seth's efforts; he has made life easier by coordinating and arranging all events. Our IT Admin Sam, took care of all our software and hardware issues and both have been instrumental in the success of this thesis.

I would like to thank all my student colleagues with whom I have spent countless hours in the Lab – Karan, Bin, Jinseok, Jeesung, Sungkeun, Sameer, Tiefu, Liyu, Xin, Anand, Peter, Wenchao, Xiaohu, and Jun helped create the fun and stimulating environment that it was. I've had great friends Karan, Abhishek, Deep, Nilesh, Swanand, Kaushal, Maitrik and Gunjan over the course of three and a half years studying, working on projects and assignments or just having fun. Life at NC State was complete thanks to all these guys. I want to thank Rahul for the countless hours of discussion and jovial midnight-food sessions; his thought process and dedication has inspired me to carry on with my goals. I would also like to thank my friends Sounak, Anirudha and Sushrath back home, for their constant support. Finally, I thank Prashanth and Ranjith, my roommates, for bearing with me through the final semesters. Lastly, but most importantly, I would like to thank God for seeing me through this journey and keeping his ever watchful eye on me.

TABLE OF CONTENTS

LIST OF FIGURES viii
LIST OF TABLES xii
1. INTRODUCTION 1
1.1. Rationale 1
1.2. Organization of the chapter 1
1.3. Power from Renewable energy sources 2
1.4. Key enabling technologies 4
1.5. Organization of the thesis 8
2. COMPONENT LOSS ANALYSIS 10
2.1. Rationale 10
2.2. Organization of the chapter 10
2.3. Calculation of the system voltages and currents 11
2.4. Loss characterization of the semiconductor devices 12
2.5. Losses in other power components 13
2.6. Introducing the Emitter Turn-Off Thyristor (ETO) 14
2.7. Loss Characteristics of the Emitter Turn-Off Thyristor 16
2.7.1. Switching loss 16
2.7.2. Conduction loss 18
2.8. Loss Characteristics of the Anti-parallel Diode 5SDF 10H4520 19
2.8.1. Switching Loss 20
2.8.2. Conduction loss 26
2.9. Loss calculation of the devices in the H-Bridge 27
2.10. Clamp component losses 31
2.11. Conclusion 36
3. THERMAL MANAGEMENT OPTIONS 37
3.1. Rationale 37
3.2. Organization of the chapter 37
3.3. Basic mechanisms of heat transfer 37
3.3.1. Conduction 38

3.3.2. Convection 39
3.3.3. Radiation 40
3.3.4. Phase change 42
3.4. Heat-Pipes for the ETO Converter 42
3.4.1. 2.2kW Heat-pipe for ETO device thermal management 43
3.4.2. 1.2 kW heat-pipe for clamp diode 44
3.5. Thermal Resistance 46
3.5.1. Heat-sink 47
3.5.2. Cold-plates 48
3.5.3. Heat-pipe 50
3.6. Comparison and Conclusion 53
4. MECHANICAL DESIGN 54
4.1. Rationale 54
4.2. Organization of the chapter 54
4.3. Judging design parameters 54
4.3.1. Parasitic or stray inductance 56
4.3.2. Design for minimum contact resistance between two Bus-bars 70
4.3.3. Bus-bars for the Voltage Source Converter 82
4.3.4. Discussion of the support for the H-bridge (12) 94
4.3.5. Support for the RCD Clamp circuit components: 100
4.4. Interconnection of the major power components 104
4.5. Conclusion 110
5. THERMAL MANAGEMENT DESIGN 111
5.1. Rationale 111
5.2. Organization of the chapter 111
5.3. Equivalent electrical circuit for heat-transfer 112
5.4. Air flow design 119
5.5. Conclusion 126
6. Conclusions 127
6.1. Construction of ETO Light Converter 127
6.2. Thermal management 128

6.3. Future work 129
6.4. Conclusion 129
Bibliography 131

LIST OF FIGURES

Figure 1-1: Usage of switched capacitor banks and STATCOM for regulating voltage..... 2
Figure 1-2: One line diagram of the 10 MVA STATCOM connected to the PCC 3
Figure 1-3: Voltage balancing components used for devices in series..... 4
Figure 1-4: Voltage Source Converters in series 6
Figure 1-5: Water cooled 1.5 MVA voltage source converter..... 7
Figure 1-6: Air cooled, heat-pipe based Voltage source converter 8
Figure 2-1: Topology of a Cascaded 5-level STATCOM 11
Figure 2-2: Circuit diagram of the H-Bridge converter..... 12
Figure 2-3: Self Powered Emitter Turn-Off thyristor..... 14
Figure 2-4: Cross section of the Emitter Turn-Off Thyristor 15
Figure 2-5: Turn Off transient of the ETO device..... 16
Figure 2-6: Pulse tester for calculating the switching loss of the ETO 17
Figure 2-7: Experimental data from a series of pulse tests at various temperatures..... 18
Figure 2-8: On-state voltage across the ETO..... 19
Figure 2-9: Reverse recovery current vs. Forward current of the diode (9) 20
Figure 2-10: Reverse recovery charge vs. the rate of change of forward current (9)..... 21
Figure 2-11: Experimental setup for measuring diode parameters..... 21
Figure 2-12: Diode turn-off energy calculation..... 23
Figure 2-13: Diode turn-on energy calculation..... 23
Figure 2-14: Double pulse test for the clamp diode..... 24
Figure 2-15: Reverse recovery current of the clamp diode..... 25
Figure 2-16: Forward recovery voltage of the clamp diode 25
Figure 2-17: The forward voltage drop of the diode at various temperatures (9)..... 26
Figure 2-18: Switching angles of a phase leg of the H-Bridge..... 27
Figure 2-19: The waveforms of the switches and diodes in the H-Bridge 28
Figure 2-20: Clamp circuit components 31

Figure 2-21: Voltage and current waveforms in clamp circuit components 34
Figure 3-1: A high-performance copper, extruded-fin type heat-sink. 38
Figure 3-2: Semiconductor devices mounted on a cold-plate 39
Figure 3-3: Black colored fins of the heat-pipe 40
Figure 3-4: Water cooling system for semiconductor devices 41
Figure 3-5: Principle of heat-pipe. (Courtesy: Thermacore Inc.) 43
Figure 3-6: 2.2 kW isolated heat-pipe for ETO thermal management 43
Figure 3-7: Thermal loading (1.8k-2k-2.2k) characteristics of the 2.2 kW heat-pipe 44
Figure 3-8: 1.2 kW isolated heat-pipe for clamp diode's thermal management 44
Figure 3-9: Thermal loading (0.8k-1k-1.2k) characteristics of the 1.2 kW heat-pipe 45
Figure 3-10: Aluminium bonded-fin heat sink, A = 18.59", B = 8.0", C = 16.0" 47
Figure 3-11: 3-D rendered image of a de-ionized water circulator for hockey-puck devices 49
Figure 3-12: Ceramic tubes in the heat-pipes for electrical isolation 51
Figure 3-13: Arrangement of heat-pipes with the Emitter Turn-Off Thyristor 51
Figure 4-1: Loop inductance and a method to minimize it 56
Figure 4-2: Parasitic inductance due to unequal lengths of conductor. 57
Figure 4-3: Parasitic loop inductance with the power stage 58
Figure 4-4: ANSYS simulation showing the flux density in case 1 61
Figure 4-5: Voltage Overshoot due to parasitic inductances 62
Figure 4-6: ANSYS simulations for flux density for case 2 63
Figure 4-7: Arrangement of devices leading to stray inductance in series with diode 64
Figure 4-8: Arrangement of devices leading to minimum stray inductance in an H-Bridge .. 65
Figure 4-9: CH4 (green) shows the negative current flowing through the GTO 66
Figure 4-10: Arrangement of devices leading to optimal and useful stray inductance 67
Figure 4-11: Stray inductances L1 < L2, due to difference in bus-bar length 68
Figure 4-12: Stray inductances L1 = L2 = L 69
Figure 4-13: Contact area under pressure 71
Figure 4-14: Experimental setup for observing streamline effect 72

Figure 4-15: Streamline effect curve 73
Figure 4-16: Experimental setup for constriction resistance measurement 74
Figure 4-17: Current density lines showing constriction 74
Figure 4-18: Spreading resistance curve 75
Figure 4-19: Contact resistance under clamping force 76
Figure 4-20: Current flow along the edges of contact between two bus-bars 78
Figure 4-21: Current constriction because of bus-bars of different resistivity 79
Figure 4-22: Trimming edges to force current away from edges 79
Figure 4-23: Guideline for implementing proper overlap joint between bus-bars 81
Figure 4-24: Arrangement of bus-bars for optimal stray inductance in half-bridge 83
Figure 4-25: ETO with the heat-pipes 84
Figure 4-26: Exploded figure of components of the half-bridge circuit 85
Figure 4-27: Isometric view of bus-bar 1 86
Figure 4-28: Isometric view of bus-bar 2 87
Figure 4-29: Isometric view of bus-bar 3 88
Figure 4-30: Isometric view of bus-bar 4 88
Figure 4-31: Arrangement of the half-bridge circuit 89
Figure 4-32: Right view of the half-bridge arrangement 89
Figure 4-33: Exploded view of RCD clamp circuit 90
Figure 4-34: Isometric view of bus-bar 5 91
Figure 4-35: Isometric view of bus-bar 6 92
Figure 4-36: Isometric view of bus-bar 7 93
Figure 4-37: Isometric view of bus-bar 8 93
Figure 4-38: Half-bridge circuit clamped together with ABB glass-epoxy clamp 94
Figure 4-39: Pointing to surfaces selected for mounting on support 95
Figure 4-40: Half-bridge support structure 97
Figure 4-41: Assembly diagram of the support 98
Figure 4-42: Half-bridge ciruit on the support 99

Figure 4-43: Electrical circuit of the RCD clamp 100
Figure 4-44: RCD clamp support structure 101
Figure 4-45: RCD support with diode clamp 102
Figure 4-46: Clamp circuit arrangement 103
Figure 4-47: Clamp circuit with half-bridge 104
Figure 4-48: H-Bridge with clamp circuit 105
Figure 4-49: Isometric view of H bridge with clamp resistor 107
Figure 4-50: Top view of H-Bridge with clamp resistor 108
Figure 4-51: Isometric view of H-Bridge with snubber inductor 109
Figure 4-52: Top view of H-Bridge with snubber inductor 109
Figure 4-53: Clamp resistor stack arranged with the DC capacitors 109
Figure 5-1: Two possible arrangements of devices in an H-Bridge Phase leg 112
Figure 5-2: Electrical equivalent model for arrangement in Figure 5-1.i 113
Figure 5-3: Electrical equivalent model for arrangement in Figure 5-1.ii 115
Figure 5-4: Summary of results for first arrangement 118
Figure 5-5: Summary of results for second arrangement 118
Figure 5-6: Analysis of the 2.2 kW Heat-Pipe 120
Figure 5-7: Analysis of the 1.2 kW Heat-Pipe 121
Figure 5-8: Heat-sink for the clamp resistor array 122
Figure 5-9: Air-flow electrical equivalent model for the system 124
Figure 5-10: Simplified version of the model shown in Figure 5-9 125

LIST OF TABLES

Table 2-1: Circuit parameters of the experimental setup 22
Table 2-2: Anti-parallel Diode turn-off loss summary: 24
Table 2-3: Anti-parallel Diode forward recovery summary: 24
Table 2-4: Clamp diode turn-off loss 26
Table 2-5: Clamp diode forward recovery voltage 26
Table 2-6: Device losses in the capacitive mode 30
Table 2-7: Device losses in the inductive mode 30
Table 2-8: Losses in the clamp circuit 35
Table 3-1: Comparison between various thermal management options for the VSC 53
Table 4-1: Voltage spike generated for a particular parasitic inductance 59
Table 5-1: Temperature profile of devices in capacitive/inductive mode (t_{amb} = 35 °C) 114
Table 5-2: Temperature profile of devices in capacitive/inductive mode (t_{amb} = 55 °C) 114
Table 5-3: Temperature profile of devices in capacitive/inductive mode (t_{amb} = 35 °C) 116
Table 5-4: Temperature profile of devices in capacitive/inductive mode (t_{amb} = 55 °C) 116
Table 5-5: Air-flow requirement on the 2.2kW heat-pipe 121
Table 5-6: Air-flow requirement on the 1.2kW heat-pipe 122
Table 5-7: Inductor parameters 123
Table 5-8: Obtained air-flow values as compared to the minimum required values 126

1. INTRODUCTION

1.1. Rationale

Energy generation and conservation are topics of great research value today. This is vastly true because of the rapidly decreasing reserves of fossil-fuels in the planet. Concerns over the rising concentration of the harmful gases in the air we breathe and pollutants destroying the environment around us have lead to a great interest in the use of free renewable sources of energy. There are different kinds of free renewable energy sources that can be found in any given environment, such as solar, wind and geothermal energy. Depending on the geographical location and concentrations of the available energy either of the three mentioned energy generation centers can be setup.

The varied geographical layout of the North American continent, comprising of vast deserts, volcanic regions and windy grasslands make it most suitable to setup different kinds of free renewable source generation centers. The vast deserts could be used to harness solar power, the active volcanic regions to tap the geo-thermal energy and the windy-grasslands for harnessing wind power. At some locations near river dams and water reservoirs, hydro-generation plants could also be established. Even if a tenth of all the free renewable energy is harnessed and utilized, a large number of polluting and hazardous fossil-fuel powered generation units could be decommissioned.

1.2. Organization of the chapter

The chapter gives an overview of the presented thesis. It is divided into two sections; the problem followed by a best suited solution selected from a pool of other possible solutions. The problem is explained briefly in context to the actual application viz. a wind-farm project. The proposed solution is also explained in short and in relation to the actual application.

1.3. Power from Renewable energy sources

Power obtained from renewable energy sources greatly depends on the availability of the natural resource being converted into usable energy. If the case under discussion is solar energy, then there will be zero energy produced during night or when the sky is severely overcast. If wind-power is being discussed, then only the average flow of wind during a particular day can be estimated accurately, to a certain degree only. There can be days when the wind in the region is very low and insignificant amount of energy is produced that day; alternatively there can be days when too much power is produced. The production of energy in hydro-power plants depends on the availability and rate of flow of water. This can again fluctuate depending on the varying conditions.

In short, the power obtained from renewable energy sources is fluctuating very rapidly and can change every hour. It is not just the frequency at which the voltage level changes, but also the voltage itself. The power output obtained from the renewable sources can vary from 0% to up to 150% of the rated output. These conditions severely limit the ability of the power obtained from the renewable sources to be directly fed back to the grid for distribution purposes.

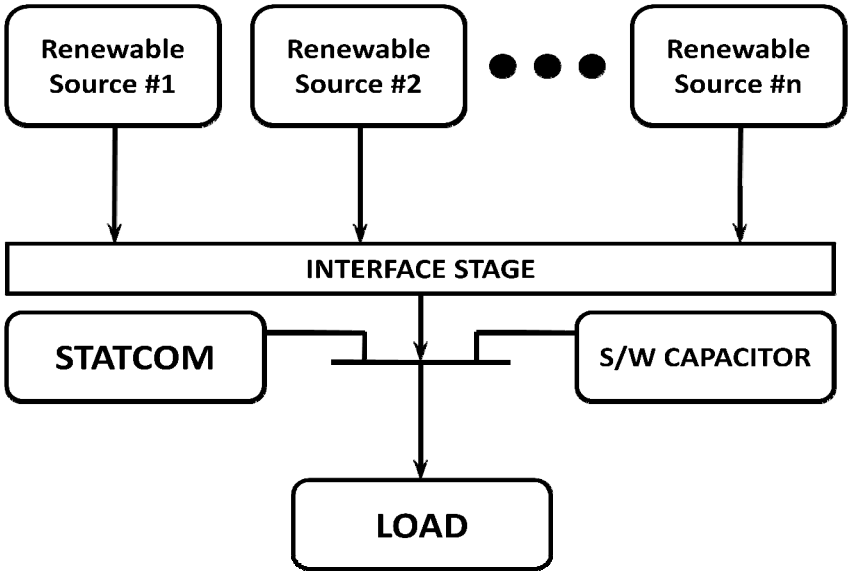


Figure 1-1: Usage of switched capacitor banks and STATCOM for regulating voltage

Figure 1-1 shows n-number of renewable sources connected in series/parallel, depending on the voltage and current requirements. Here the energy obtained from the renewable sources is conditions at the point of common coupling (PCC) by switched capacitor banks and a STATCOM. If the power delivered is about 100 MVA, then the capacitors are rated for 90 MVA and the STATCOM is rated for 10 MVA. The switched capacitor banks provided a slower response than the STATCOM, but are installed at a higher rating because of a cheaper cost of installation and maintenance. The STATCOM provides a faster sub-cycle response to the fluctuations in the voltage of the PCC (VPCC). Together the response of the system is much better than the s/w capacitor connected by itself. Ideally, a 100 MVA STATCOM should be connected to the PCC, but it will be very expensive as compared to the combination of s/w capacitor and a smaller rated STATCOM. The motivation to upgrade to a full 100 MVA STATCOM depends largely on the success of the smaller initiative.

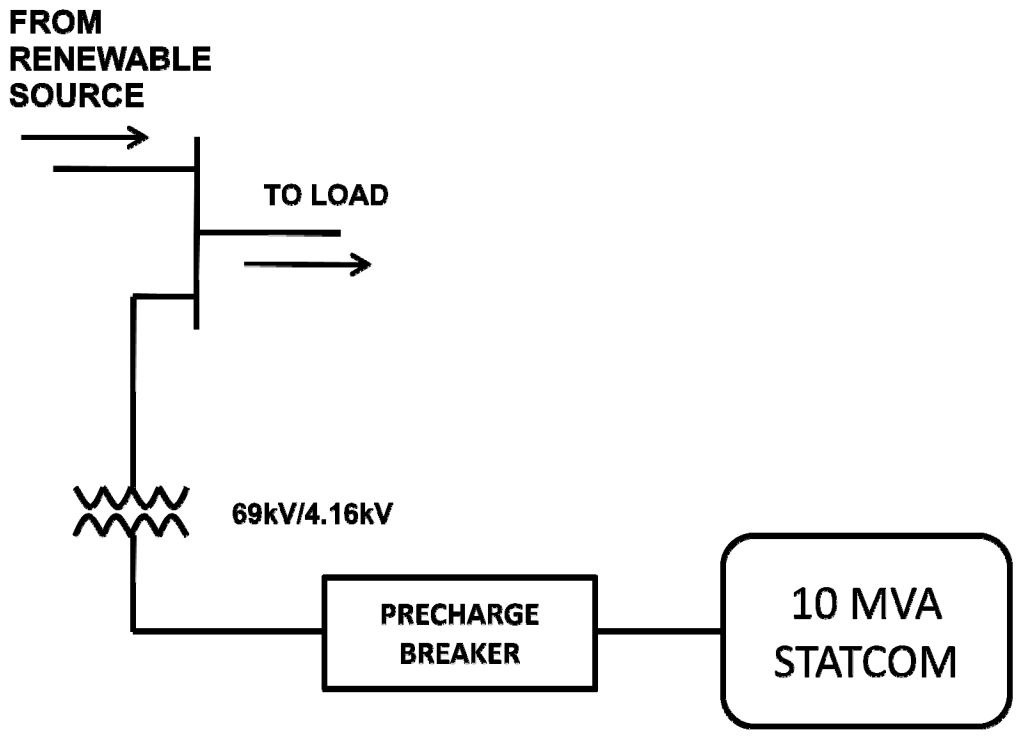


Figure 1-2: One line diagram of the 10 MVA STATCOM connected to the PCC

1.4. Key enabling technologies

The 10 MVA STATCOM is the first step to installing similar interfacing setups for other renewable sources. This makes the flexibility to upgrade or change the configuration of the system an important feature that the system should have. Thus special focus must be given to make the system as modular as possible, both electrically and thermally. Electrically, a modular design can be obtained by using the most suitable topology for the given application. In this case since the converter has to be tied to the PCC of the grid, a high voltage output is desired to reduce the size of the coupling transformer or if possible to eliminate it. A high voltage converter can be designed by either using semiconductor devices in series to obtain large voltage blocking capacity or by using smaller converters in series. Using semiconductor devices in series may seem feasible initially, but there are a number of problems associated with connecting devices in series. These problems mainly arise from the mismatches the devices have at the silicon level. Extra components and efforts form the control system have to be put to ensure correct and safe operation of such a system (1). Thus the system becomes more complicated and cannot be easily upgraded for a higher voltage level.

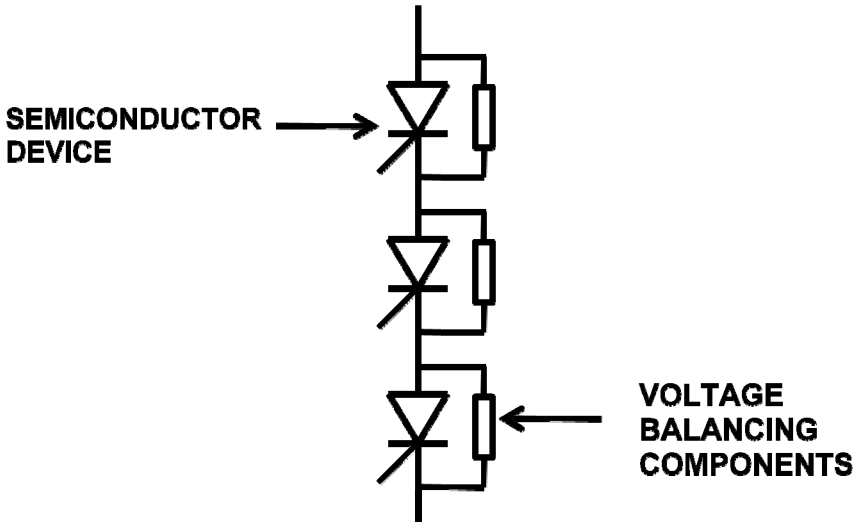


Figure 1-3: Voltage balancing components used for devices in series

The Figure 1-3 shows voltage balancing components connected across each device in the stack. The components are usually resistors and capacitors connected in series/parallel combinations. Any failures occurring in the device stack could halt the operation of the converter, unless more devices had been added to the stack previously. In any case the entire system would have to be offline to service/replace stacks containing faulty devices.

Another approach of obtaining a high voltage output would be to use smaller converters connected in series. This configuration is called as the cascaded multilevel converter (1). The immediate advantage of using such a converter is that it is modular, both electrically and thermally. It has a smaller component count than the previously mentioned converter as the voltage balancing components are not required anymore. An added advantage to having smaller converters is that the voltage levels of each converter can be monitored and controlled independently. Additional redundant converters can be added in case of fault scenarios and there will be no need of halting the operation of the entire system in case of a fault in one of the converters. The faulty converter can be turned off and serviced while the entire converter remains on-line. The fundamental advantages provided by the cascaded converter topology make it an obvious choice for the presented requirements of the system. The Emitter Turn-Off Thyristor (2) is a key enabling technology used to build the cascaded VSC. The onboard sensors provide telemetry signals required for control, thus eliminating use of expensive sensor arrays.

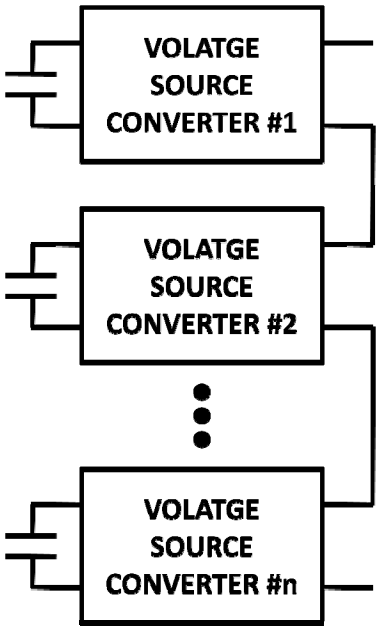


Figure 1-4: Voltage Source Converters in series

Previously, high power converters had used water or fluid based cooling to meet their thermal management requirements. The thermal system thus was non-modular and had to be completely re-configured to adapt any change (increase) in the thermal load. The water cooling system had to be continuously monitored for leaks, ionization and calcification. Periodic maintenances had to be conducted keeping the converter offline, thus the outage times were significantly more than a system which did not use water based cooling. Also the system was bulkier, occupied more volume and had a larger foot-print. The cooling system was a complicated real-time control system by itself. Thus alternative options for handling the thermal load had to be explored to ensure minimal outage times and more reliable operation of the converter.

Figure 1-5 shows an example of a 1.5 MVA water cooled VSC. Notice the complicated mesh of water tubes throughout the cabinet. Routing of the water tubes must be carefully done to avoid mixing hot and cold water in the system. Electrical conductivity of the water has to be continuously monitored to prevent any failure/trip occurring due to conduction of current through water.

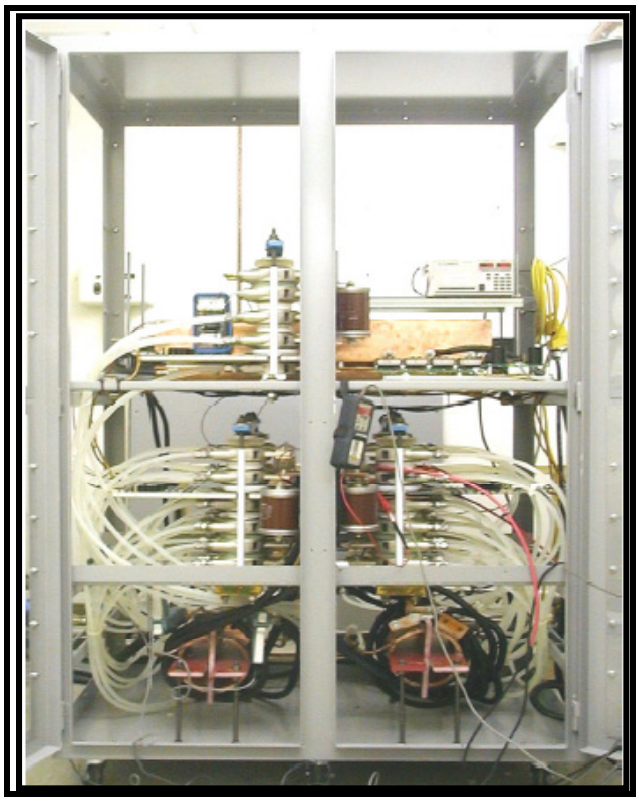


Figure 1-5: Water cooled 1.5 MVA voltage source converter

The Figure 1-6 shows a more compact version of the voltage source converter, but working at a higher rating of 1.667 MVA. All the components shown above are air cooled by 'passive' heat-pipes. The heat-pipes are nothing but heat transporting agents with zero thermal resistance between two ends of a pipe. Their thermal resistance arises because of the fact that there is a thermal resistance between the heat-pipe and the ambient. The pipes are flexible and are used to effectively spread the heat over a larger area for efficient cooling performance. The thermal resistance of the heat-pipes is only slightly higher than the water based cooling option. However, it does not have any of the previously mentioned disadvantages of 'active' water cooled systems. It is compact and modular. Thus this technology enables the power converter to be modular, flexible and reusable for other applications. Thus, overall cost of components and manufacturing reduces greatly.

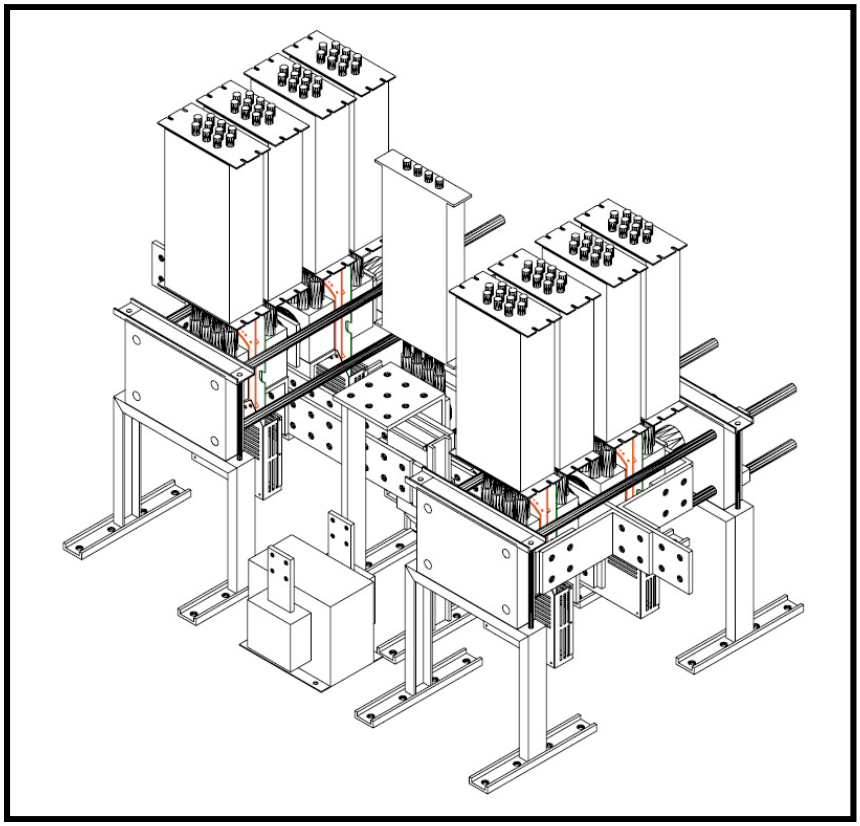


Figure 1-6: Air cooled, heat-pipe based Voltage source converter

1.5. Organization of the thesis

The thesis is organized into six chapters chronologically arranged as per the tasks that were undertaken leading to the final design.

Chapter one is the basic introduction to the research conducted. The motivation behind the research work and thesis is explained. The issues with similar work done previously and techniques to overcome those problems are also discussed. The reader should use this chapter to get an insight of what can be expected in the following chapters.

Chapter two deals with the loss characteristics of all major components used in the power converter. This investigation leads to calculation of the actual losses in the power converter

at different modes of operation. The loss information is used to calculate the temperature rise of the system and aid in the selection of heat-transfer/ dissipation components.

Chapter three uses loss information from the previous chapter to select the most suitable heat-transfer medium. Before the selection process, the available four methods of heat-transfer are discussed and compared in detail.

Chapter four discusses the mechanical design of the power converter. The impact of mechanical design parameters on the electrical parameters is discussed in detail e.g. the length and routing of copper bus-bars on the parasitic/ stray inductances of the system. The effect of improper mechanical contact between two bus-bars and the techniques of ensuring a good contact are highlighted. Other details that are covered in this chapter include the mechanical layout of the major components in a cabinet/ enclosure aimed to optimize the foot print and the volume of the converter.

Chapter five deals with the air-flow design in the cabinet. Calculations leading to reasonably accurate estimation of the static pressure head along the various air flow paths are shown. These results are utilized for the proper selection of an air-mover that has to be installed in the power converter cabinet. The performance of the air-flow system is also examined using analytical methods.

Chapter six is the concluding chapter of the thesis where all major analysis and various conclusions are compiled to represent the work done in a meaningful manner.
A list of references can be found at the end of the thesis.

2. COMPONENT LOSS ANALYSIS

2.1. Rationale

Semiconductor devices have proved to be far superior to mechanical valves and switches in terms of response time and power handling density. However, these devices are not 100 % efficient and have their own loss characteristics. The loss characteristics of semiconductor devices mainly depend on the voltage, current and temperature at which the devices are operating. A good understanding of the loss characteristics of the device being used for a power converter is essential to determine the losses, performance and true efficiency of the converter. The determined losses enable the designer to accurately calculate the nominal and worst case operational temperature of the devices. This study of temperature variation of the devices is essential to determine the life of the converter and its reliability under high temperature operation. A good understanding of loss characteristics and the ability to calculate device losses accurately can lead to reliable and robust power converter design.

2.2. Organization of the chapter

The chapter introduces the devices utilized for the voltage converter application and their loss characteristics. The trends of the device losses are highlighted in detail. Based on the application, the ratings of the devices are determined and appropriate commercially available devices are selected. Experiments on the diodes were carried out to emulate the turn-on loss in the diode. Similar experiments were also carried out to determine the switching loss in the Emitter Turn-Off thyristor (1). Empirical equations were derived for the switching and conduction losses based on the current and nominal operating temperature (1), (3). Detailed waveforms are shown; these waveforms and empirical equations are used to determine the actual losses of the system. The advantages and disadvantages of using the selected devices and various components are discussed throughout the chapter. Finally, a tabulated summary of the losses is presented to conclude the chapter. The information derived will be utilized in the next chapters for thermal design of the system.

2.3. Calculation of the system voltages and currents

The STATCOM is grid tied using a 69 kV/ 4.16 kV transformer. The series line connected inductance is decided as 0.6886 mH, based on the peak-to-peak ripple on the input line current. The DC bus voltage of the VSC is chosen as 2170 V. Keeping the IEEE 519 (4) specification in mind a series of switching angles are calculated for a seven level three phase 10 MVA STATCOM (5). However, the discussion of the STATCOM in this thesis is based on the cascaded five-level converter topology shown in Figure 2-1. The two modes of the converter operation are inductive compensation and capacitive compensation. These two modes of operation are achieved by using different sets of modulation index for the converter. The maximum RMS current of the STATCOM can be calculated by using the rating of the STATCOM viz. 10 MVA and the VPCC voltage viz. 4.16 kV. Thus a maximum RMS current of 1.39 kA is obtained for both inductive and capacitive compensation. This Maximum RMS current obtained will be useful to calculate the losses in various semiconductor devices and components.

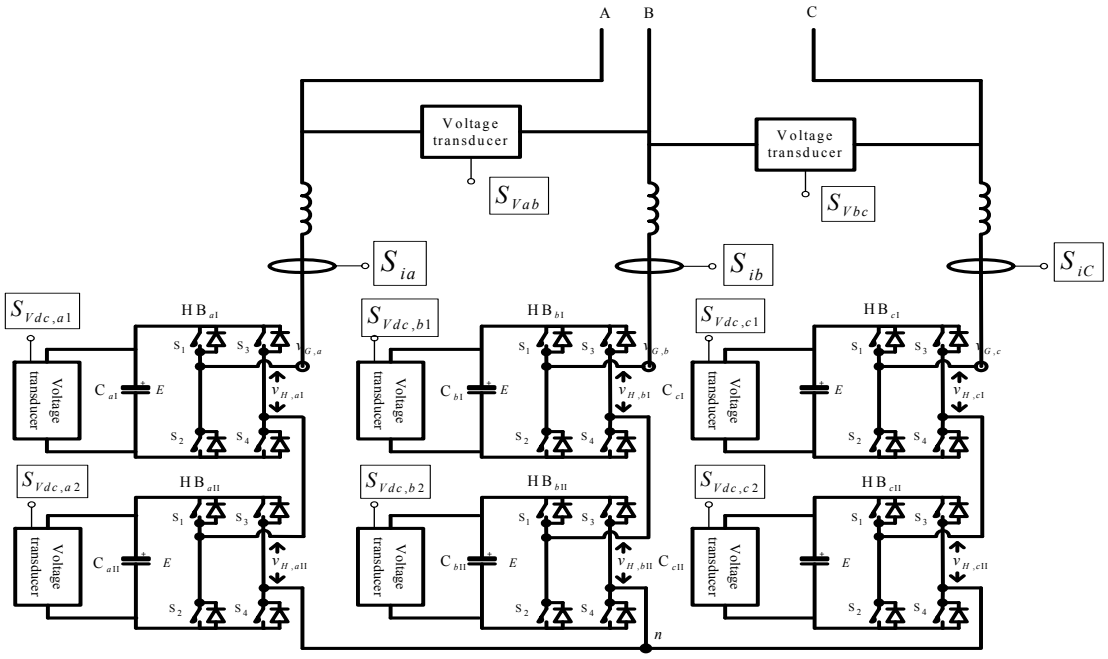


Figure 2-1: Topology of a Cascaded 5-level STATCOM

Operating the STATCOM at a modulation index of 0.904 runs it in full capacitive compensation mode and changing the modulation index to 0.6 runs the STATCOM in full inductive mode. The losses at these two extremes have to be calculated based on the switching angles for the given modulation index. Waveforms of the component voltages and currents are drawn to get an idea of the switching and conduction losses in the components. Since the losses are unequal in the H-Bridge levels, the switching patterns will be cycled through the various levels to average out the losses. If this procedure is not implemented there will be unequal thermal loading of the components in different levels which may cause unexpected thermal failure of the components resulting in a system trip. In the H-bridge itself, the switching patterns leading to a zero vector output will be toggled between the top two and the bottom two switched to equalize the losses within the components in a single H-Bridge.

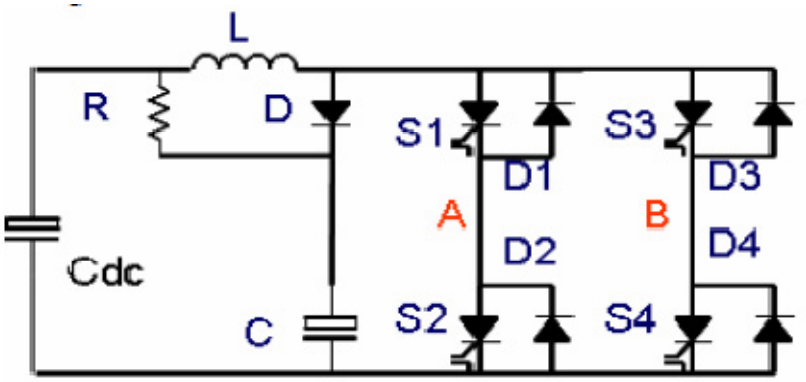


Figure 2-2: Circuit diagram of the H-Bridge converter

Thus, to equalize losses in the H-Bridge, as shown in Figure 2-2, the zero vector output is generated by switches S1/S1 and S2/S4 alternatively.

2.4. Loss characterization of the semiconductor devices

The electrical parameters of a semiconductor device are a function of operating temperature of the device. Thermal conditions have a significant effect on the performance of power electronic devices. High temperature usually degrades the electrical properties of silicon. In

unipolar devices like the MOSFET, the phenomenon occurs due to the reduction of carrier mobility with rising temperature.

$$\mu_T(T) = \mu_{300}\left(\frac{T}{300}\right)^{-2.3} \quad \text{..... Equation 2-1}$$

Where μ_T is the electron mobility and μ_{300} is the mobility at 300K. In bipolar devices such as the ETO the decreased mobility at higher temperatures leads to higher losses and poorer switch performance. The leakage current also increases at higher temperature. To characterize the loss performance of any semiconductor device, the switching loss, conduction loss and leakage currents must be calculated at various operating points and at different temperatures.

The total loss in a semiconductor device is a summation of the major loss components mentioned above. Previous work done in (1), (3) and (6) gives us empirical formulae for calculating the device losses at different operating points and temperatures. For the sake of convenience, worst case losses are calculated at the maximum possible safe operating temperatures.

2.5. Losses in other power components

There are significant losses in the other components of a power converter such as the clamp circuit resistor R, the clamp diode D and the Snubber inductor L, as shown in Figure 2-2. There are losses in the bus-bars also. However, the losses in the clamp resistor, bus-bars and Snubber inductor are mainly due to the resistivity of the material. A large current flows through a resistor, causes significant I^2R losses which have to be accounted for while summarizing the system losses. The losses in the diode can be divided in to three components; the conduction loss, reverse recovery loss and the forward recovery loss. The conduction loss parametric equation can be obtained from the datasheet of the diode itself. The reverse recovery loss and the forward recovery losses are calculated by experimentation.

2.6. Introducing the Emitter Turn-Off Thyristor (ETO)

The ETO is discussed in various articles and a lot of research work has already been done to call the technology mature (2), (3), (7) and (8). The basic principle of operation is briefly discussed here for the sake of completion and to aid in further discussion of the loss calculations. The ETO can be thought of a hybrid fab-less MOS controlled thyristor. As compared to a conventional GTO, the ETO has a large reverse biased safe operating area (RBSOA), built in closed loop compensated current, voltage and temperature sensors, can turn off snubber-less under hard driven conditions and has full optical control. The latest generation of the ETO can draw its own gate drive power from the voltage bus and can be called a "light triggered self-powered device" shown in Figure 2-3.

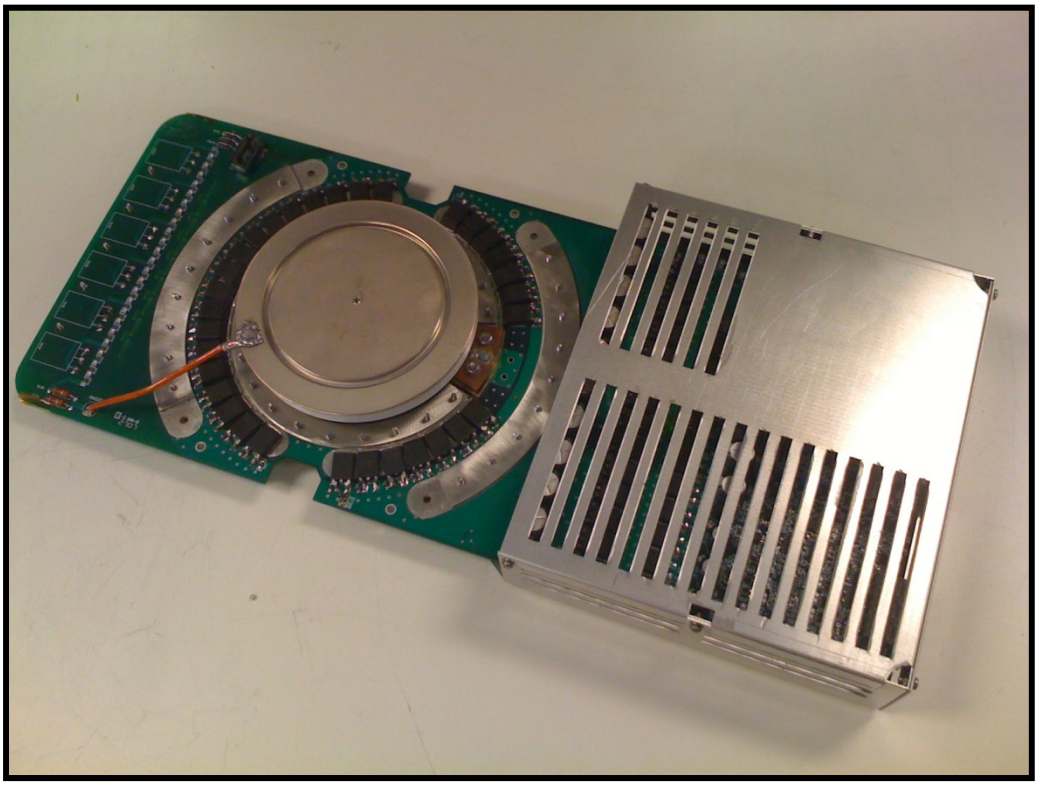


Figure 2-3: Self Powered Emitter Turn-Off thyristor

The cross section of the ETO is shown in Figure 2-4. It can be seen that the two MOSFETs are operating as a complementary pair to turn-off the GTO. To turn off the GTO device, the

emitter switch Q_e is turned off and the gate switch Q_g is turned on, the cathode current of the GTO will be diverted to the gate, in effect results a unity-gain turn-off condition, where the anode current equals the gate current. In this scenario the GTO can be turned off safely without using any R/C voltage clamp across it. There are two benefits of having a unity-gain turn off. First, the time required for the gate current to remove all minority charges from the p-base region decreases significantly. Secondly, the turn-off of the ETO is changed to an open base PNP process ensuring uniform distribution of current among the GTO cells on the device during the transient turn-off period.

Figure 2-3 shows the photograph of a 4.5 kV, 5 kA ETO. It utilizes double side press-pack cooling packages to get smaller thermal resistance. The thermal resistance of the ETO form the junction to the case is 12.6 K/kW.

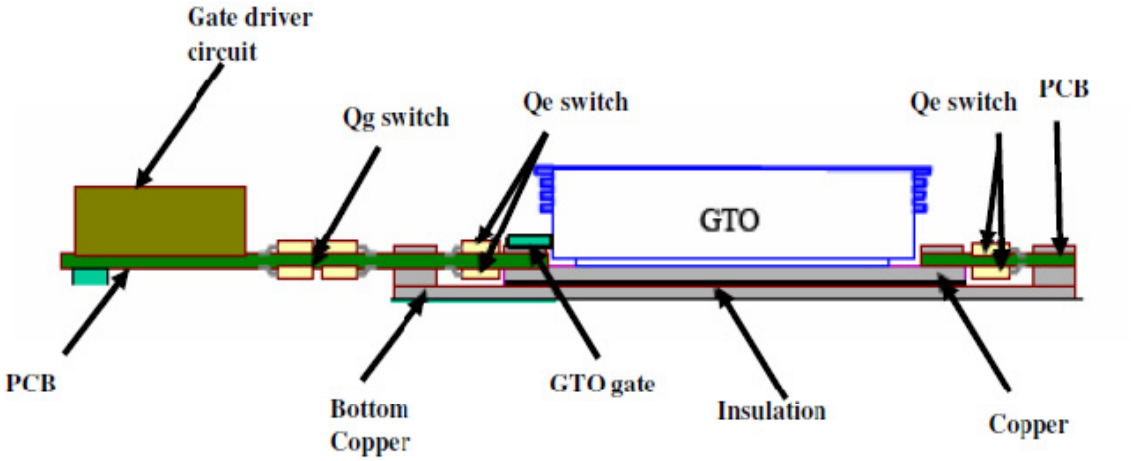


Figure 2-4: Cross section of the Emitter Turn-Off Thyristor

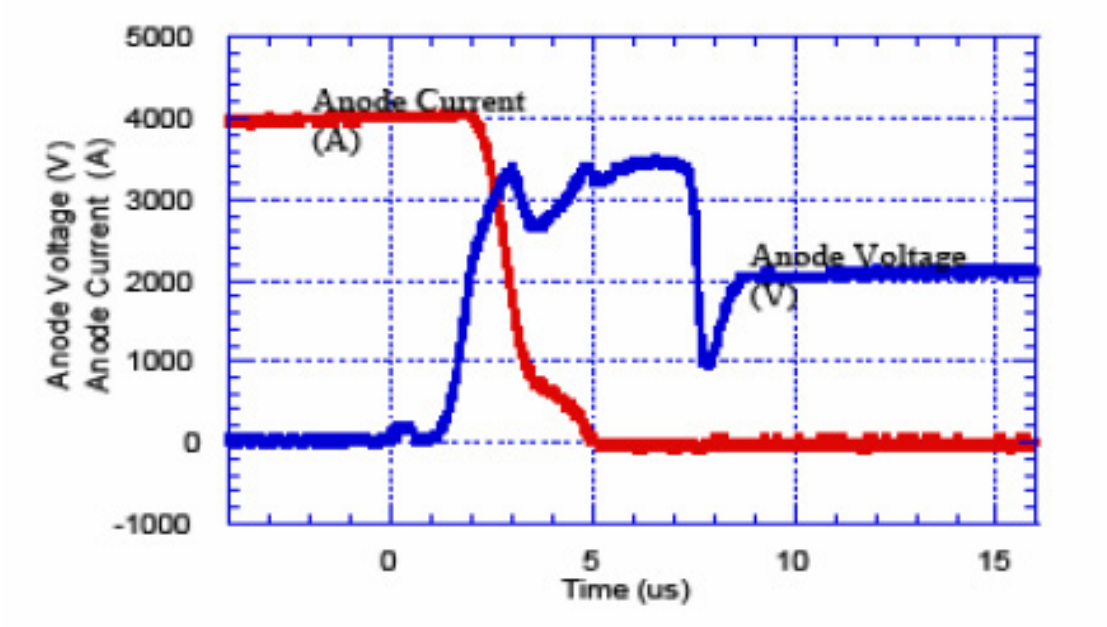


Figure 2-5: Turn Off transient of the ETO device

2.7. Loss Characteristics of the Emitter Turn-Off Thyristor

Empirical formulae for the switching, conduction and leakage loss are calculated based on data obtained from experimental results at different operating voltage current and temperature. Such analysis has already been done in previous work (1), (6). The process of obtaining the empirical formulae is explained briefly for the sake of completion. The formulae have been derived at the worst operating temperature for silicon, 125 °C.

2.7.1. Switching loss

The switching loss of the emitter turn off thyristor was measured using a pulse tester, with a temperature controlled base. The setup basically discharges a high voltage charged capacitor bank through the device under test (DUT) and an inductive load. The inductive load also acts as a di/dt snubber for the DUT and limits the rate of rise of the anode current through the device. Single pulses are fed to the DUT to trigger it on and off, the on time usually being in the order of microseconds. The heater base-plate is used to change the junction temperature

of the DUT. The turn off current is measured at regular intervals of temperature to obtain a set of data which is used to calculate the turn-off loss.

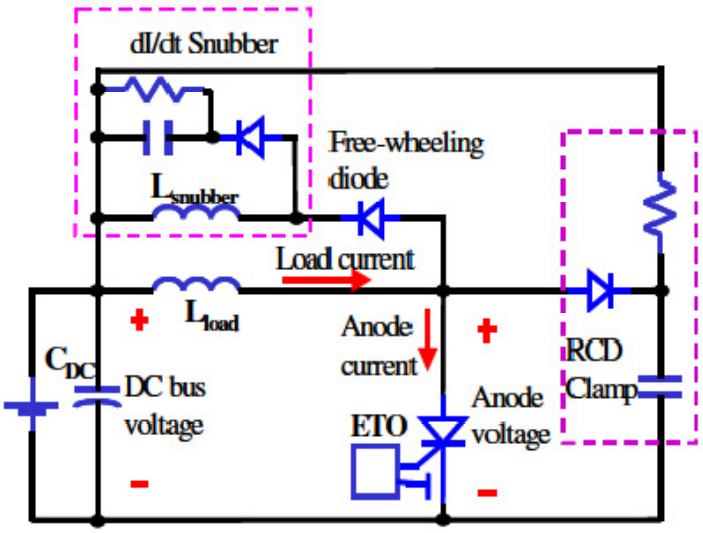


Figure 2-6: Pulse tester for calculating the switching loss of the ETO

When the ETO is turned on, the anode current in the DUT builds up linearly. The snubber inductor determines the rate of rise of the current in the DUT. When the desired anode current is reached the device is pulsed to be turned off. The anode current will keep flowing through the ETO till its anode voltage is equal to the DC bus voltage. The ETO anode current then commutates to the freewheeling diode and partly to the clamp circuit. Due to parasitic inductances the DUT may see a voltage spike but this is limited by using a RCD clamp across it. The ETO switching losses are the highest when it is turning off maximum current at and the anode to cathode voltage has risen to a maximum value. The ETO blocks a voltage equal to the DC bus after completion of the turn-off process. The DUT commutated current is still flowing through the load, snubber and freewheeling diode.

The integration of the DUT voltage and current during the switching transient period gives the turn-off loss at that particular operating voltage and current of the DUT. The turn-on loss of the ETO is negligible as compared to the turn-off loss because of the presence of the di/dt snubber inductor which limits the rise of current through the DUT. Since the ETO will

always be utilized with a series di/dt snubber inductor, the turn-on losses will continue to remain negligible, and as a result will be discarded throughout the discussion.

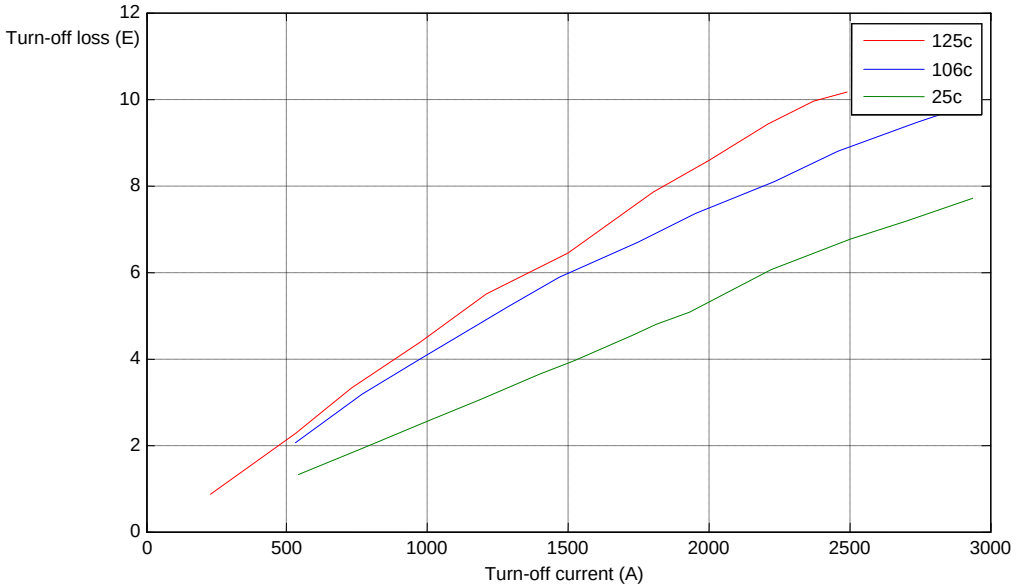


Figure 2-7: Experimental data from a series of pulse tests at various temperatures

The empirical formula for turn-off loss at worst-case junction temperature 125 °C is given by:

$E_{off}(I) = 0.0042*I + 0.169$ ……...…… Equation 2-2

This formula is valid for a generation 4 ETO device shown in Figure 2-3.

2.7.2. Conduction loss

The conduction loss can be measured by measuring the on-state voltage of the ETO when a controlled DC current is flowing through it. Since the current is very high, a low voltage source has to be used for the test. The easiest way to do this is to obtain large current from a parallel current capacitor bank. The ETO is connected to a capacitor bank through a current limiting di/dt snubber. When the ETO is turned on, the capacitor bank gets discharged and a large current flows through the ETO. The conduction voltage and current waveforms are

recorded over a range of operating points and temperatures. The on-state voltage drops are measured across the GTO and MOSFET separately and then added to get a total voltage drop across the ETO device. This is done at different temperature points, using the base heater of the pulse tester.

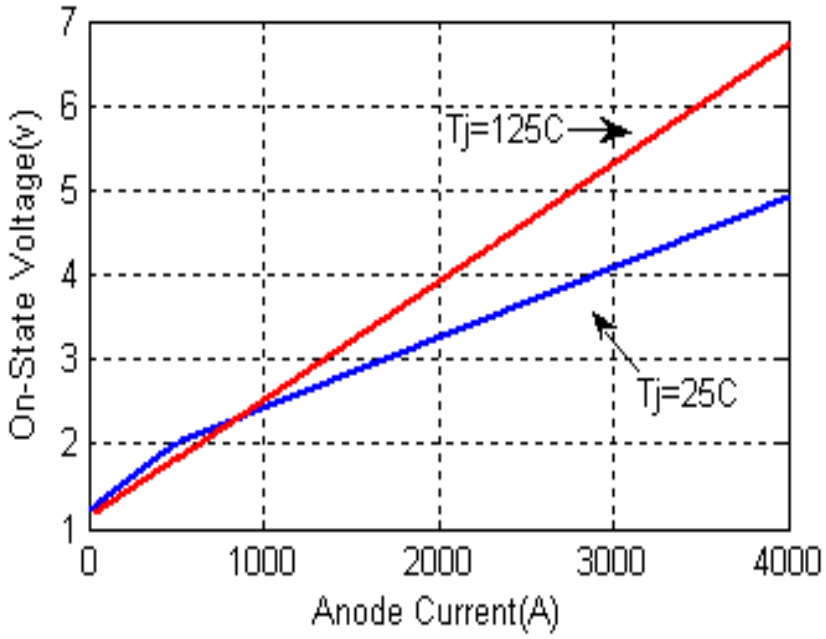


Figure 2-8: On-state voltage across the ETO

The empirical formula for depicting on-state voltage at the worst case temperature of 125°C is given by:

$V_{ON}(I) = 0.0041*I + 1.1$ …… Equation 2-3

The conduction loss can be obtained by multiplying the V_{on} voltage with the anode current.

2.8. Loss Characteristics of the Anti-parallel Diode 5SDF 10H4520

A similar experimental analysis has to be performed for the diode to obtain loss characteristics of the diode over a wide temperature and operating condition range. A first estimation of the loss numbers can be done by looking into the datasheet of the diode under

discussion. But a detailed experiment must be done at the desired operating point to obtain an accurate number for the device losses.

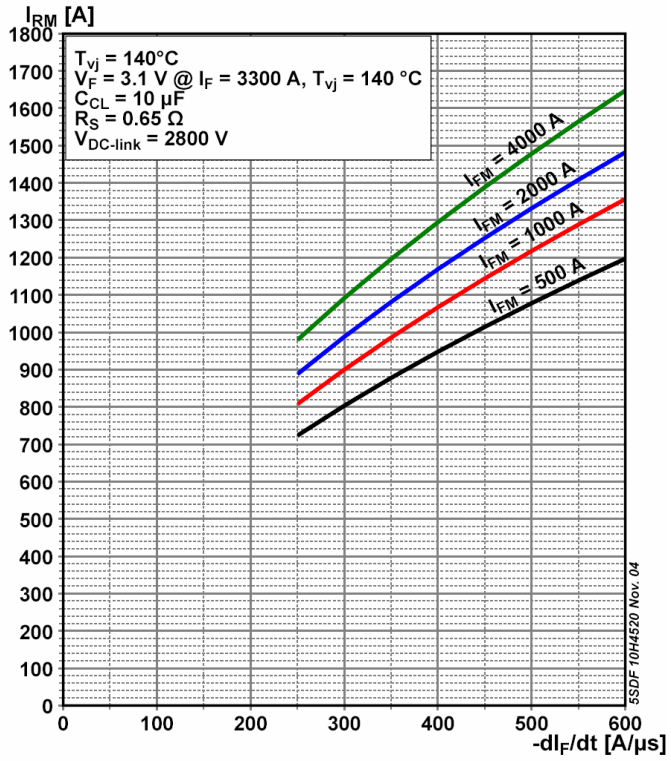


Figure 2-9: Reverse recovery current vs. Forward current of the diode (9)

2.8.1. Switching Loss

The operating point of the anti-parallel diode in the voltage source converter is similar to the operating point of the switching device it is coupled with in the power topology. The diode forward current will be 1965.7 A and its maximum blocking voltage will be equal to the DC bus voltage viz. 2170 V. The operating point information can be used to obtain the necessary calculate the reverse recovery current and the reverse recover charge, Q_{rr}. There is a curve already available for obtaining the value of Q_{rr} in the datasheet.

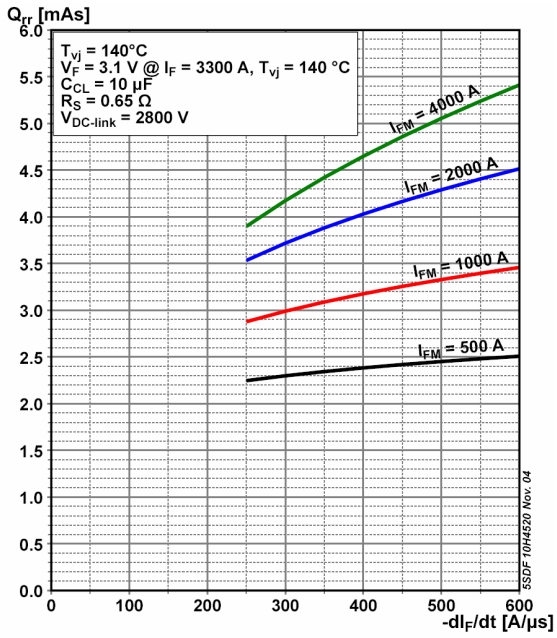


Figure 2-10: Reverse recovery charge vs. the rate of change of forward current (9)

However, it can be seen from both Figure 2-9 and Figure 2-10 that the circuit parameters under which the diode is tested does not match the circuit parameters where the diode will actually be used. Hence a detailed experimental analysis was conducted to obtain the accurate values of switching loss of the diode.

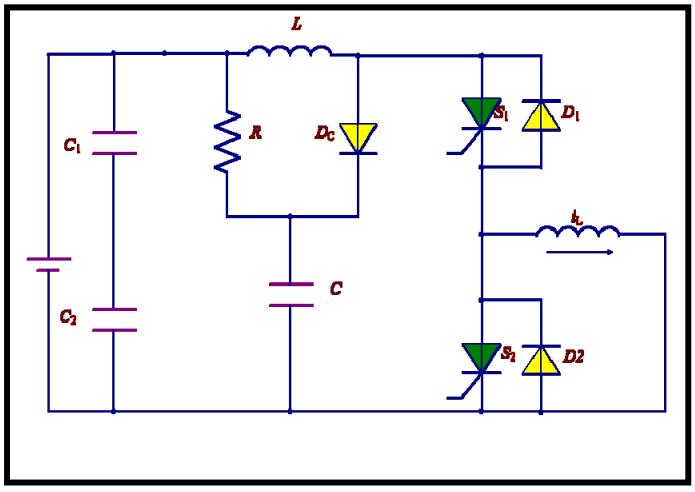


Figure 2-11: Experimental setup for measuring diode parameters

The experimental setup for diode testing consists of identical circuit passive as used in the actual H-Bridge converter. The values of the circuit parameters are highlighted in Table 2-1.

Table 2-1: Circuit parameters of the experimental setup

DC Capacitor	850 µF/2
di/dt inductor L	10 µH
Clamp resistor R	1 Ω
Clamp capacitor C	12µF
Load inductor	120 µH
S1&S2	ETO 4.5 kV/ 4 kA
D1&D2	5SDF 10H4520
Dc	5SDF 10H4502
Temperature	22 °C

From the pulse-test results, shown in Figure 2-12 and Figure 2-13 below, the switching loss parameters such as the diode turn-off and turn-on energies of the diodes were calculated and used in the loss calculation.

The Table 2-2, shows the diode turn-off loss results and the Table 2-3, shows the diode's forward recovery experimental results. It can be seen that the forward recovery transient voltage exceeds the maximum reverse blocking voltage of the Gate Turn-Off Thyristor used in the ETO. However, as this transient lasts for only 10-12 µs the impact of the heat generated by the voltage pulse can be directly related to the material characteristics of silicon. There will be a certain rise in temperature of the die (ΔT) because of the voltage

pulse. The silicon die can sustain a finite number of such voltage pulses during the normal course of operation; this number is given by X, where X is:

$$X = \left(\frac{300}{\Delta T}\right)^9 \quad \text{..... Equation 2-4}$$

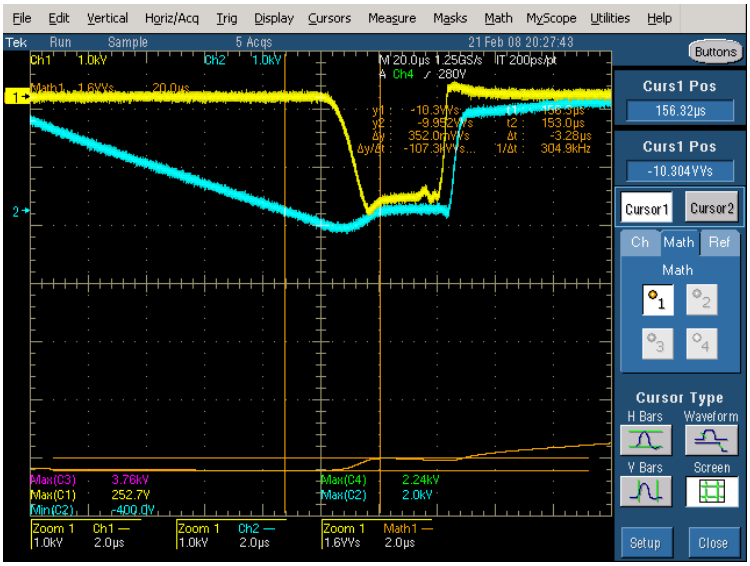


Figure 2-12: Diode turn-off energy calculation

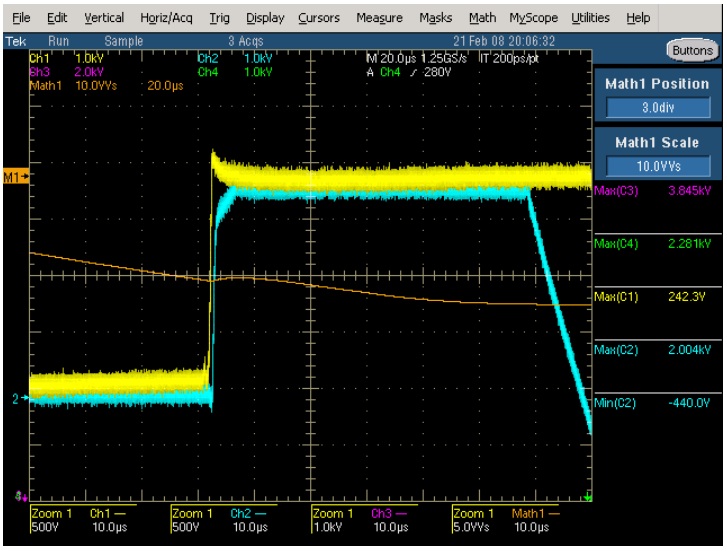


Figure 2-13: Diode turn-on energy calculation.

Table 2-2: Anti-parallel Diode turn-off loss summary:

I_{fm} (A)	di/dt (A/µs)	E_{rr} (J)	I_{rm} (A)
2000	181	0.352	400

Table 2-3: Anti-parallel Diode forward recovery summary:

di/dt (A/µs)	V_{fr} (V)	E_{fr} (J)
2.25e3	251	0.24

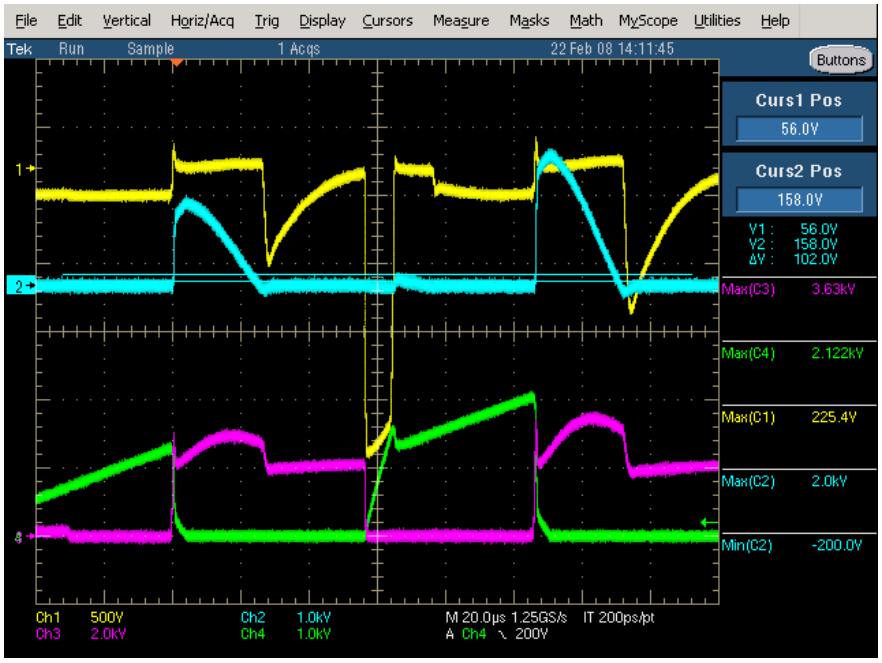


Figure 2-14: Double pulse test for the clamp diode

For obtaining the switching loss parameters of the clamp diode, a double pulse test was utilized. In this test, the switch S1, shown in Figure 2-14, is turned on. The load current builds up in the inductor. When the desired current level is reached a second pulse turns off

the switch and the load current commutated to diode D2. The waveforms were captured as shown in Figure 2-14, Figure 2-15 and Figure 2-16.

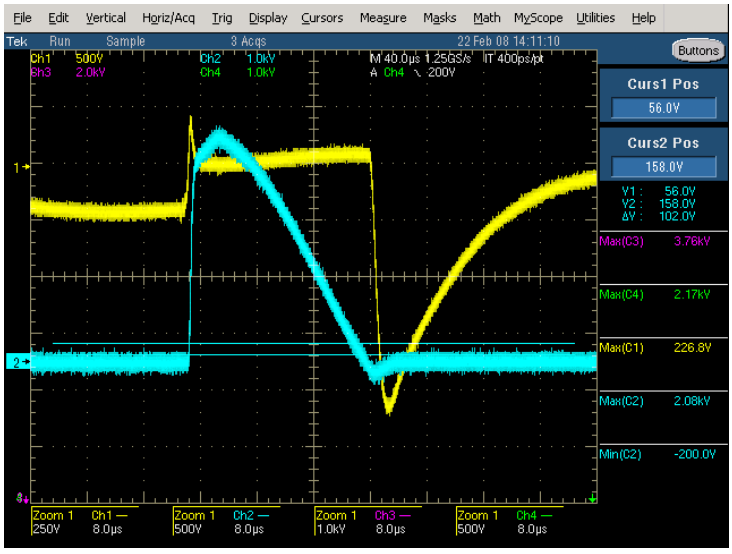


Figure 2-15: Reverse recovery current of the clamp diode

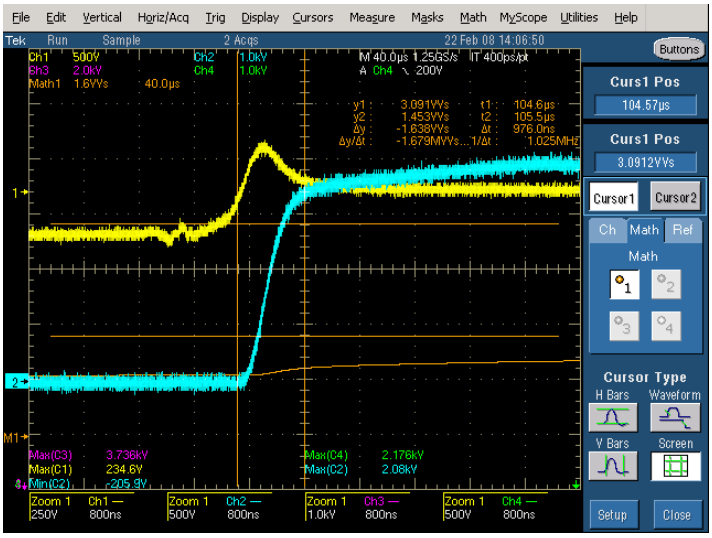


Figure 2-16: Forward recovery voltage of the clamp diode

Table 2-4 and Table 2-5, show the clamp diode's turn-off loss experimental results and the forward recovery voltage respectively.

Table 2-4: Clamp diode turn-off loss

I_{fm} (A)	di/dt (A/µs)	E_{rr} (J)	I_{rm} (A)
0	102.5	0.18	104.9

Table 2-5: Clamp diode forward recovery voltage

di/dt (A/µs)	V_{fr} (V)	E_{fr} (J)
2.74e3	226	0.163

2.8.2. Conduction loss

The worst case conduction loss of the diode is obtained by multiplying the forward voltage drop of the diode with the diode current. The forward voltage drop characteristics can be obtained from the data-sheet of the diode used.

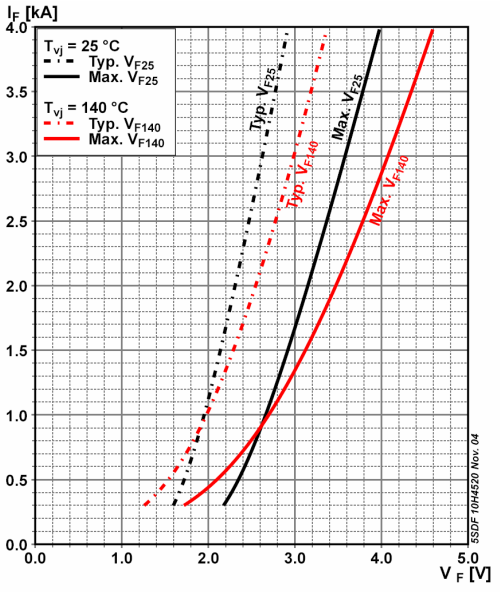


Figure 2-17: The forward voltage drop of the diode at various temperatures (9)

Since the forward voltage drop of the diode does not depend on the circuit parameters, the worst case forward voltage drop of the diode (@ 125 °C) can be empirically put as:

$V_{ON}(I) = 0.00088*I + 1.75$ …… Equation 2-5

2.9. Loss calculation of the devices in the H-Bridge

The modulation technique used in the H-Bridge is optimal PWM modulation (5), which uses a switching pattern that has been optimized to generate low current harmonics at the output of the voltage source converter (VSC). Since the STATCOM has to be in service both in the capacitive and inductive modes, a different modulation index for each makes this feasible. A case study showing calculation of the switching angles for a seven level converter has been done (5). A set of simultaneous equations, depicting the magnitudes of the 5^{th} 7^{th} 11^{th} and 13^{th} harmonic is drawn up and each of these equations is equated to zero and solved simultaneously. The set of equations is solved for different modulation index and various switching angles for different modulation index are obtained.. The region from zero degrees to $\pi/2$ is divided into six regions using five angles θ_1, θ_2, θ_3, θ_4 and θ_5. Figure 2-18 shows the switching patterns of the VSC.

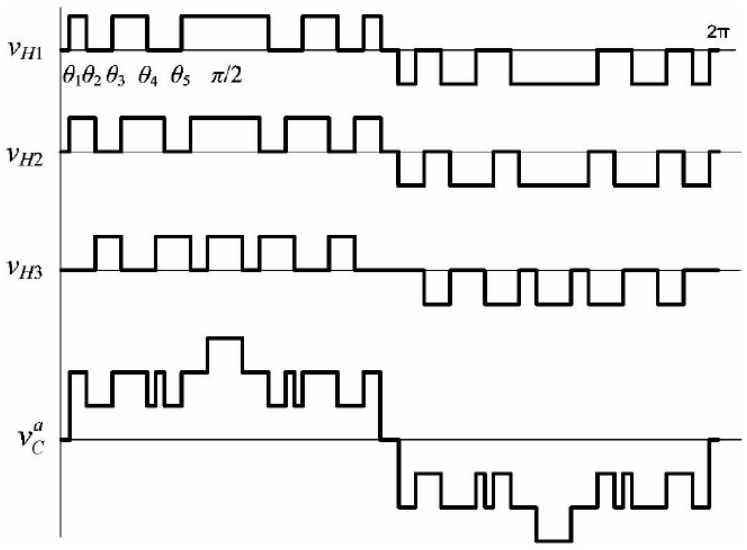


Figure 2-18: Switching angles of a phase leg of the H-Bridge

Based on the above switching angles, a simulation is carried out for a five level cascaded multi level converter system. The current and voltage waveforms of the switches and diodes used in the system are shown in Figure 2-19.

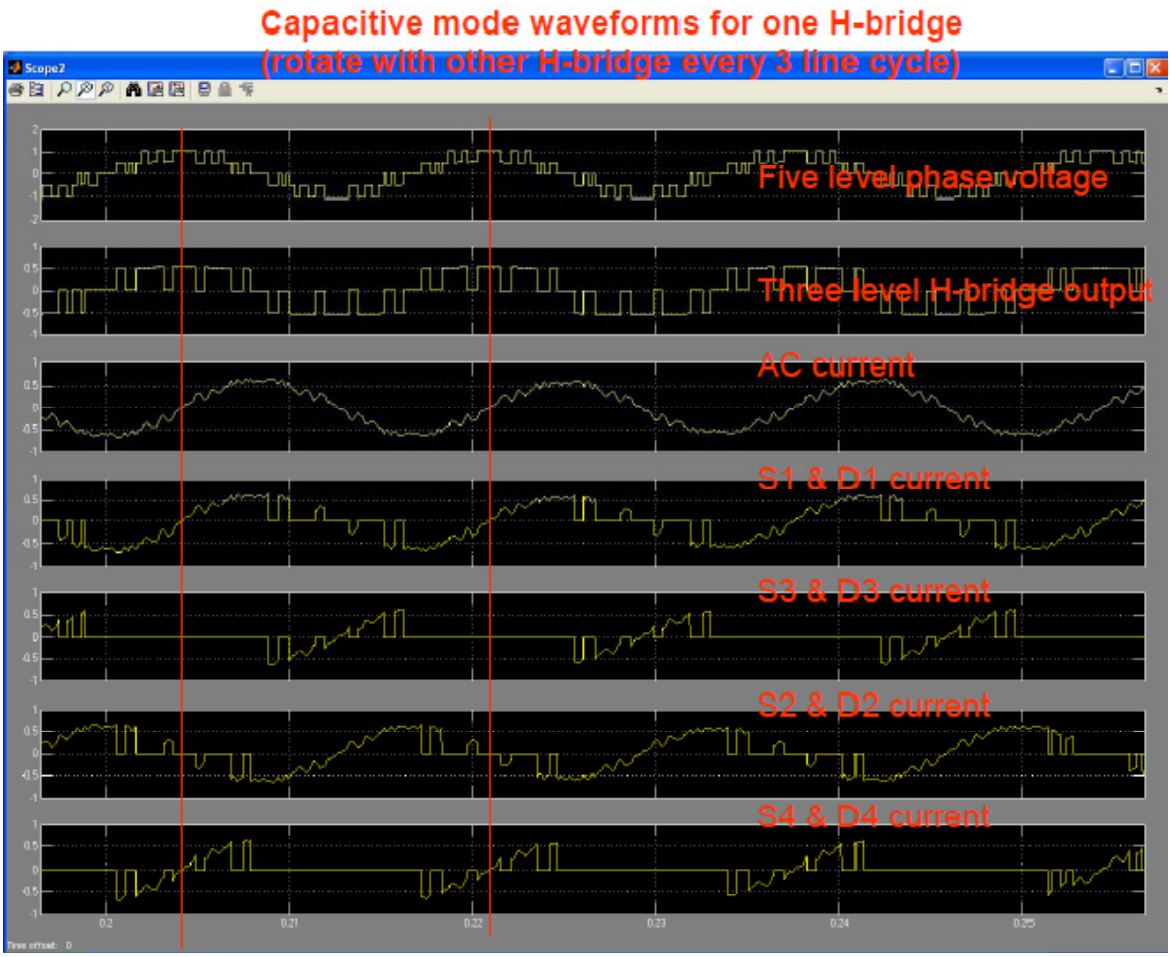


Figure 2-19: The waveforms of the switches and diodes in the H-Bridge

Because of the differences in the current conduction times occurring in the two H-Bridges making the five-level voltage, the losses in the two H-Bridges are different. Hence the switching pattern is rotated every three line cycles to equalize the losses. The currents going through the devices at turn-on and turn-off are recorded along with the conduction times through them. The switching losses can be calculated from the empirical turn-off loss equations of the ETO and the diodes experimentally derived at 125 °C. The conduction

losses can be calculated by integrating the product of the forward voltage of the device with the forward current, over the time for which the current flows through the device. The calculated device losses are tabulated in Table 2-6 for the capacitive mode and in Table 2-7 for the inductive mode of compensation of the STATCOM.

Table 2-6: Device losses in the capacitive mode

	$P_{switching}$ (W)	$P_{conduction}$ (W)	TOTAL (W)
S1	1099.5	1076	2175.5
S2	1099.5	1076	2175.5
S3	1099.5	1076	2175.5
S4	1099.5	1076	2175.5
D1	82.95	1049	1131.95
D2	82.95	1049	1131.95
D3	82.95	1049	1131.95
D4	82.95	1049	1131.95

Table 2-7: Device losses in the inductive mode

	$P_{switching}$ (W)	$P_{conduction}$ (W)	TOTAL (W)
S1	740.31	1062	1802.31
S2	740.31	1062	1802.31
S3	740.31	1062	1802.31
S4	740.31	1062	1802.31
D1	116.07	1024	1140.07
D2	116.07	1024	1140.07
D3	116.07	1024	1140.07
D4	116.07	1024	1140.07

As seen from the table above the total losses of the devices are more in the inductive mode although the output power in both the cases is 10 MVA. This occurs because in the capacitive mode the switches are hard switched thrice in every cycle, as compared to just twice in the inductive mode of operation. In the inductive mode of operation, the diode switching losses are more because the diode has a hard turn-off thrice during one cycle. The conduction losses in both modes of operation are nearly same because the conduction angles remain the same; the subtle differences have occurred because of small difference in the load currents for the two modes of operation.

2.10. Clamp component losses

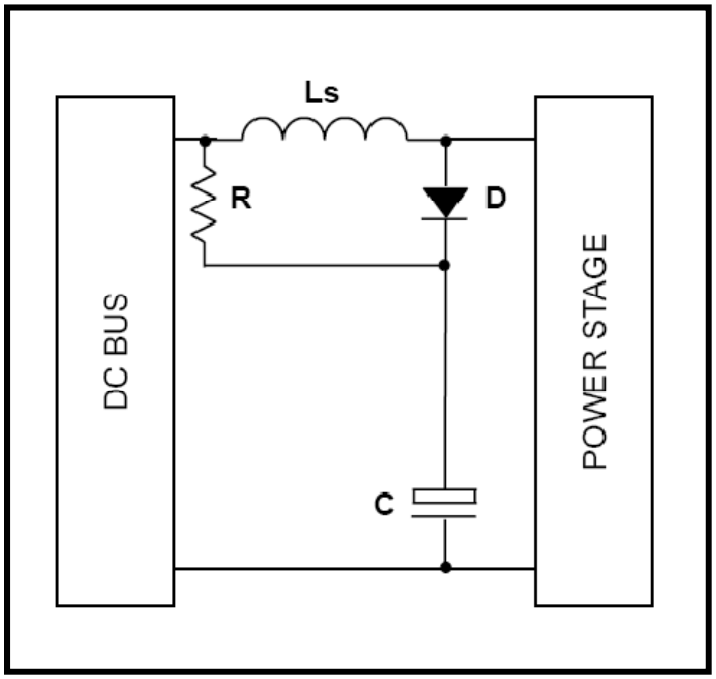


Figure 2-20: Clamp circuit components

The voltage clamp consists of the usual resistor, capacitor and diode. The inductor is used to limit the rate of change of current (di/dt) going through the device when the device is turned on. It also limits the rate of change of reverse recovery current going through diode. The two circuits can be combined together to get a hybrid snubber and voltage clamp circuit as shown in Figure 2-20. The diode and the resistor help reset the current in the inductor, before the

next switching cycle occurs. The major loss components in the above circuit are the diode, resistor and the inductor. The losses in the inductor arise from the presence of parasitic resistance in the inductor.

The minimum value of the snubber inductor can be chosen using,

$$L_{min} = \frac{V_{DC\,MAX}}{di/dt}$$ ..... Equation 2-6

Where,

L_{min} is the minimum required inductance

V_{DCMAX} is the maximum allowable DC bus, considering all overshoots possible on the devices ,

di/dt is the rate of change of current in the device.

Given the DC bus of 2200 V maximum and a maximum 500 A/µs; the minimum value of inductance is 4.4 µH. The resistor is sized at 1 Ohm to limit the Ohmic losses incurred in the resistor to a minimum. The L/R time constant will then be equal to 4.4 µs. A lower reset time is usually desired, but this would mean increasing the value of the resistance to decrease the L/R time constant. Increasing the value of R increases the Ohmic losses in the resistor. There is thus a trade-off between the losses and the inductor current reset time. For practical purposes and ease of availability an inductor value of 5 µH and a resistor value of 1 Ohm is considered for the design. The clamp capacitor is used to limit the voltage across the switching device when the device is turning off large current. There are voltage spikes on the device during the turn-off transient because of the parasitic inductance between the power stage and the clamp circuit. A well designed clamp is ineffective if this loop parasitic inductance is not minimized by proper mechanical design guidelines. This is discussed in detail in chapter four. To minimize stray inductances, the clamp capacitors are packaged to have minimal lead stray inductances. They are small in size to fit alongside semiconductor devices in a stack and they do not have any long protruding connection leads; instead they

have buried threaded contacts which can be used with the help of bolts. For this application the clamp capacitor value is chosen to be 13.2 µF. This is realized by connecting two 6.6 µF capacitors in parallel. Special consideration has to be taken to equalize stray inductance in the path of these capacitors. Details of mechanical design of the bus-bars to minimize strays are in chapter five.

In the STATCOM H-Bridges, the di/dt inductor is chosen to be 5 µH. The clamp resistor is chosen to be 1 Ohm and the capacitor 13.2 µF. A fast recovery diode ABB 4500 V diode is chosen as the clamp diode. With the above clamp and snubber parameters, the maximum di/dt seen by the devices during turn-on are limited to 220 A/µs; which leaves enough margin for ETO shoot-through protection. The peak current in the inductor is same as the peak reverse recovery current of the diode which is commutating current to the switch. The energy stored in the inductor could be calculated as:

$E = \frac{1}{2} L I_{RR}{}^2$ …….. Equation 2-7

At the ETO turn-off event, the energy stored in the inductor is discharged and clamped by means of the RCD clamp circuit. The discharged energy is equal to:

$E = \frac{1}{2} L I_{LOAD}{}^2$ ……..……. Equation 2-8

Not all the magnetizing energy is discharged through the RCD circuit. Some of it is dissipated in the semiconductors and a certain amount is restored back to the input source. It can be estimated that more than 90 % of the energy is dissipated in the clamp resistor.

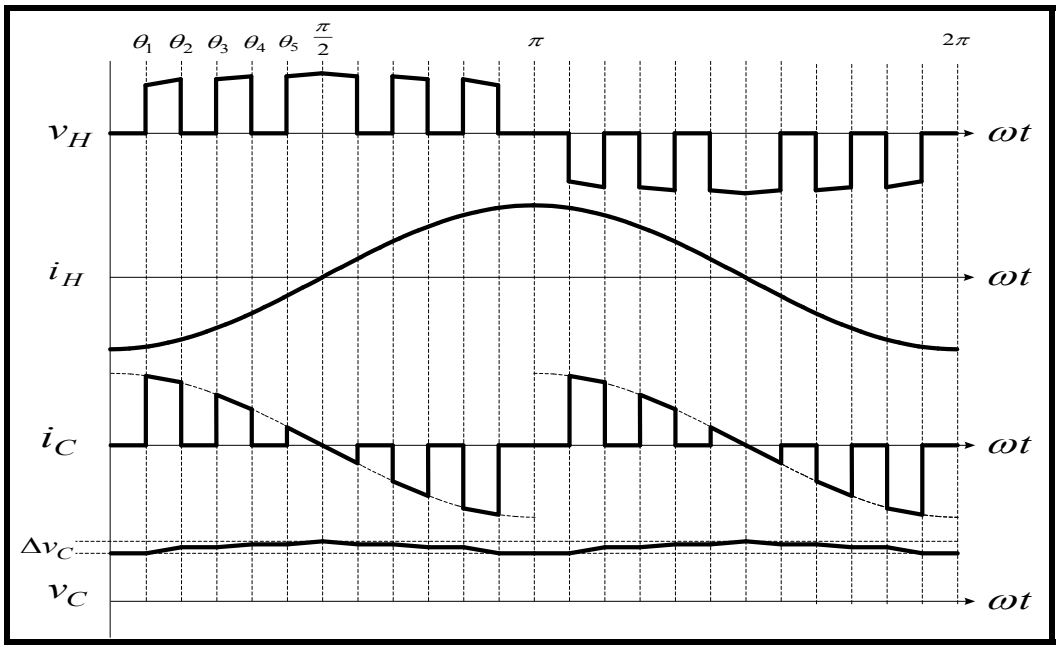


Figure 2-21: Voltage and current waveforms in clamp circuit components

In the Figure 2-21, the V_H and i_H denote output voltage and current of a selected H-Bridge, the i_C and v_C are the capacitor current and voltage respectively. The Δv_C denotes the voltage ripple seen by the capacitor. The losses in the RCD components are tabulated below:

Table 2-8: Losses in the clamp circuit

<table>
<tr><td rowspan="4">Clamp Circuit Loss</td><td rowspan="4">5.32 kW
(resistor loss + diode loss)</td><td>Resistor Loss</td><td colspan="2">4.85 kW</td></tr>
<tr><td rowspan="3">Diode Total Loss :
472W</td><td>Diode Forward recovery</td><td>196 W</td></tr>
<tr><td>Diode conduction</td><td>61W</td></tr>
<tr><td>Reverse recovery</td><td>216 W</td></tr>
<tr><td>DC Capacitor (ESR Loss)</td><td colspan="4">382 W</td></tr>
<tr><td>Di/dt Inductor</td><td colspan="2">Copper Loss
(Resistance = 1.7 mΩ)</td><td colspan="2">663.63 W (CAP)
486.58 W (IND)</td></tr>
<tr><td>Maximum Clamp Capacitor Voltage @4000A</td><td colspan="4">3900 + 200 (ripple) = 4100 V</td></tr>
<tr><td>Reset time @ 2000A</td><td colspan="4">16 μs</td></tr>
</table>

The losses of the inductor are significant at 663.63 W for the capacitive mode and 486.58 W for the inductive mode of operation of the STATCOM. The purchased inductor is however, rated to operate at 3000 A RMS, as compared to the 1435 A RMS current in both modes of the STATCOM; thus it must be built with high temperature materials to sustain the thermal load. The capacitor losses are minimal and can be easily dissipated using forced air cooling.

Since the losses on the clamp resistor are excessive, there has to be some form of dedicated cooling system for the resistors. Since water/ liquid cooled system cannot be used, the resistors have to be spread over a large area for air-cooling to be feasible. Discussion on the cooling of the clamp resistor is undertaken in chapters three and five.

The diode is single sided cooled with a 1.2 kW heat-pipe, as shown in chapter four. The losses on the diode are less than 500 W; however, this number will be slightly more when the STATCOM is operated in the inductive mode. This happens because the anti-parallel diode in the power stage undergoes three turn-offs in the inductive mode as compared to two turn-offs in the capacitive mode of operation. Since the heat-pipe is already rated at more than twice the thermal load presented in the capacitive mode, there has to be no change in the rating of the selected heat-pipe. The design could be modified to cool the diode in double-sided configuration for better thermal performance and lower junction temperature.

2.11. Conclusion

The losses of the major components of the H-Bridge have been calculated for both capacitive and inductive modes of operation. Using these loss parameters the thermal management components have to be selected. The selection of the thermal management options is briefly discussed in chapter three. Further, an electrical equivalent model will be derived using these loss parameters and the temperatures of the devices can be estimated using the model. This will allow verification of the selected thermal management components and a starting point for optimizing the overall design.

3. THERMAL MANAGEMENT OPTIONS

3.1. Rationale

Energy conversion always results in emission of thermal energy as a by-product of the process. This energy is usually non usable and needs to be dissipated from the system quickly. If the energy is allowed to accumulate the components used to build the system undergo thermal stress and may be damaged. The thermal stresses sustained by the components also reduce the reliability of the system. It is thus a good practice to include thermal design considerations while working on power/energy conversion systems. There are four fundamental methods of dissipation or transporting heat away from a system to the ambient. All of the four options should be briefly explored before deciding on a single option for a particular system.

3.2. Organization of the chapter

The basic heat transfer mechanisms will be explored. The most effective heat transfer mechanism will be further discussed and systematically explained. Details on the heat transfer mechanism such as the actual process of transfer of thermal energy through the system will be highlighted. Since the heat-transfer that is selected for the voltage source converter is non-conventional and not widely used at high-power conversion systems, its pros and cons will be discussed in depth. The selected heat-transfer mechanism will be compared with the existing conventional mechanisms used today at high-power levels. The problems encountered while adapting the process for the current requirements and their possible solutions are also listed. The chapter is concluded with experimental results obtained using a heat-pipe prototype.

3.3. Basic mechanisms of heat transfer

There are four ways of transmitting the heat generated in a system. they can be listed as:

a. Conduction

b. Convection

c. Radiation, and

d. Phase change

3.3.1. Conduction

It is a heat-transfer mechanism where the actual transportation of thermal energy occurs by the virtue of vibration of molecules in the system. E.g. heat spreading in a heat-sink or a metal object. The efficiency of this process largely depends on the surface area of the heat-dissipating body exposed to the ambient environment. Various ways of increasing the surface area of the heat dissipating body are used to increase the efficiency of conduction. Heat-spreaders are sometimes used on heat-sinks with large base plate to quickly transport heat to the entire effective area available for dissipation of thermal energy. The non-uniformity of heat-energy through the surface of the heat-sink may arise because of a number of reasons. It could be because of improper placement of components or because different components are dissipating different amounts of heat-energy.

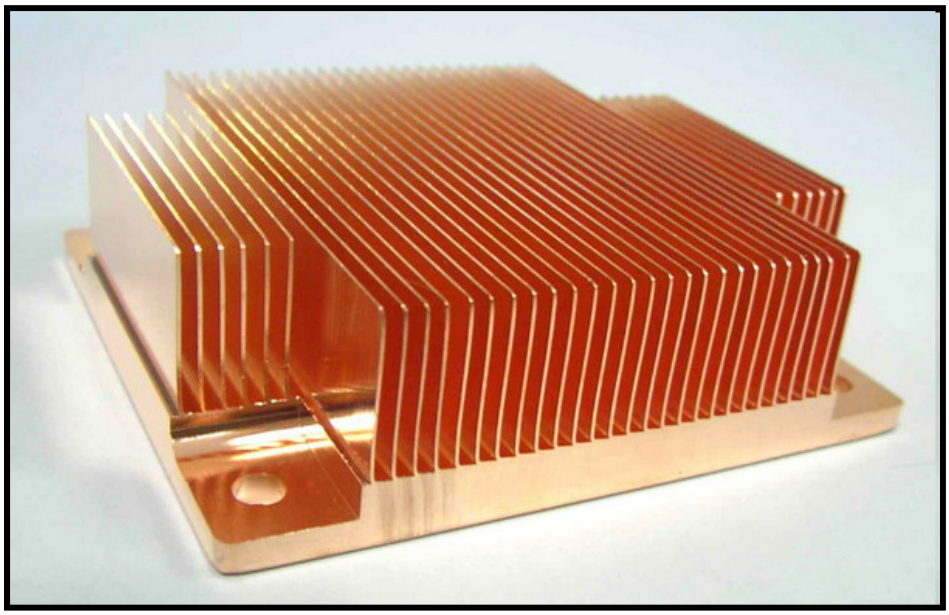


Figure 3-1: A high-performance copper, extruded-fin type heat-sink.

Since conduction aids only in the transportation of thermal energy from one point to the other, it cannot be the only medium used for dissipating heat to the ambient. Convection is one of the mechanisms that is used along with conduction to transport heat energy form the source to the ambient. The heat-sinks are usually made using a base plate and fins, as shown in Figure 3-1. Air flowing through these fins aids in transportation of heat from the fin surface to the ambient.

3.3.2. Convection

Convection is the heat transfer mechanism where the flow of heat-energy occurs by the virtue of transportation by the molecules of the medium itself. E.g. The movement of water molecules when it is heated in a beaker, the movement of hot and cold air in a closed room. The movement of the medium is called as convection current.

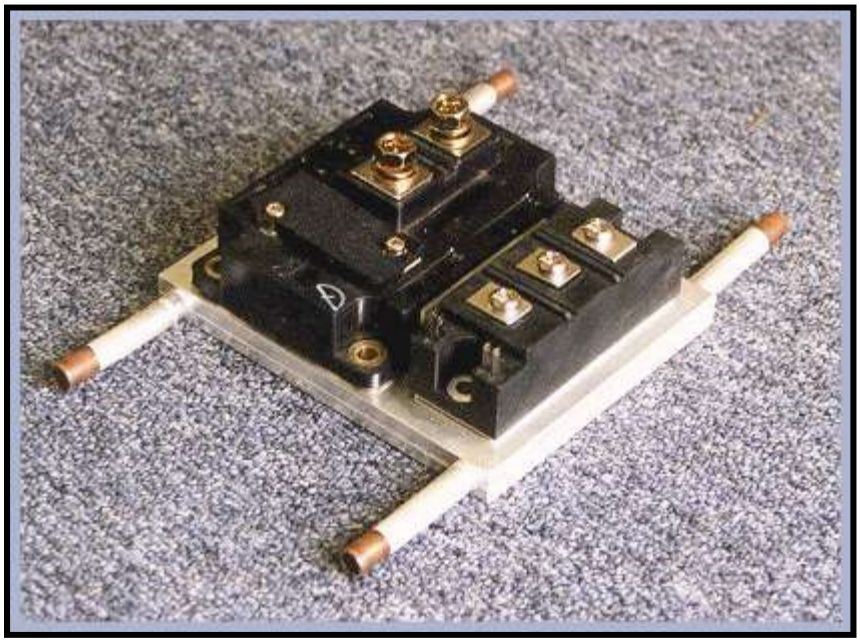


Figure 3-2: Semiconductor devices mounted on a cold-plate

Water is usually used as a fluid for heat transfer applications in high-power applications as shown in Figure 3-2. An IGBT device is mounted on the cold-plate. A cold-plate is basically used as a medium to circulate the heat carrying fluid. The circulation of fluid absorbs thermal

energy from the surface of the cold-plate and transports it to a heat-exchanger to dissipate the absorbed heat. A heat-exchanger could be a radiator with fans or a water circulator which passes hot water through pipes submerged in cold water. Convection cooling also occurs when cold air flows through hot fins of a heat-sink. The cold ambient air absorbs thermal energy form the surface of the fins and dissipates the energy in the surroundings, while passing through the fins.

3.3.3. Radiation

Radiation is the only method of heat-transfer wherein no medium is required. Thermal energy is transported by the virtue of electromagnetic waves going from one point to the other in space. Radiation does not play a significant role when heat transfer is occurring at very high power levels. It helps in the transportation of a very small fraction of heat-energy.

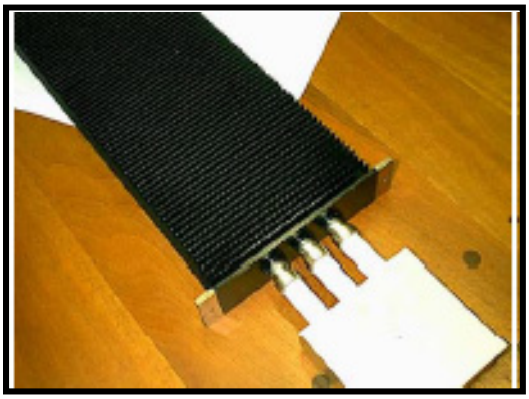


Figure 3-3: Black colored fins of the heat-pipe

A very significant theory of radiation is called as the 'black body absorption'. A black body is defined as a body/mass with perfect absorption/radiation characteristics. Coloring the fins of a heat-pipe with black paint allows transportation of heat from the surface of the fins by radiation. Although the amount of heat transported in the above example is not as large as compared to convection, it aids the process of heat-transfer. It does the process devoid of any medium between the heat-source and the ambient surroundings.

Amongst all the processes mentioned above, conduction and radiation are not capable of handling large thermal loads as seen in high-power converters. Convection aided cooling, such as water cooling does provide the necessary capacity required for dissipating large amounts of heat-energy, even to the tune of several hundred kilowatts.

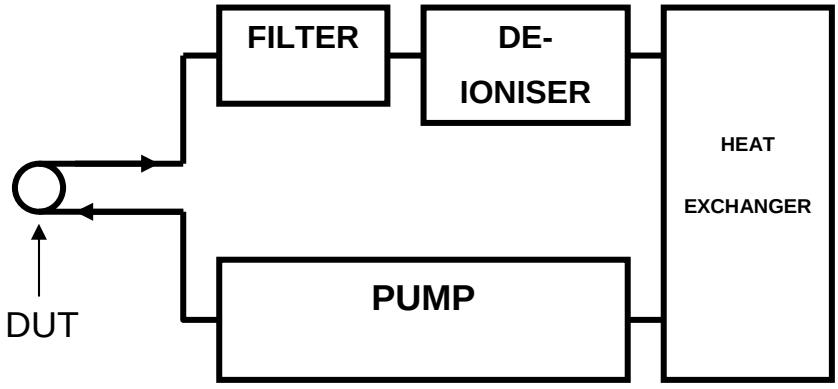


Figure 3-4: Water cooling system for semiconductor devices

A water cooling system is shown in Figure 3-4. The system includes a DUT (device under test), a pump to drive the water through the system, a filter to collect all the sediments and a de-ionizer to maintain the isolation property of de-ionized water. The heat-energy is carried from the DUT to the ambient by the water. It is dissipated to the ambient when the hot water flows through the heat-exchanger/ radiator. The entire system is very intricate and as the thermal load increases the size and complexity of the system increases exponentially. The de-ionizer is an essential part of the water cooling system as it maintains close to zero conductivity of the circulating water. If the water becomes ionized, then it will form free electrons which will help conduct electricity and increase conductivity of water. Since the water circulators directed touch the terminals of the device, allowing ionized water to flow through the system will trip the system. Water-cooled systems have to be custom designed every time a high-power converter is installed. If the power capacity of the converter is increased the cooling system has to be re-designed again if enough design margin is not considered during the first installation. Because of the complex and inflexible nature of

water-cooled systems, it is necessary that further study is conducted into alternative methods of heat transfer and dissipation.

3.3.4. Phase change

Phase change is the phenomenon of transfer of heat-energy wherein the medium undergoes a phase change to aid in transportation of heat energy. E.g. heat energy is absorbed to convert water to steam and the steam can then be transported to a desired location and condensed to dissipate heat to the ambient. The principle of operation of heat-pipes is based on the theory of phase change.

3.4. Heat-Pipes for the ETO Converter

In the Figure 3-5, the principle of operation of a heat-pipe is explained. The red arrows indicate heat-energy being applied to the evaporator plate of the heat-pipe. The liquid inside the heat-pipe condenses and moves towards the condenser due to a vapor pressure gradient created inside the heat-pipe. As the liquid reaches the condenser it cools down and changes back to its liquid state, dissipating all the heat-energy it carried in the vapor phase to the ambient. The cycle repeats itself and after reaching a stable point the heat-transfer rate becomes constant.

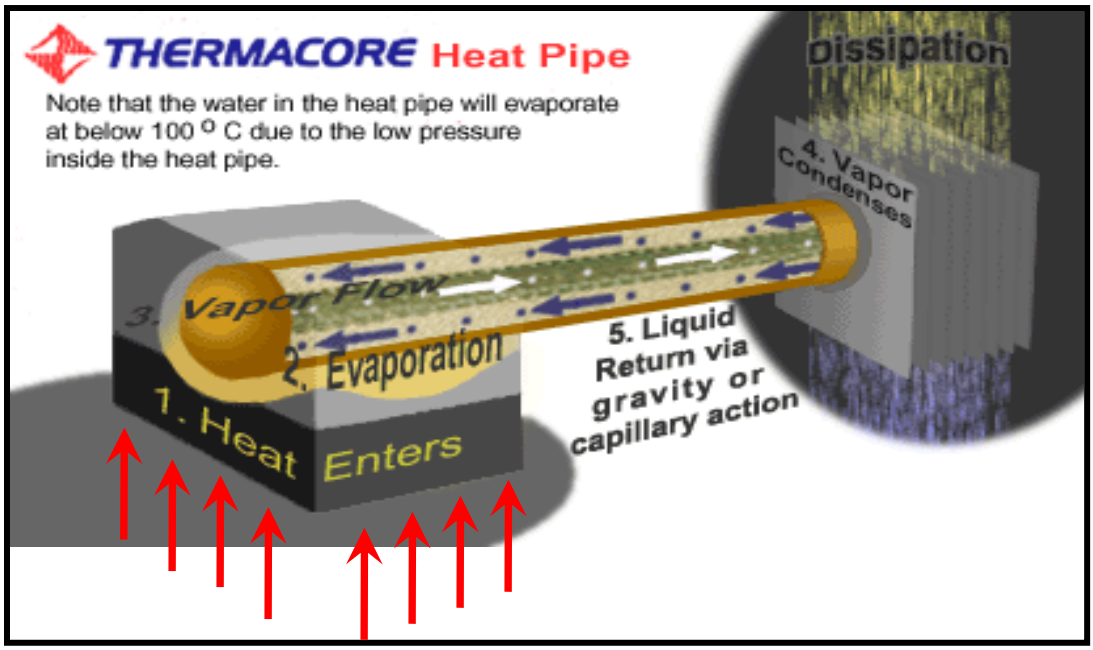


Figure 3-5: Principle of heat-pipe. (Courtesy: Thermacore Inc.)

3.4.1. 2.2kW Heat-pipe for ETO device thermal management

The 2.2 kW electrically isolated heat-pipe shown in the figure above is used for the double sided cooling of the ETO device. The combined capacity of two heat-pipes is about 4 kW, from experimental results.

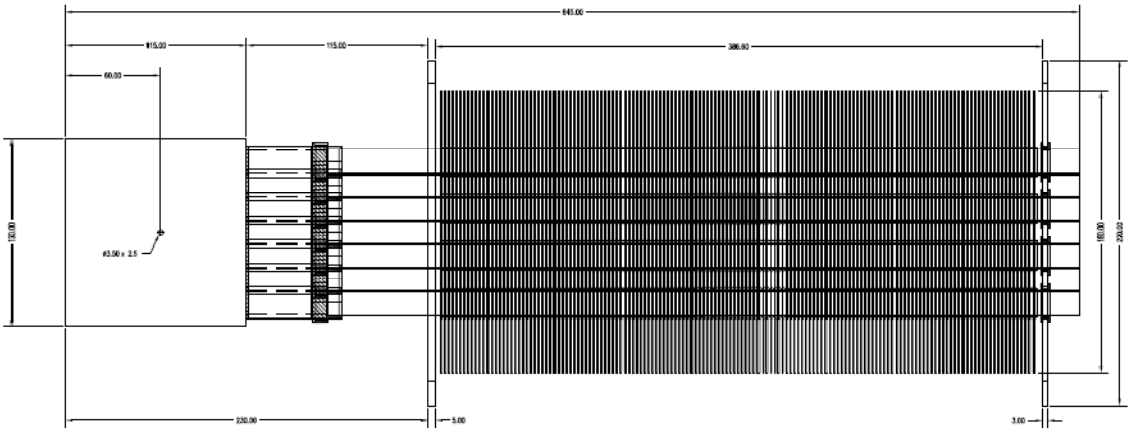


Figure 3-6: 2.2 kW isolated heat-pipe for ETO thermal management

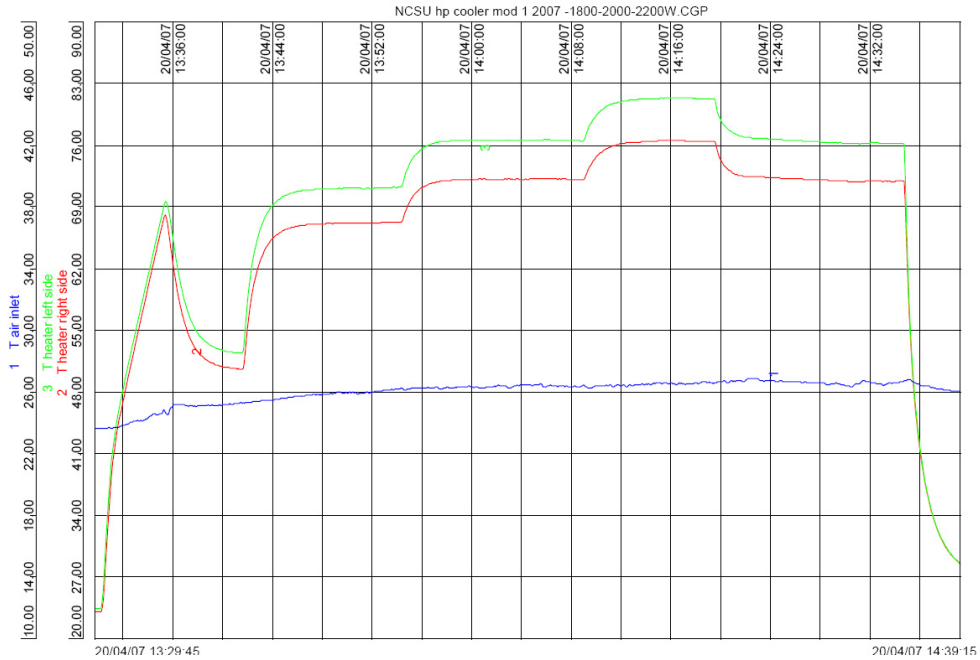


Figure 3-7: Thermal loading (1.8k-2k-2.2k) characteristics of the 2.2 kW heat-pipe

3.4.2. 1.2 kW heat-pipe for clamp diode

The 1.2 kW heat-pipe is used for single sided cooling of the clamp diode in the RCD clamp circuit. The thermal loading characteristics of the heat-pipe are presented below in figure 3.9.

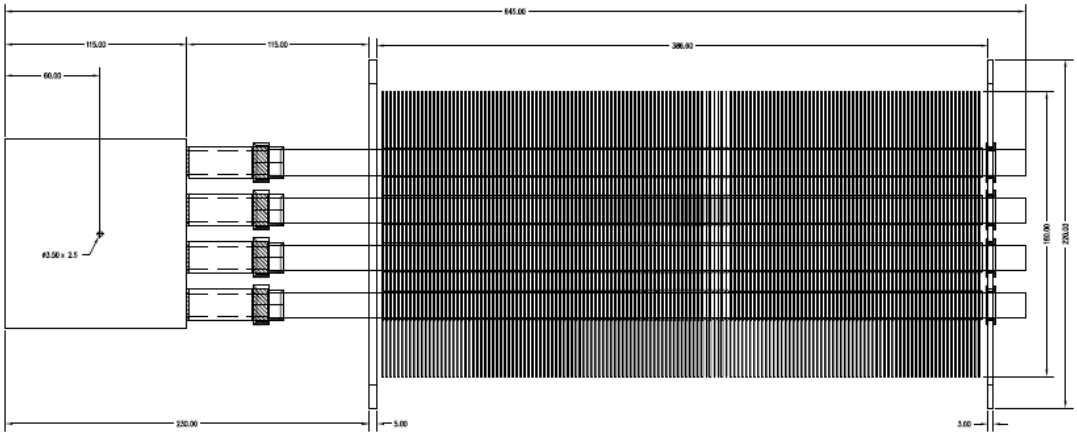


Figure 3-8: 1.2 kW isolated heat-pipe for clamp diode's thermal management

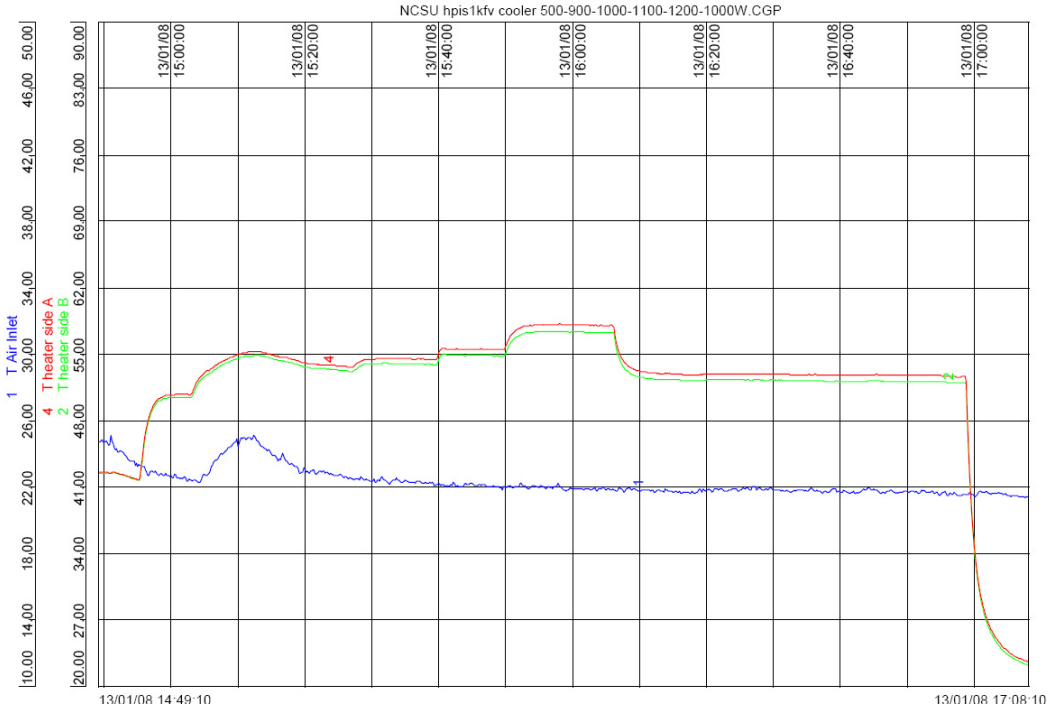


Figure 3-9: Thermal loading (0.8k-1k-1.2k) characteristics of the 1.2 kW heat-pipe

Comparison of the discussed heat-transfer mechanisms has to be done specifically for the voltage source converter application. For any given heat-transfer system, the thermal resistance of the system is a good measure of its performance. The application, for which the heat-transfer mechanism is to be designed, is a high voltage application. Voltage isolation between the evaporator plate and the heat-sink/ radiator-fins becomes an important design parameter. Thus the two factors that have to be investigated before a selection is made are:

a. Thermal resistance obtained for a given surface area of the evaporator plate.

b. Electrical isolation between the evaporator plate and the heat-dissipating mechanism.

The following sections of the chapter would discuss the above mentioned points in detail before drawing up a conclusion.

3.5. Thermal Resistance

Thermal resistance is the temperature difference across a structure when unit heat energy flows through it in unit time (10). There is an electrical analogy of the concept of thermal resistance, which is why it is referred to as a 'resistance'. The temperature difference is analogical to the potential difference in an electrical circuit. The flow of thermal energy is similar to the flow of electric current. The Ohm's law in electrical engineering relates the voltage across a component and the current flowing through it by their ratio given as:

$$R = \frac{V}{I} \quad \text{Equation 3-1}$$

Where, R is defined as the resistance of the component

V is defined as the voltage across the component

I is defined as the current through the component.

Similarly, the thermal resistance which is denoted by R-theta is defined as the ratio of the temperature difference across a component by the thermal load on it. The equation representation of this statement is as follows:

$$R_\theta = \frac{\Delta T}{W} \quad \text{Equation 3-2}$$

Where, R_θ is defined as the thermal resistance of the component under question

ΔT is the temperature difference between the measured points

W is the thermal load on the component.

Lower the thermal resistance, better the heat dissipating quality of a heat-sink/cold-plate/heat-pipe. However, a given heat-sink can have the lowest possible thermal resistance, if there are no constraints on the dimensions and weight. The true measure of performance of any heat-dissipating agent can be compared only when there is a comparison of its weight and volume with other available options.

3.5.1. Heat-sink

For the sake of simplicity, the thermal resistance will be kept the same for all three types of heat-transfer mechanisms; heat-sinks, cold-plates and heat-pipes. It will be around 20K/kW. No detailed theoretical analysis will be conducted to make this comparison; only available off-the-shelf products will be selected for comparison.

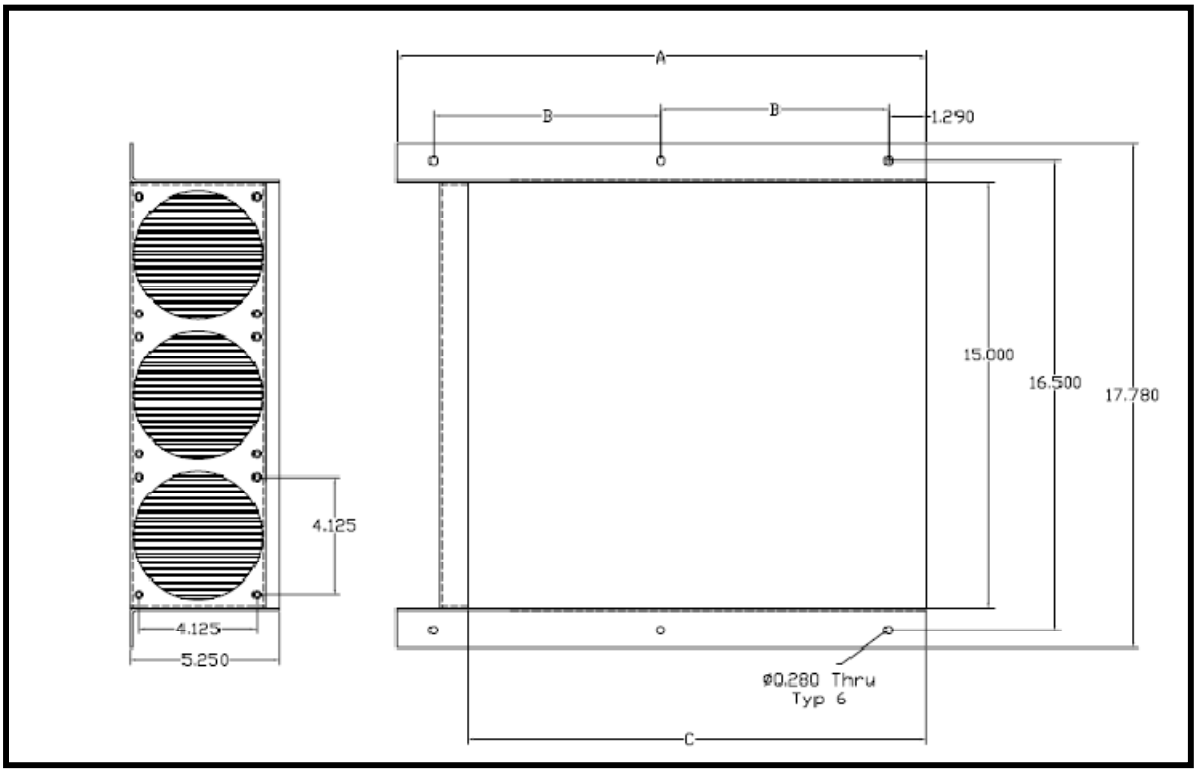


Figure 3-10: Aluminium bonded-fin heat sink, A = 18.59", B = 8.0", C = 16.0"

(Courtesy: Vette Corp.)

Heat-sinks are available in various types, shapes and sizes. For this analysis an aluminium bonded-fin heat-sink will be selected. The thermal resistance of this particular heat-sink is 17K/kW when the air-flow through the fins is 100 cubic feet per minute (CFM). The heat-sink assembly employs a bracket for three axial fans to be put on one side of the heat-sink. Consider the area of the evaporator plate of the heat-sink, its 278.85 sq. inches. The voltage source converter employs 70 mm hockey-puck devices as the main current carrying devices.

These devices are also the main heat-generating devices; hence require more attention in terms of cooling arrangements. If we calculate the surface area of a 70mm diameter device it is 5.965 sq. inches. This number should be taken as reference while comparing the surface areas of the three heat-transfer mechanisms under question. Here we can clearly see that the surface area of the heat-sink is 46 times larger than the area of the device. Since the device would need two sided cooling; putting two large heat-sinks to obtain the specified thermal resistance would be impractical. Also the two surfaces of the device have to be under a force of 40kN for correct and safe current turn-off capability. Assembly such large area heat-sinks under such force would cause buckling of the structure because they are made of a soft metal like aluminium. The ABB glass-epoxy clamp would have to be specially modified to accommodate large heat-sink. The fact that the heat-sinks are in direct contact with the devices severely limits the possibility of isolation of the device anode and cathode voltages. Since the heat-sinks would have to be sandwiched between the devices the air flow would not be optimal because the bus-bar network would always block the flow of air and require usage of ducts and high-power air movers to get required thermal performance.

3.5.2. Cold-plates

Cold-plates have been traditionally used in the thermal management of high-power converters; therefore they have good thermal performance characteristics. Their thermal resistance is very low, in the range of 3K/kW to 20K/kW, depending on the gallons per minute (GPM) of the thermal fluid (usually de-ionized water) flowing through the system. The 3-D rendered image of a de-ionized water circulator is shown in figure 4.11. There is an inlet and an outlet for water. Cold water flows into the inlet and hot water is taken out of the outlet and sent to the heat-exchanger. The overall area of the water circulator is 19.32 sq. inches. This is about three times bigger than the actual contact area of the semiconductor device making this proposition more efficient in terms of thermal resistance per sq. inch as compared to the heat-sink.

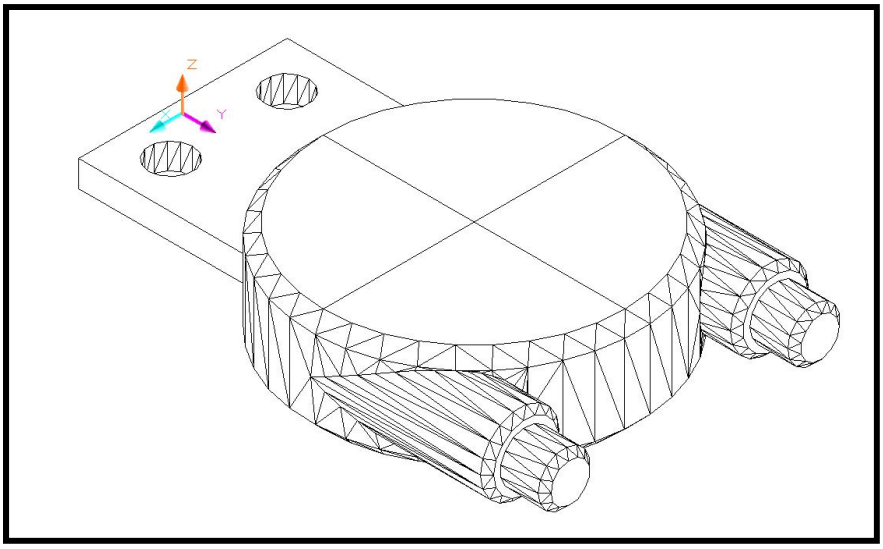


Figure 3-11: 3-D rendered image of a de-ionized water circulator for hockey-puck devices

Although, the usage of the water circulator with a heat-exchanger system may seem to be the best thermal management alternative for the voltage source converter applications, we have to still look into the electrical isolation that this system can offer. Since this system uses a thermal fluid to transport heat from the devices to the ambient (via the heat-exchanger) the electrical isolation between the device and the heat-exchanger (usually made of metal) is a function of the electrical conductivity of the thermal fluid. Water is the best fluid in terms of thermal energy carrying capacity, but it is also a good conductor of electricity and highly corrosive to metals when used in its impure form as obtained from various bodies. Due to the mentioned problems with regard to water being used as a thermal fluid, other alternatives are used as thermal fluids. However, no fluid can provide a wide operation temperature or thermal energy carrying capacity as water. Water is thus distilled and de-ionized to rid it of all corrosive metallic salts and other harmful impurities. The de-ionization process also reduces the conductivity of water to acceptable values for use in a high-power converter. But this forces the system to include a highly sophisticated filtration and de-ionization system to maintain the chemical inertness and low conductivity of the circulating water. The inclusion of such blocks in the cooling system would also imply inclusion of an intricate control system to monitor the status of the circulating water through the system. Overall, the system

becomes very complicated, requiring constant maintenance and supervision. The system is custom made and has to be redesigned for different systems. The design parameters include the selection of fluid for the system, selection of the pump for circulating the fluid and heat-exchanger. If the power converter is upgraded for more power output, the thermal load also increases proportionately. The previously installed system then has to be completely redesigned to accommodate the additional load, if sufficient design margin was not included during the first design iteration. In short, the fluid based cooling system is not modular. This is one of the main disadvantages of using system in today's age of cascaded multi-level converters.

3.5.3. Heat-pipe

A heat-pipe uses phase change mechanism of a thermal performance fluid (again, usually de-ionized water) for transporting heat from the evaporator plate to the ambient. In terms of thermal performance the custom designed heat-pipes shown in Figure 3-6 and Figure 3-8 are well suited for the voltage source converter. Each of them has a thermal resistance of 17 K/kW. The surface area of the evaporator plate is 21.39 sq. inches, which is 3.6 times the surface area of the actual contact area of the hockey-puck devices. It matches the water cooling system in terms of thermal resistance per unit area. In terms of electrical isolation, there are ceramic tubes connecting the evaporator plate to the heat-pipes providing up to 10kV of isolation between them. The inclusion of ceramic tubes in between the evaporator plate and the heat-pipes may seem to degrade the thermal performance of the system; however, it does not because the section of tubes closer to the evaporator plate is used to transport the fluid to the section of the heat-pipe which has fins (radiator section). It is in the fin-section of the heat-pipes where actual heat-transfer occurs between the heat-pipe and ambient. The ceramic section of the heat-pipes is shown in Figure 3-12.

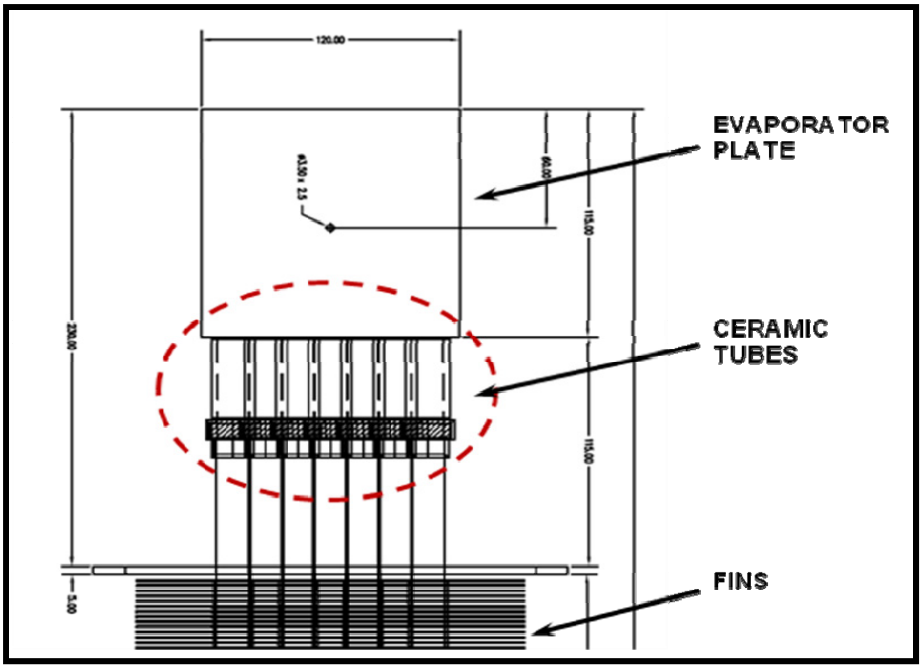


Figure 3-12: Ceramic tubes in the heat-pipes for electrical isolation

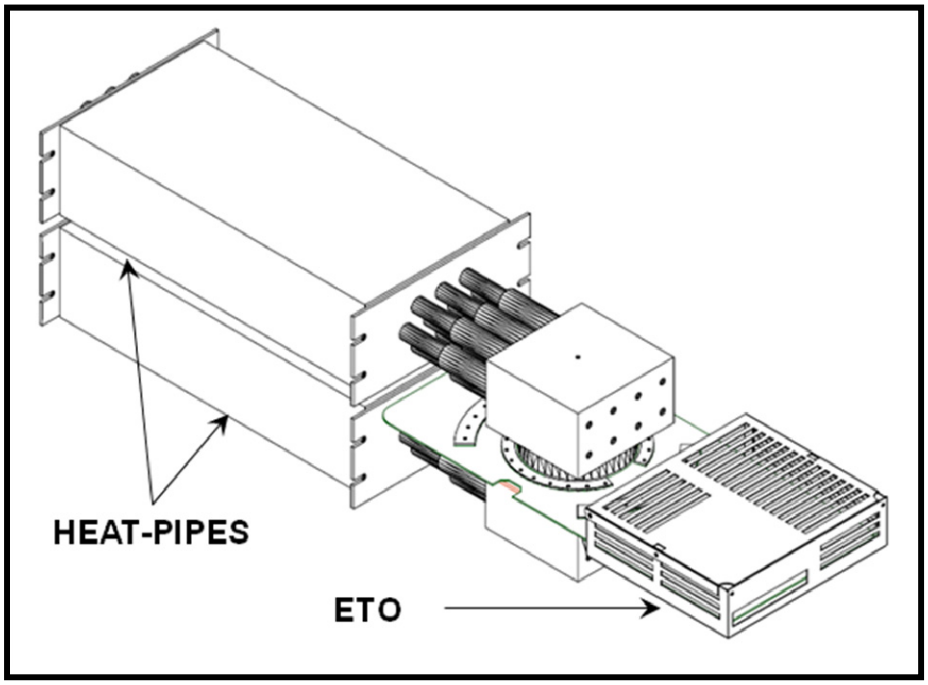


Figure 3-13: Arrangement of heat-pipes with the Emitter Turn-Off Thyristor

The Figure 3-13 shows the arrangement of the ETO device with the heat-pipes. The arrangement is similar to the arrangement of water circulators. In general the hockey-puck devices are double-side cooled to obtain better heat removal performance.

Since the thermal fluid is vacuum sealed inside the heat-pipe, its flow velocity is not as high as the fluid flowing in a water cooled system. Although this limits the performance of the heat-pipes marginally, it provides a greater advantage over the water cooled system. The rate at which corrosion or calcification of the metal in the tubes would occur is slowed down to a great extent as compared to a water circulating system. The heat-pipes do require maintenance, but only once in 12-15 years, as quoted by the leading vendors of the product. The heat-pipes are a self-contained heat-transfer mechanism and depending on the cooling requirement and the size constraints can be either cooled by natural air convection or by forced air cooling. In the application under discussion, the forced air convection option is selected and the air-flow requirement is specified to be about 350-400 CFM. The air-mover can be installed on the same cabinet as the rest of the voltage source converter.

The rating of power converters is usually increased by increasing the voltage of the overall system. This is done by simply adding a level of voltage source converters to the system, thus increasing the out-put voltage. Since there is not additional requirement on the heat-pipes to meet cooling requirement; a simple connection between the previous power converter system and the new voltage source converter stages will achieve the goal. Thus the power converter now becomes modular, which is a very great advantage when using cascaded multi level converters. It is also essentially a passive cooling system, requiring no power input like the water cooled system (pump, heat-exchanger). The overall system is an order in magnitude smaller as compared to the water cooled system when all the necessary accessories are included (pump, heat-exchanger and water reservoir).

3.6. Comparison and Conclusion

The table 3.1 summarizes the discussion on the selection of cooling components for the hockey-puck packaged devices. It can be clearly seen that there are a lot of advantages of using a heat-pipe based thermal management system for the voltage source converter.

Table 3-1: Comparison between various thermal management options for the VSC

Thermal resistance 17K/kW	Area	R_θ / Area	Disadvantages
Heat-sink	278.85	16.40	No electrical isolation
Cold-plate	19.32	1.136	Heavy maintenance required to sustain electrical isolation
Heat-pipe	21.39	1.258	-NA-

The fluid circulation based cooling matches and could even exceed the thermal performance characteristics of heat-pipe based solutions. It can be seen in Table 3-1 that the thermal resistance per unit area of the fluid based cooling system is higher than the heat-pipe based system. The difference is however marginal, about 0.122 K/kW/sq. inch. But the maintenance-free high-voltage isolation characteristics offered by the heat-pipe based system clearly wins over the thermal performance of the fluid based cooling systems.

4. MECHANICAL DESIGN

4.1. Rationale

Mechanical design and integration of all the components of the power stage has significant impact on the performance and reliability of the system. Usually the word 'mechanical design' brings up thoughts of frame-work, supports, cabinets and fork-lifts required to set up electrical equipment on-site. However, it is a key factor in determining the final 'real-world' performance of the electrical equipment. Depending on the details, time and effort put into the mechanical design, the equipment may work as expected, or perform non-satisfactorily, or sometimes under unfavorable circumstances fail completely.

Design considerations that should be taken into account while designing power electronics equipment are:

a. Minimization of parasitic inductances
b. Providing rigid support for floating components
c. Proper distribution of overall weight.
d. Minimizing volume of overall system

The above criteria are listed in terms of order of importance.

4.2. Organization of the chapter

The discussion on mechanical design will not be just limited to mechanical forces, stress and strain. It will include discussions on key electrical parameters such as stray inductances, contact resistances and various methods to eliminate or reduce them. Using finite element analysis tools the stray inductance of a loop was calculated. Results obtained from the software are compared with hand-analysis numbers. The chapter is concluded with the design process of the bus-bars and the support system for the power components.

4.3. Judging design parameters

When looking into mechanical design considerations for electrical engineering applications such as designing electrical machines or high-power converters, one has to be judgmental

about the parameters selected for design consideration. The field of mechanical engineering is too vast to cover all aspects affecting the electrical parameters of the system. However, the parameters having the most effect should be selected out and analyzed in depth. This exercise helps in improving the performance of the electrical system by as much as an order under special conditions.

The power-stage consists of large area semiconductor devices in hockey-puck package, heavy gauge wires, wide bus-bars, heavy passive components and large heat-pipes. The semiconductor devices are clamped together with the heat-pipes using a force of 40 kN. The 200-250 lbs. capacitors and the 500 lbs. power stage have to be supported on a stable frame. The frame has to be rigid enough to support this weight and flexible enough to endure transportation with the heavy passives in it. Components have to be placed in an orderly manner to avoid unnecessary stress on the weld joints of the frame as this may cause the structure to buckle. Usually selecting a heavy gauge steel beam will solve this problem, but this design would come with substantial weight which is not favorable for good design. Proper placements of components along with some basic design rules could be used to avoid such design issues and come up with a much lighter product.

Parasitic inductances could be one of the most primary reasons for a power electronic system to under-perform or fail completely; hence serious thought must be put into design of the bus-bars. Reducing the length of copper buses, overlapping the bus-bars where possible and proper placement of components can reduce parasitics in the system significantly.

Contact resistances arising from the joints of the bus-bars lead to Ohmic losses. The losses add up and eventually affect the overall efficiency of the power converter. Proper implementation of design rules and guidelines help reduce these contact resistances, improving system performance. The Ohmic loss in the conductors leads to heating of the bus-bars. The thermal cycling loosens the joints of the bus-bars further increasing the contact resistance. This leads to a degenerating cycle which eventually causes the system to trip.

Controlling the contact resistance thus becomes conducive for long term operation of the power converter.

Weight distribution and minimizing volume are parameters that need to be considered for the final product to be easily portable, compact and manufacturable. They should, however, be strictly secondary as compared to the parameters discussed earlier. There is no benefit of designing a system that is light and portable, but doesn't function.

4.3.1. Parasitic or stray inductance

The stray inductances could be broadly categorized as the ones arising from a loop formation between components and the bus-bars, and the other arising from the actual length of copper bus-bar used to connect components.

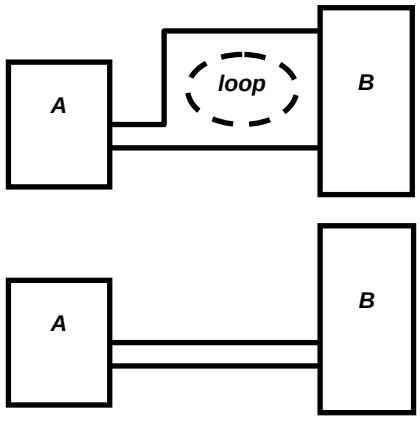


Figure 4-1: Loop inductance and a method to minimize it

The loop stray inductances can be reduced and even eliminated by reducing the area of the loop of the stray inductance. The Figure 4-1 shows a stray loop inductance between components A and B, and how it can be reduced by bringing the bus-bars closer to each other. However, stray inductance can never be zero because of the parasitics associated with the length of copper bus-bar. A conservative estimate of about 10 nH per inch can give a good idea of system parasitics without involving time-consuming math.

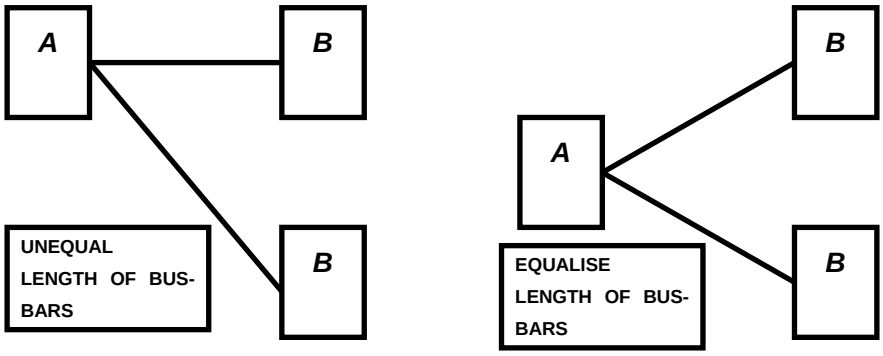


Figure 4-2: Parasitic inductance due to unequal lengths of conductor.

An adverse effect of parasitic inductances is that they alter the time constants of the system leading to transient voltage spikes on components connected in parallel. This occurs because of difference in the lengths of bus-bar connecting the parallel components. In Figure 4-2 component A and b are in parallel. Notice the difference in the length of the bus-bar connecting A to B. The longer length of bus-bar translates into additional parasitic inductance and hence increases the time constant of that path. The only solution to this problem is equalizing the lengths of bus-bars from A to B. This ensures similar signal response along both the paths.

4.3.1.1. Voltage Source Converter parasitics

Three major parasitic inductances were identified during the course of design and experimentation of the voltage source converter. These inductances were found between the power stage and clamp circuit, within the clamp circuit and in the half-bridge sub-system itself. All three stray inductances will be explained in order and methods of mitigating them or reducing them follow.

4.3.1.2. Loop parasitic Inductances:

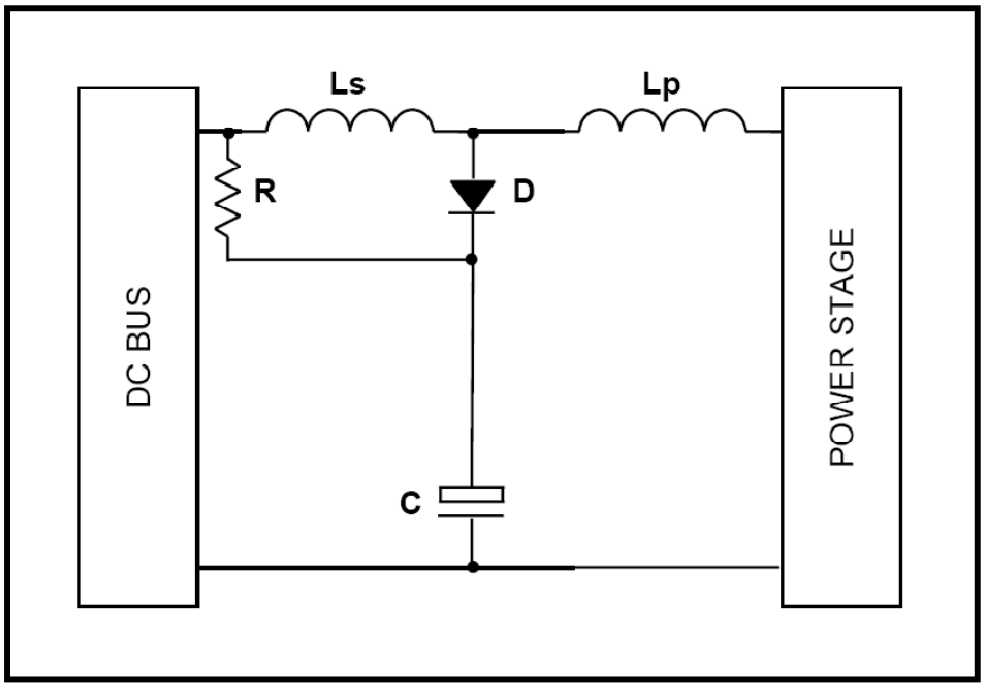


Figure 4-3: Parasitic loop inductance with the power stage

The Figure 4-3 above shows one of the most important parasitic inductances Lp on the power stage. Its importance comes with the fact that improper design of the bus-bars could lead to large values of L_p. Semiconductor devices are capable of turning-off large amount of current in microseconds, resulting in very high di/dt. A high di/dt coupled with the parasitic inductance leads to voltage spikes on the devices which can be as large as twice the DC bus voltage. Since the parasitic inductance is not very controllable in terms of design; large voltage spikes occurring on the device due to these stray inductances can lead to a voltage-breakdown failure of the devices. The term 'parasitic' and 'stray' are used interchangeably in this context.

For a turn-off current di/dt of 4000A/μs, the voltage spikes are listed below:

Table 4-1: Voltage spike generated for a particular parasitic inductance

Parasitic Inductance	Voltage Spike
100 nH	400 V
150 nH	600 V
400 nH	1600 V

The data presented in Table 4-1 clearly shows that if the parasitic inductance is high the voltage spike on the DC bus can be as high as 1600 V. This severely compromises the chances of increasing the DC bus voltage to increase power output without putting the semiconductor devices under too much voltage stress. Occasionally, if proper design considerations are not applied the voltage spike might be high enough to cause a breakdown of the semiconductor device. Proper care should be taken in laying the bus-bars of the system to minimize stray inductances. The aim should be to reduce the area of the loop forming the stray inductance. Ideally the bus-bars should overlap completely leading to zero area between them, however this is usually not viable because of the strike and creep distance limitations imposed by the high voltage levels in the power converter. Usually a distance of one inch per kV is taken as rule of thumb while determining the minimum safe distance between two live bus-bars. The use of insulators/ coatings on the bus-bars can significantly reduce the distance between the bus-bars safely thus allowing a tighter and compact design.

4.3.1.3. Finite Element Analysis for parasitic inductances

Finite Element Analysis (FEA) tools can provide insight to the actual behavior of the parasitic inductances with complex loop areas in three dimensions. The bus-bar between the power stage and the clamp circuit went through several iterations of design to minimize the stray inductance. Using ANSYS© FEA tool the interconnecting bus-bar was modeled in

CAD. Appropriate test conditions were setup in the program and the simulation was run to obtain the inductance value.

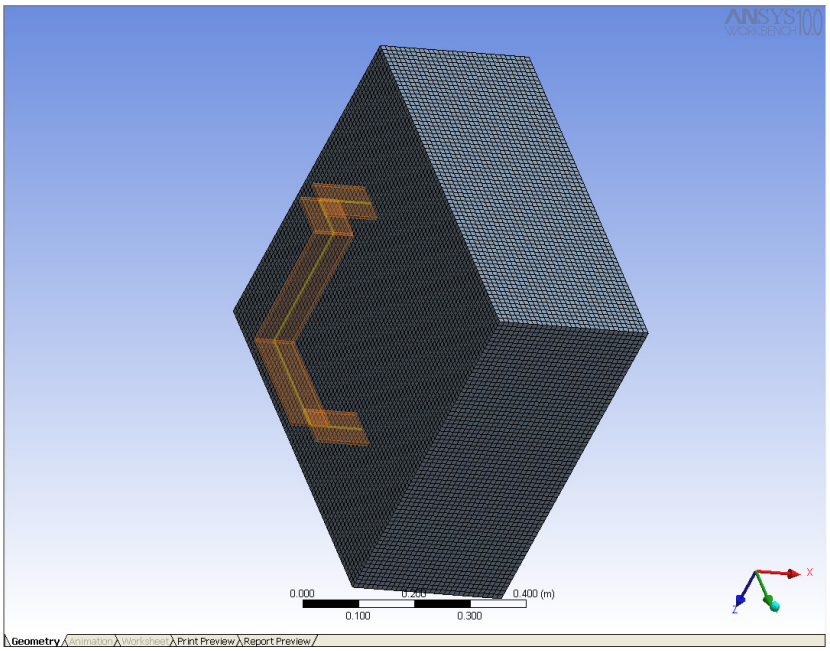
Three design iterations are discussed below:

a. First design run with no optimizations applied.
b. Design optimized by bringing bus-bars as close as possible within minimum strike distance for air.
c. Design optimized for bus-bars being coated and covered with insulation.

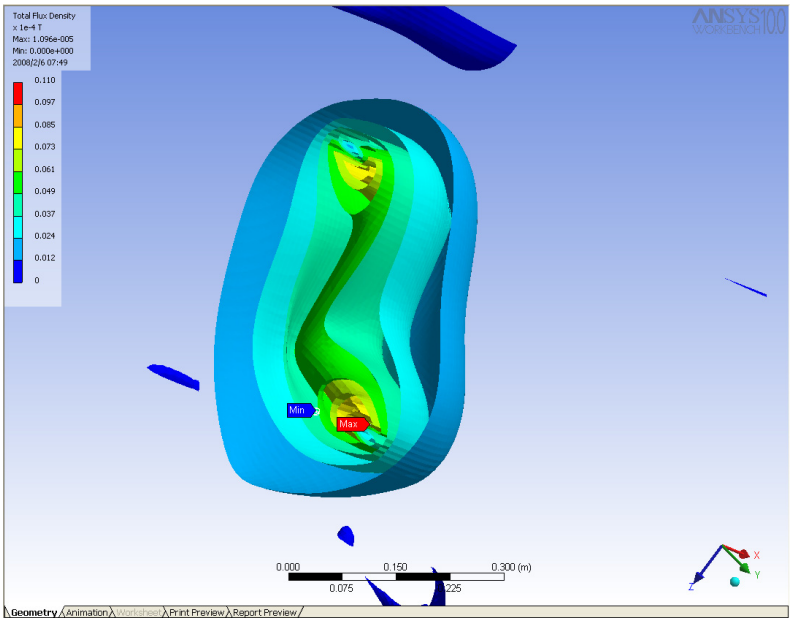
The first design run was finished assuming ideal conditions, so that the all problems arising within the system could be better understood. No consideration was given to reducing the parasitic inductance loop or the stray inductances due to the length of the bus-bars. When the voltage spikes were calculated using the inductance values obtained from ANSYS© the design was considered infeasible and design optimizations were considered for the second iteration of design.

In the second design iteration, the design was optimized without further addition of any material to the system. Hence bringing the bus-bars close up to only the minimum allowable strike distance was possible. The basic rule of thumb for the strike distance was kept as one inch per kV; thus for an overshoot of 4kV, 4 inch spacing between the bus-bars was considered optimal.

For the third design iteration, the use of insulation material was considered. The insulation material reduced the strike distance by 50% to 75% depending on the grade of the insulation material ANSYS© simulations for the above cases are shown in Figure 4-4 and Figure 4-6.



(i)



(ii)

Figure 4-4: ANSYS simulation showing the flux density in case 1

Figure 4-4-i shows the meshing procedure that is carried out in any FEA tool. The main motivation to carry out meshing or dividing the object into finitely small elements is to use numerical techniques to solve the set of differential equations generated by the problem specification. The object is divided into small finitely sized elements so that the fields over the small section of the object are uniform e.g. electric field over the entire object would be equi-potential. Each section then has its own set of differential equations which are solved by an iteration process until a convergence point for the solution is reached and the error of the results is within acceptable set parameters. Meshing also reduces complex geometries unlike the one being discussed into regular shaped cuboids or polygons to ease the process. The granularity of the meshing is a key factor in determining convergence. If the mesh is too fine the results would be more accurate, however, at the cost of increased computing resources and time taken to obtain the solution. Usually, a balance between the two should be maintained to obtain the most accurate solution in least time. As the object is meshed to obtain certain parameters, the volume around the object also has to be meshed to obtain specific details such as electric-magnetic fields, air flow parameters, temperature profile of still air etc. The same balance between the accuracy of the solution and the computing resources/ time has to be maintained.

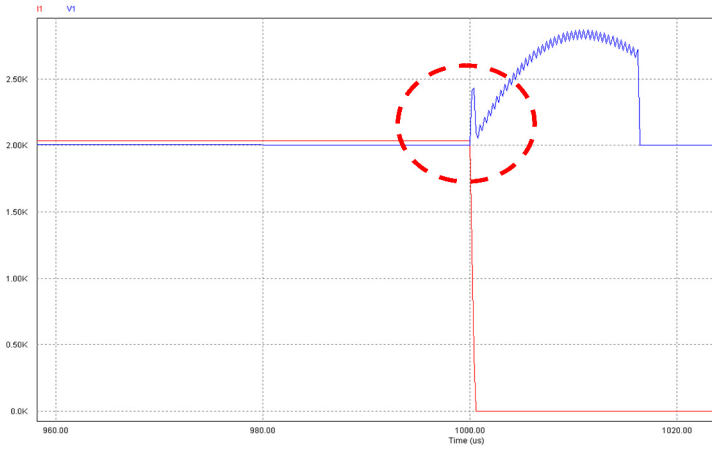
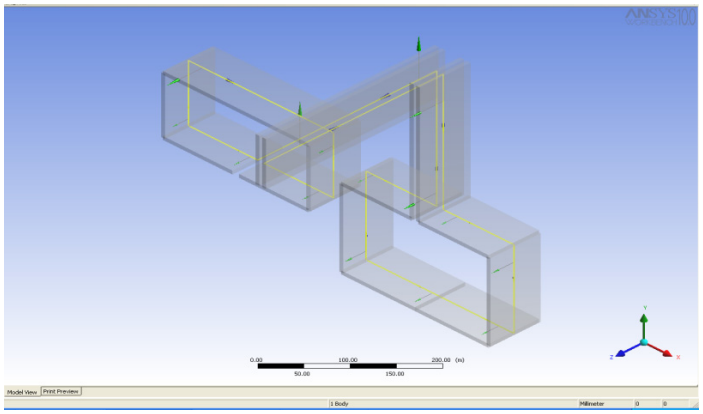


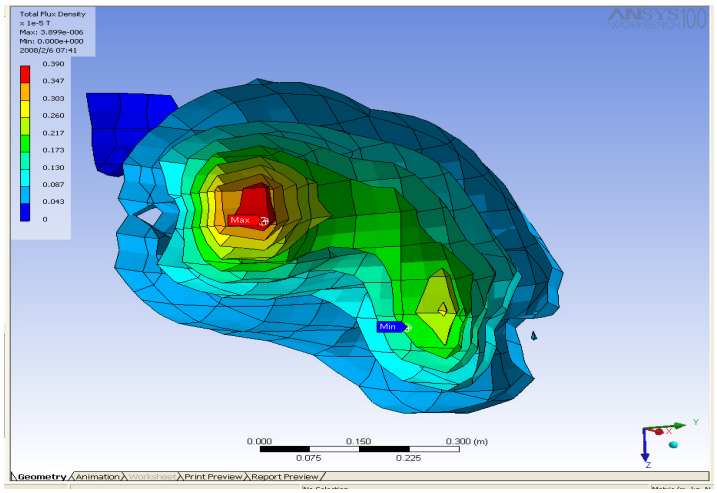
Figure 4-5: Voltage Overshoot due to parasitic inductances

Figure 4-4-ii, shows the magnetic field density solution obtained after an analysis run. This was done to see the volume of influence of the magnetic field on the surrounding

components. It is especially important to understand the effects of magnetic fields on surrounding components. Varying magnetic fields have detrimental effects on electronic components such as controllers, sensors and gate drive circuits. The components mentioned above have some measure of Electromagnetic Compatibility (EMC), however, it is always beneficial to reduce the source of EMI. The pulsating current in the loop can give rise to such EMI. The inductance resulting from this loop also results in voltage overshoots which directly reflect on the power devices, as shown in Figure 4-5.



(i)



(ii)

Figure 4-6: ANSYS simulations for flux density for case 2

Figure (i) of Figure 4-4 and Figure 4-6 show how the CAD modeling is done for the bus-bar and the figure (ii) shows the flux within the loop and surrounding area. The maximum flux for the first design run was 1.096e-005 T and for the second design run the flux was 3.09e-004 T. The significance of showing the flux is that now we can see that in the second optimized design run the flux had significantly reduced indicating lower inductance. Similarly the actual simulated values of inductance were 540 nH and 200 nH respectively.

4.3.1.4. Parasitic inductance due to length of the copper bar

Copper bus-bars have some inherent inductance which can be quantified as 'inductance per inch'. Although the inductance also depends on the cross-sectional area of the conductor, but it's the length of the conductor that contributes to the inductance. Let us consider two arrangements of devices in the power stage to see how this length of conductor may affect our design. It can either be helpful to us, or in many cases cause harm.

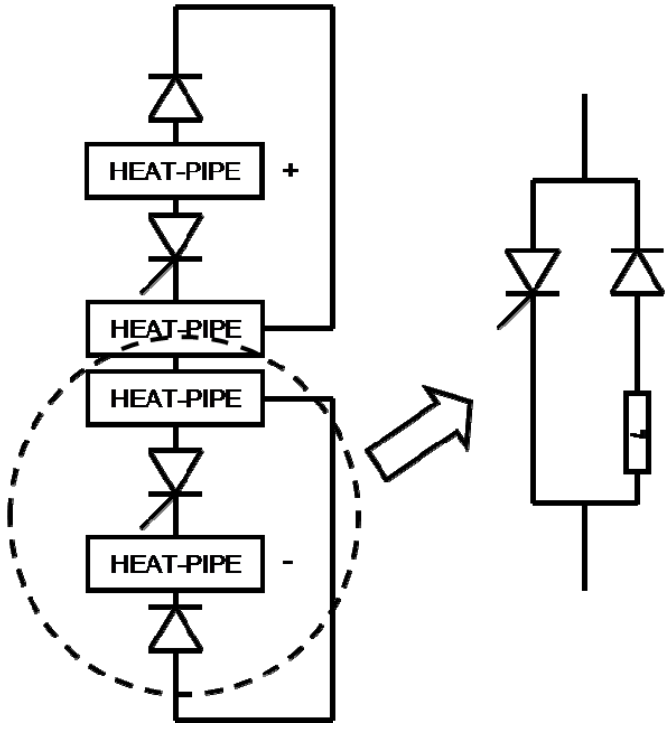


Figure 4-7: Arrangement of devices leading to stray inductance in series with diode

In Figure 4-7, the arrangement of the semiconductor switch and the anti parallel diode devices are shown. Ideally in water-cooled systems the device and diode are placed side by side and clamped together in a single wide clamp structure. This arrangement gives the minimal inductance possible between the diode and the switching device.

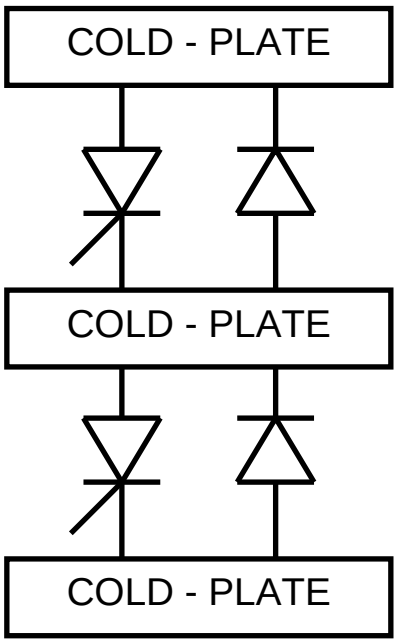


Figure 4-8: Arrangement of devices leading to minimum stray inductance in an H-Bridge

The arrangement shown in Figure 4-7 was adopted for the first design iteration. When the power stage is operational, the current in the switching device is commutated to the diode and then back to the device and the cycle repeats. As the current commutates from the switching device to the diode, the current has to overcome a large inductance in series with the diode as shown in the figure on right. As the transition occurs the stray inductor sees rapid change in the current and a large voltage is generated across the inductor to oppose this change in voltage. This voltage spike is added to the diode forward recovery voltage; thus a large reverse-bias voltage is applied to the switching device until the forward recovery of the diode is over (for about a period of 10us for selected diode). This large voltage spike across the switching device causes some negative current to flow through the device. This current can be as high as 20%-30% of actual load current which is getting commutated. If any

attempts are made to turn of the device during that period, the device might fail due to junction breakdown. Other device arrangements were tried to minimize the amplification of the diode forward recovery voltage due to the stray inductance.

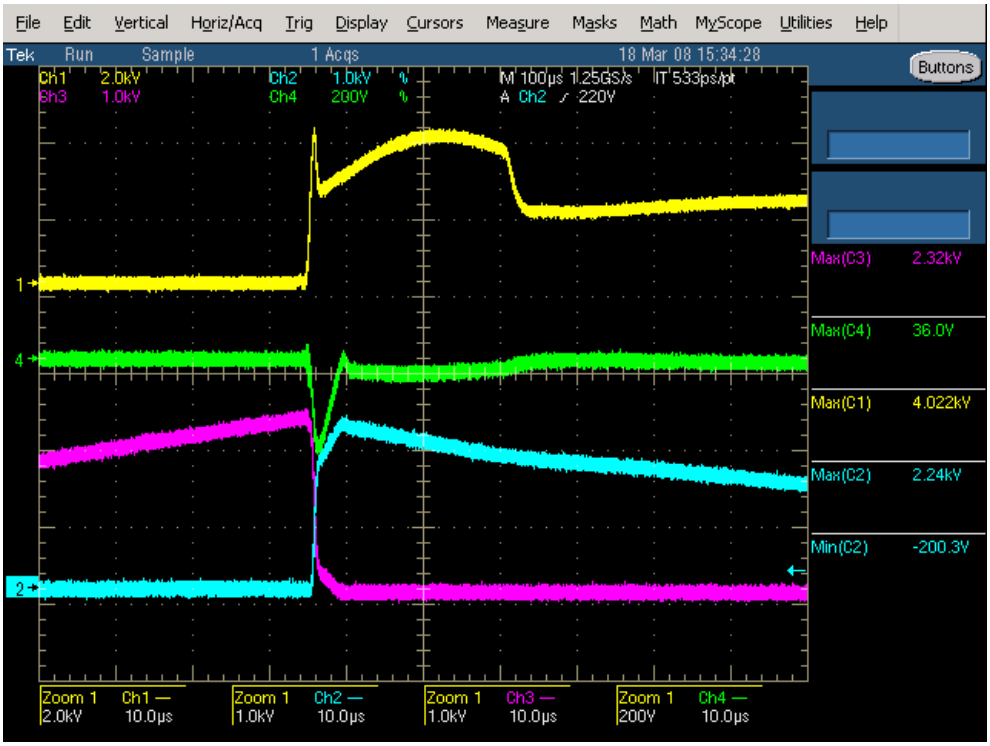


Figure 4-9: CH4 (green) shows the negative current flowing through the GTO

The Figure 4-9 above shows the negative current flowing through the GTO during current commutation from the switch to the diode. The load current is shown here in pink, CH3, which is rising until the device turns-off. The current is then commutated to the diode in the same phase leg. The diode current is shown here in blue, CH2. It can be clearly seen that the diode current is cut off at the rising edge, indicating that the some portion of the load current has taken another route. The only other route possible would be through the GTO, but in the opposite direction. The reverse current through the GTO is not completely avoidable, however there must be some effort put in to reduce its magnitude and tail. If the magnitude of the current is large, it will have a longer tail current. The switch cannot be turned on until the tail current reduces to zero, else it will result in the failure of the semiconductor switch. Thus

the time taken to turn the device on for the next switching-cycle will increase, decreasing the overall switching frequency of the converter. A shorter reverse GTO current will result in a higher switching frequency to be possible.

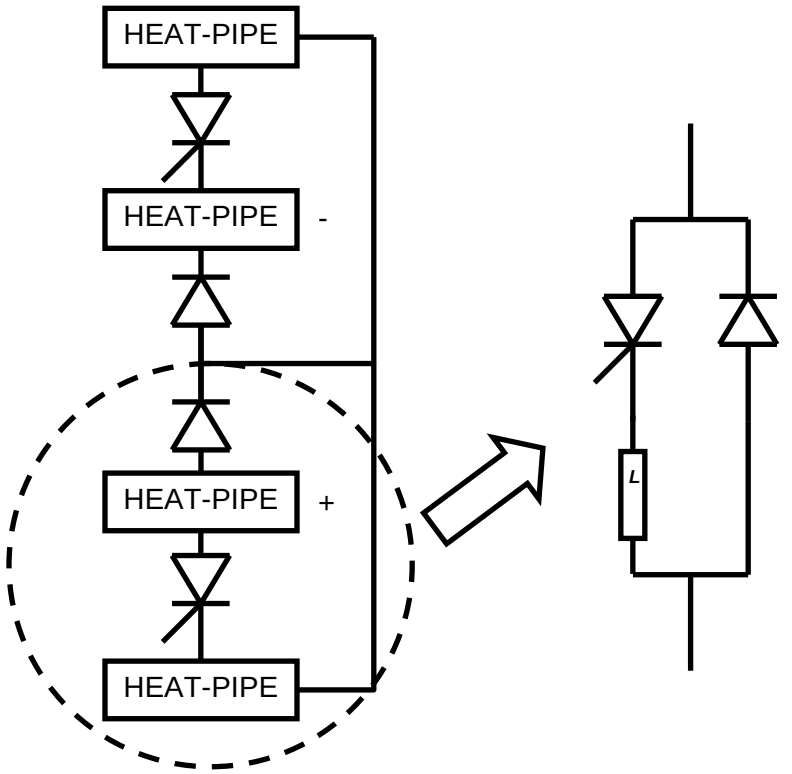


Figure 4-10: Arrangement of devices leading to optimal and useful stray inductance

In Figure 4-10, shown above, the position of the diode and the semiconductor switch are exchanged. The location of the positive and negative terminals of the DC bus is also interchanged to maintain the correctness of the topology. It should now be noted that when the current commutates from the switching device to the diode, the parasitic inductance in the path of the diode is virtually eliminated or reduced to a negligible proportion. The parasitic inductance is basically shifted from the diode to the switching device. This is beneficial to the switching device because the series inductance helps suppress the turn-on inrush currents.

Suppression of turn-on di/dt is crucial for the preventing failures in the switching device due to large rate of change of turn-on current. Another advantage of this arrangement of devices

is that the diodes have better thermal performance. This is due to the fact that the diodes are now sandwiched by two heat-pipes. In the previous arrangement the diodes were at the extremes of the stack, hence cooling of the diodes was insufficient. The new arrangement is reduced in size and weight because of optimized design of the bus-bars.

4.3.1.5. Parasitic inductance due to unequal length of copper bus-bar

The running length of the bus-bars can provide a rough estimate of the stray inductance in that path. The estimate of 10 nH/ inch is a very conservative estimate for design purposes. These parasitic inductances cannot be avoided, but have to be given certain amount of consideration because they are part of the converter. The presence of such strays has to be accounted for while designing the rating of devices and parameters of the control system.

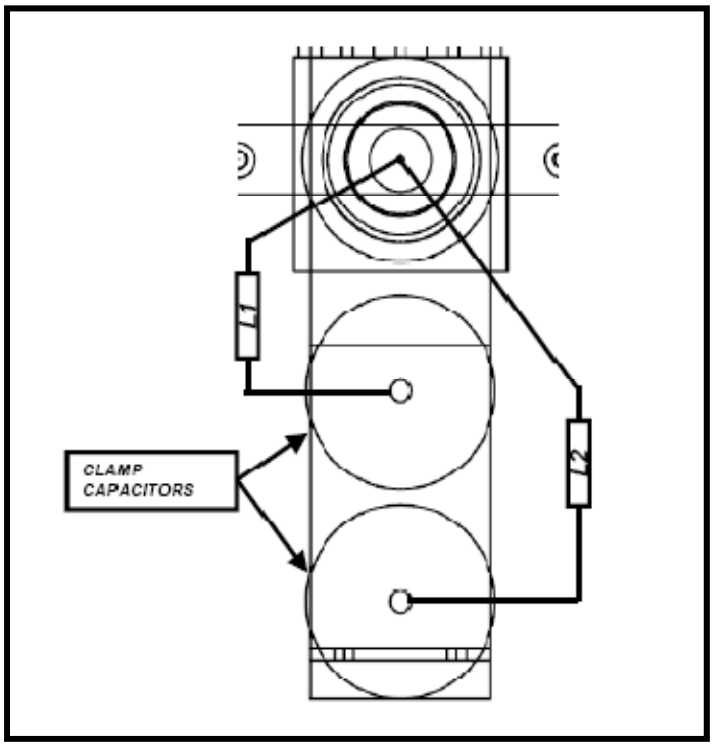


Figure 4-11: Stray inductances L1 < L2, due to difference in bus-bar length

Consider a simplistic example; connection of components in parallel, e.g. capacitors in a capacitor-bank as shown in Figure 4-11. If the capacitors connected together have different

stray inductances in the current return paths, the capacitor with more parasitic inductance will see a larger voltage during charging/discharging of the capacitors. This could probably cause the capacitor to fail because the voltage spike may exceed the capacitor's maximum non-repetitive voltage rating. To avoid such occurrences the lengths of the bus-bars connecting the components to a common point should be attempted to be nearly equal.

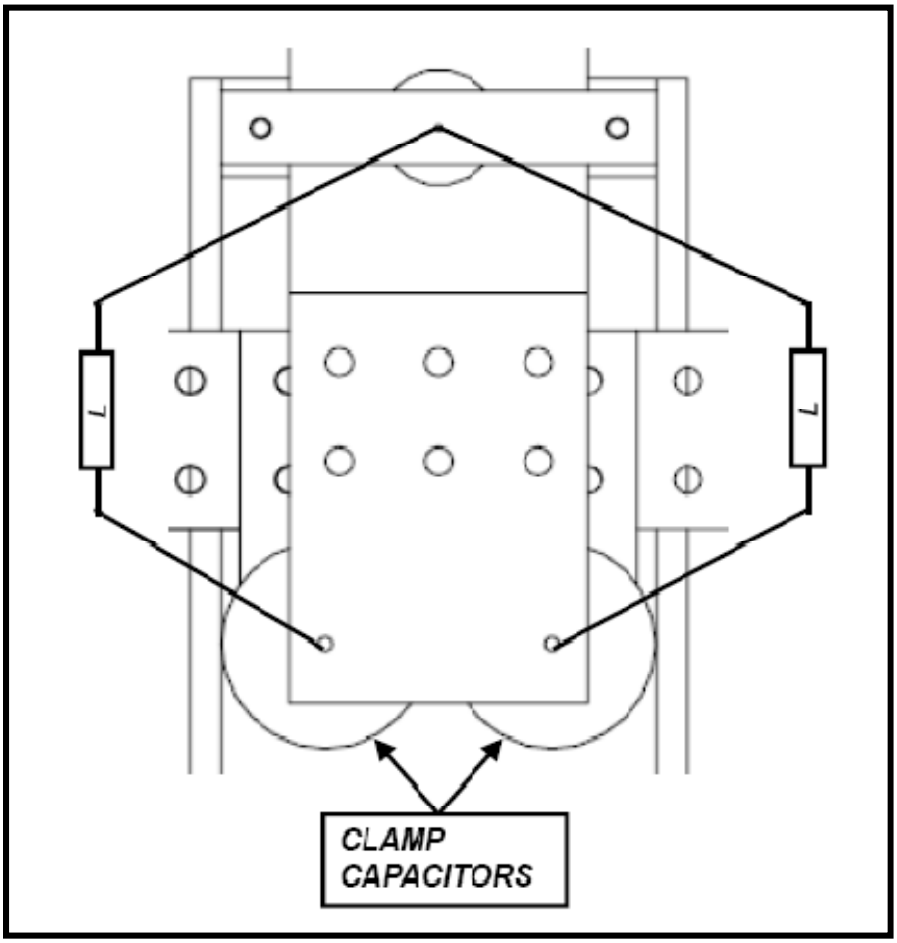


Figure 4-12: Stray inductances L1 = L2 = L

In the Figure 4-12 it can be clearly seen that the capacitors are rearranged so that the lengths of bus-bars connecting them to a common point are equal. This equalizes the stray

inductance in the capacitance thus avoiding any unwanted voltage overshoots on the capacitors.

4.3.2. Design for minimum contact resistance between two Bus-bars

It is a wrongly accepted fact that a good mechanical joint also forms a near perfect electrical connection. Imperfections in the joints lead to large stray inductances and significant contact resistances. These contact resistances add to the losses in the converter, lowering its efficiency. Also the thermal cycling that results from the varying temperature gradients at the point of contact between bus-bars, leading to joint failures. The contact resistance is inversely proportional to how perfect the mechanical connection between two bus-bars is. A joint with high contact resistance will undergo rapid thermal cycling; further increasing its contact resistance and over time will fail due to the inverse relationship. Proper design practices help lower the contact resistances, thus increasing converter efficiency.

Stray inductances do not, in general, affect the performance in low power converters; they might bring down the efficiency by a small fraction if not properly designed. However, their existence has a big influence on the proper operation and even operational stability of high power converters. This is mainly due to the fact that low power converters do not use big and hefty metal bus-bars for interconnecting all major current carrying components. The large size bus-bars lead to significant amounts of stray inductances and inter bus-bar contact resistances. This section's main focus would be the analysis of interconnection resistance and techniques to minimize the contact resistance for copper bus-bars. The discussion may also be extended to aluminium bus-bars as well.

4.3.2.1. Point of contact between two metal surfaces

A well polished metal surface also consists of microscopic hills and valleys. Theoretically, only three points of contact are required between two metal pieces to 'establish contact'. When the pressure on the two overlapping metal bars increases the initial 'three points of contact' are broken down and the area of metal that is actually touching each other increases. However, it is seen experimentally that even when a large pressure approaching the

deformation pressure of the material is applied, the actual area of contact is still a fraction of the actual area of overlap of the metal bars.

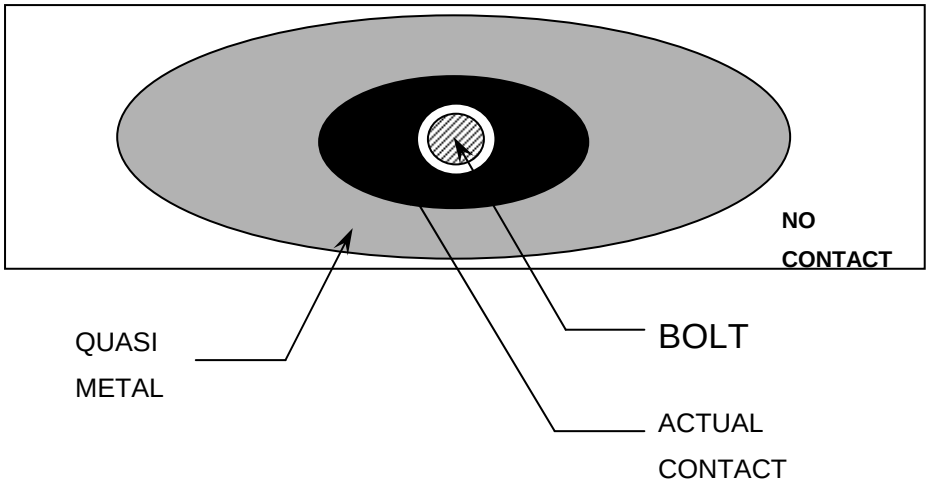


Figure 4-13: Contact area under pressure

The metal surfaces are usually covered by a thin film of oxide. When a mechanical joint is made between two metal surfaces using nuts and bolts; the metal yields. The brittle oxide film which is common to all metal surfaces exposed to air is unable to deform like the metal. Cracks and fissures are formed in the film on the metal surface leading to actual contact between the overlapping metal surfaces. These spots of perfect contact are surrounded by less-perfect spots where in actual metal-to-metal contact is not made. A single molecule layer of oxide film or lubricants may still exist in the less-perfect contact spots. These spots can be called as 'quasi-metal' spots (11) and have a very low resistance. Outside these 'quasi-metal' spots are regions where no contact has been made.

Basically, contact resistances can be broadly classified into two types (11):

a. Resistance at contact points caused by oxide layers, trapped gases/air.
b. The constriction resistance cause by non-uniform flow of current in overlapping conductors.

Point ‘a’ had been briefly discussed earlier in the introduction and shown in the figure. Point ‘b’ requires characterization to judge its impact on the resistance, depending on varying system parameters.

4.3.2.2. Streamline effect:

Experimental results have shown that resistance of a perfectly made overlapping joint (of no inter-surface resistance resulting from oxides or trapped air) is higher than the actual calculated resistance based on the formula:

$$R = \frac{l \cdot \rho}{A} \quad \text{..... Equation 4-1}$$

Where R = the resistance of the conductor

l = the actual length of the conductor

A = cross-sectional area of the conductor

This effect is called as the ‘streamline effect’ (11).

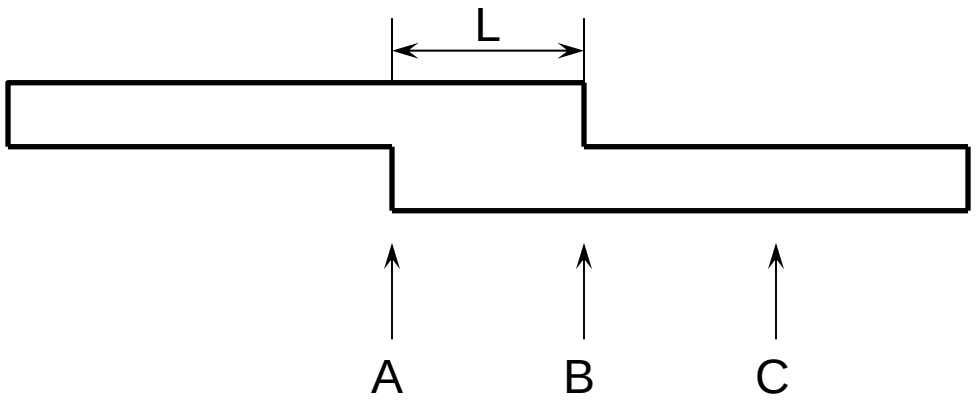


Figure 4-14: Experimental setup for observing streamline effect

The Figure 4-14, represents a uniform bus-bar with thickness t at all points expect for the region between A and B, where its thickness is equal to 2t. The bus-bar is shaped like a lapped joint, but it does not have any contacting surfaces along AB. Any variations of voltage drop measured across the entire length of the bus-bar will be due to the shape of the conductor.

A current is passed through the strip from one end to the other. Voltage drops are measured between the points A and B, and between B and C. The distance between AB = BC.

Voltage drop from A to B = V_1

Voltage drop from B to C = V_2

$$e = \frac{V_1}{V_2} = \frac{R}{R_b} \quad \text{..... Equation 4-2}$$

Where, e = streamline effect

R = total resistance of joints

R_b = resistance of equal length of single bus-bar.

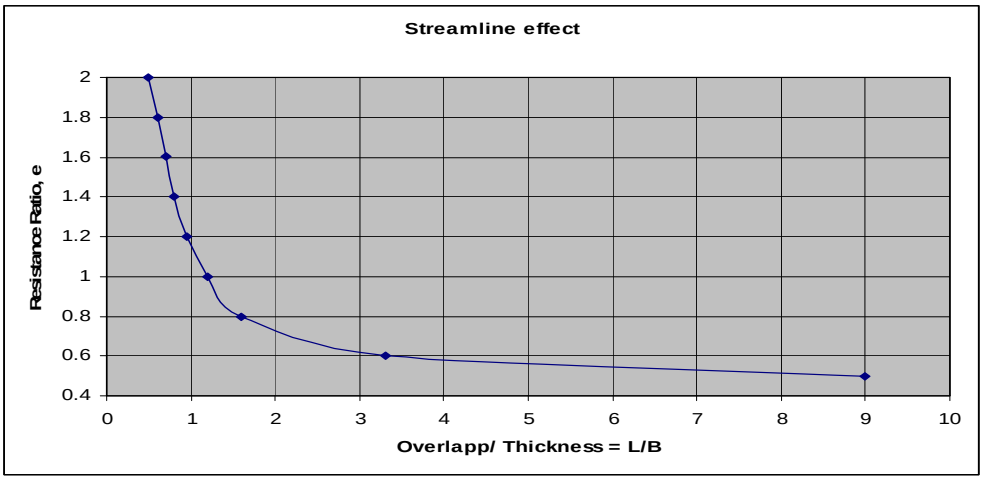


Figure 4-15: Streamline effect curve

The experiment was conducted for a large number of current samples and the graph shown in Figure 4-15 was plotted. It can be concluded that the larger the overlap area, smaller is the streamline effect resistance. The ratio e becomes less than one only when the overlap length L becomes larger than the thickness B of the bus-bars.

4.3.2.3. Constriction resistance

The distribution of current in a copper bus-bar of uniform thickness is uniform. The resistance of the rod could be calculated based on the material properties such as the conductivity, length, width and thickness of the bus-bar.

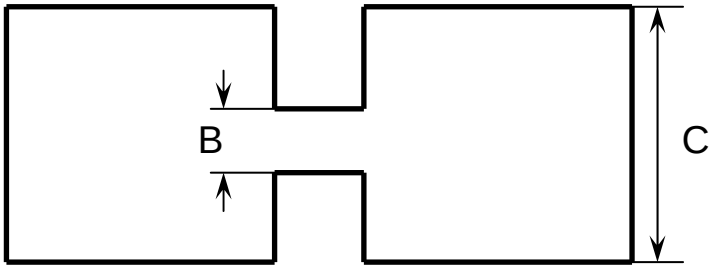


Figure 4-16: Experimental setup for constriction resistance measurement

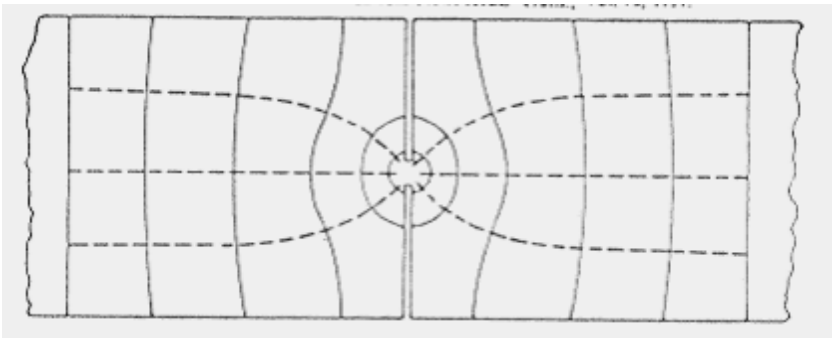


Figure 4-17: Current density lines showing constriction

When a constriction is introduced in such a bus-bar as shown in Figure 4-17, the current flow becomes non-uniform. The distortion in the lines of current flow results in an increase in resistance called as 'constriction resistance' (11). In a mechanical joint of two bus-bars, the points of actual contact are of various shapes and sizes and are located at random throughout the entire overlapping area. The actual contact points can be thought of constrictions in the

flow of the current through the bus-bars as shown in the figure. The constriction resistance is the only resistance between two surfaces that have actual contact (11). Experimental results shown in the form of a graph in figure, confirm the theory. It can also be seen that the resistance increases as the constriction in the flow of current increases.

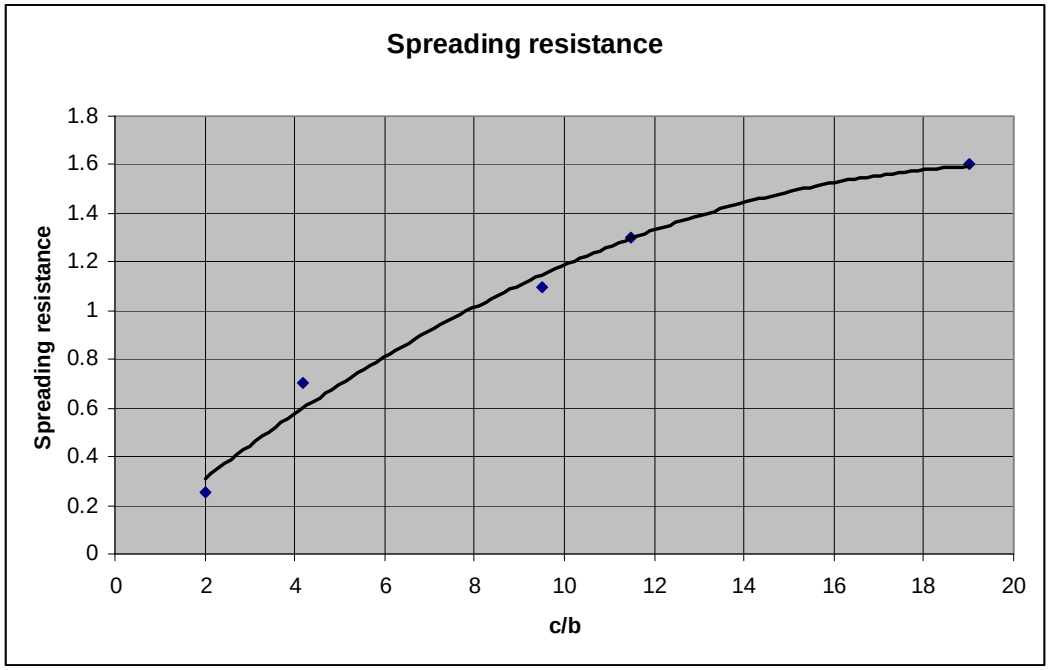


Figure 4-18: Spreading resistance curve

4.3.2.4. Film resistance

When clean metal surfaces are exposed to air, their surfaces become coated with thin layers of metallic oxides of various thicknesses, depending on the concentration of the gases and suitable conditions for oxidation reaction. During a test (11), a clean surface of copper became covered with a monomolecular film of oxygen in a few seconds; in half an hour the film grew to a thickness of about 10 to 30 Angstrom.

Conduction through very thin oxide films, according to quantum mechanics (11), that electrons in the metal can penetrate a few angstrom units into an insulating layer without receiving any excitation energy. This process of transmission of electrons through very thin

insulating metal-oxide layers is known as the quantum mechanical tunnel effect (11). Because of this effect, the electric current can pass through thin metal-oxide layers without any practically thin resistance. However, thick multi-molecular films without any surface fissures like oxides, sulfides, nitrites and others can be regarded as pure insulators. There can be no current flow through them.

4.3.2.5. Clamping force-contact resistance

There is defined relationship between contact force and the resulting contact resistance. Experimental data shows the variation of contact resistance during initial application of the clamping force (11).

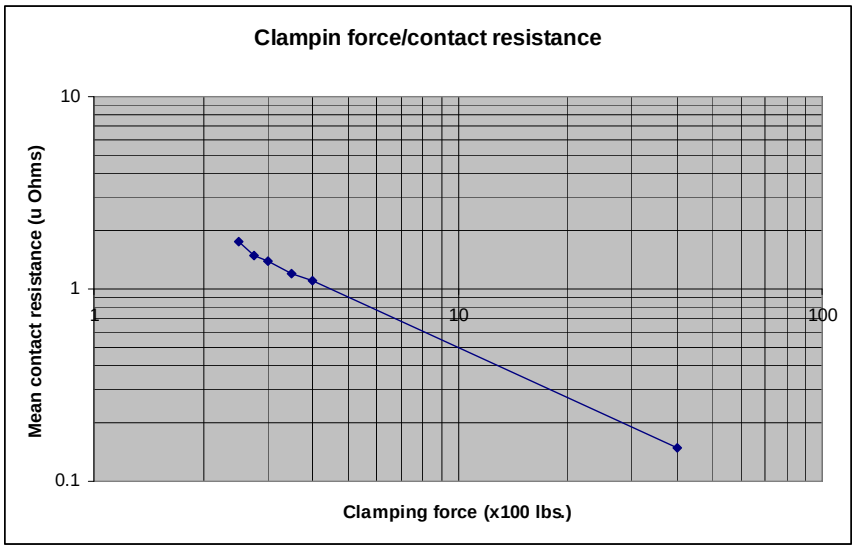


Figure 4-19: Contact resistance under clamping force

The above graph can be represented by the formula (11):

$RP^n = C$ …… Equation 4-3

Where, R = contact resistance

P = clamping force

C = constant

The initial contact resistance of two well-cleaned surfaces depends on two factors:

a. The conductivity of the materials of the surfaces in contact
b. The area of the surfaces in actual contact, devoid of any thin oxide films in between them.

The area and distribution of the points of actual contact between two overlapping surfaces depends on the magnitude of the clamping force and the techniques used to apply the clamping force on the two connecting metal objects/bus-bars. It therefore becomes essential to properly select the bolts, nuts and washers used to clamp the two connecting buses together. Also the placement of these nuts and bolts becomes crucial for uniform distribution of the clamping force. Proper guidelines must be followed while selecting the clamping components to ensure the best possible electrical connection between two bus-bars.

4.3.2.6. Contact surface preparation

The conditioning of contact surfaces before any assembly is made has a significant impact on the contact resistance of the electrical connection between the bus-bars (11). Proper preparation of the contact surfaces before any assembly or initial clamping results in a suitably low value of contact resistance. Such preparations ensure that the efficiency of the electrical joint and the contact resistance of the joint remain unchanged through a number of thermal cycles that the system will eventually go through.

It has been proved by extensive experimentation that for both aluminium and copper bus work, it is essential that the surfaces of the metals are immediately coated with some kind of suitable grease-type compound before and after machining the metal surface. This protects the newly exposed metal surface against oxidation. Better results can also be obtained when the contact surface is abraded using a wire brush or any kind of coarse abrasive paper/cloth. In case of aluminium this process becomes more important because of the fact that aluminum oxide formation is much quicker than oxide formation over copper. This protective coating/ grease should not be removed even during clamping the two bus-bars together in a lap joint. This ensures that there is no further oxidation of the contact surfaces, by sealing the joint and preventing exposure of the joint to any corrosive gases, liquids and oxidation.

Due to a variety of conditions under which bas-bar installations are made and the systems operate; the use of petroleum based compounds with higher melting points and better weather-resistant properties than petrolatum are recommended (11). Another alternative to using a protective layer of grease-like compounds on bare metal are electroplating the metal with a non-corrosive metal like tin or silver. The process can be expensive and yields more long term benefits as compared to the traditional processes.

4.3.2.7. Contact surface area

The efficiency of the joint is defined as the ratio of the conductivity of the joint to that of a bar of the same length as the joint. The design parameters that must be considered while determining the overlap area of two interconnecting bus-bars are as follows (11):

a. The current usually passes through the end points of the contact surfaces; the intermediate region is used insignificantly for the passage of current.

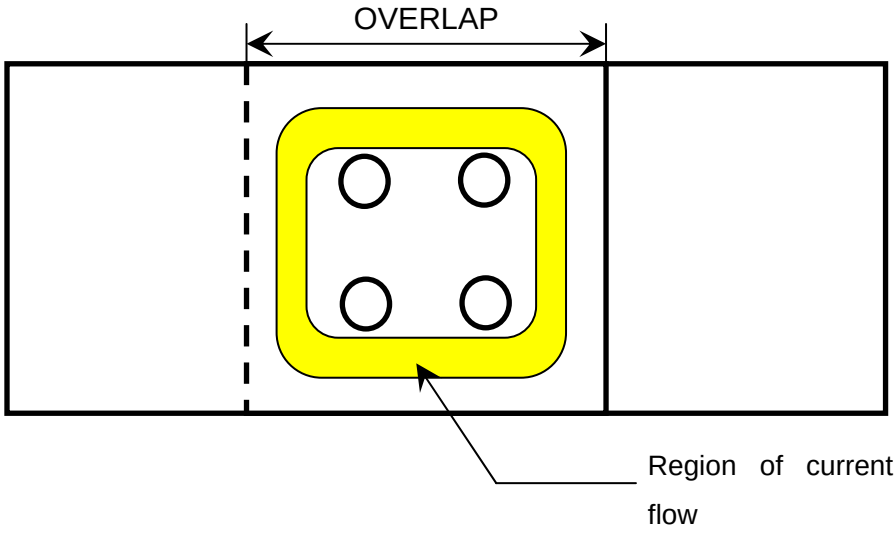


Figure 4-20: Current flow along the edges of contact between two bus-bars

b. If two materials having different conductivities are used to make a joint, the current will pass across the contact surface almost exclusively at the end of the better

conductor. While the rest of the contact surface remains devoid of any passing current.

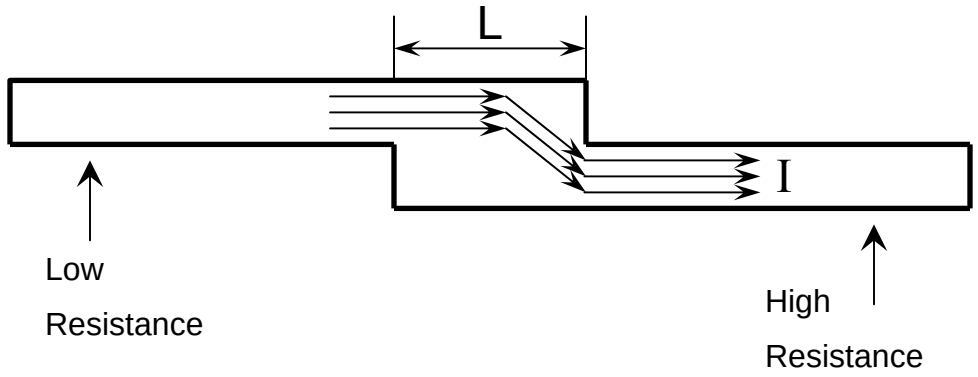


Figure 4-21: Current constriction because of bus-bars of different resistivity

c. Reduction of current density at the joints should be obtained by increasing contact surface in width rather than increasing the contact surface in length. It can also help to use the double slice plate butt joint (11).

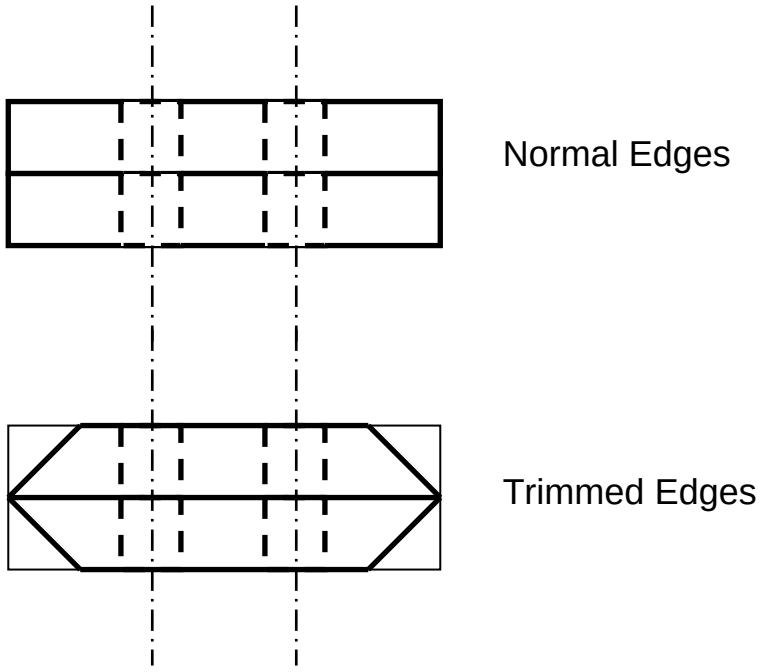


Figure 4-22: Trimming edges to force current away from edges

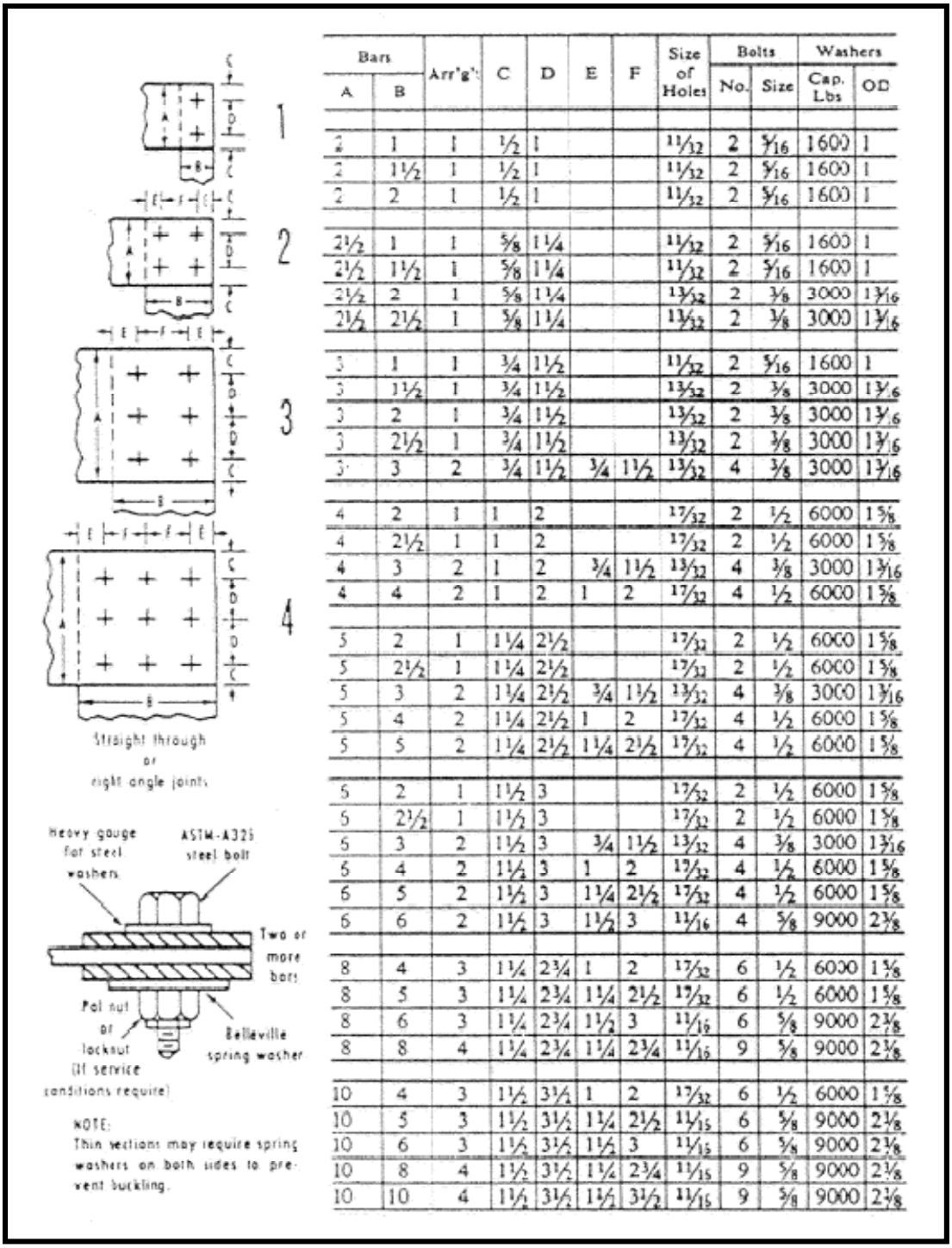
d. Since most of the current tends to flow through the end regions of the contact, it may help to increase the resistance of the ends regions of the contact surface to enhance current flow through the rest of the contact surface. The resistance can be increased by tapering the ends of the contact surface region so that the cross-sectional area in those regions is lower than the rest of the contact region. Lower cross-sectional area implies more resistance.

It has also been shown experimentally that the joints that have been dismantled must be cleaned and processed again before they are re-assembled.

Theoretical values of overlap area can be calculated using above mentioned design pointers, however there must be sufficient allowance for the area lost in drilling holes. Actual contact area is also a function of the clamping pressure on the joint. Hence a more practical rather than a theoretical approach must be taken into consideration while determining the overlap area between two interconnecting bus-bars.

For the sake of convenience, it is common practice to make overlaps equal to the width of the bus-bar. This method yields satisfactory results for the bus-bars of ordinary dimensions. But there is considerable loss of contact efficiency when using bus-bars of higher thickness-to-width ratio. An overlap of 4” on a ¼” x 4” bus-bar will give good enough contact efficiency; however, on a ¼” x 1” bus-bar an overlap of 1” will not be sufficient. The minimum overlap should be at least 8-10 times the thickness of the bus-bar to provide good enough contact, only if the current density in the contact is not more than 90 amperes per square inch.

A reasonable guide to deciding the overlap and the position of holes in bus-bars is presented in the Figure 4-23. All the data is largely based on experimental validation of the cases presented.



Bars A	Bars B	Arr'g't	C	D	E	F	Size of Holes	Bolts No.	Bolts Size	Washers Cap. Lbs	Washers OD
2	1	1	½	1			11/32	2	5/16	1600	1
2	1½	1	½	1			11/32	2	5/16	1600	1
2	2	1	½	1			11/32	2	5/16	1600	1
2½	1	1	5/8	1¼			11/32	2	5/16	1600	1
2½	1½	1	5/8	1¼			11/32	2	5/16	1600	1
2½	2	1	5/8	1¼			13/32	2	3/8	3000	1 3/16
2½	2½	1	5/8	1¼			13/32	2	3/8	3000	1 3/16
3	1	1	¾	1½			11/32	2	5/16	1600	1
3	1½	1	¾	1½			13/32	2	3/8	3000	1 3/16
3	2	1	¾	1½			13/32	2	3/8	3000	1 3/16
3	2½	1	¾	1½			13/32	2	3/8	3000	1 3/16
3	3	2	¾	1½	¾	1½	13/32	4	3/8	3000	1 3/16
4	2	1	1	2			17/32	2	½	6000	1 5/8
4	2½	1	1	2			17/32	2	½	6000	1 5/8
4	3	2	1	2	¾	1½	13/32	4	3/8	3000	1 3/16
4	4	2	1	2	1	2	17/32	4	½	6000	1 5/8
5	2	1	1¼	2½			17/32	2	½	6000	1 5/8
5	2½	1	1¼	2½			17/32	2	½	6000	1 5/8
5	3	2	1¼	2½	¾	1½	13/32	4	3/8	3000	1 3/16
5	4	2	1¼	2½	1	2	17/32	4	½	6000	1 5/8
5	5	2	1¼	2½	1¼	2½	17/32	4	½	6000	1 5/8
6	2	1	1½	3			17/32	2	½	6000	1 5/8
6	2½	1	1½	3			17/32	2	½	6000	1 5/8
6	3	2	1½	3	¾	1½	13/32	4	3/8	3000	1 3/16
6	4	2	1½	3	1	2	17/32	4	½	6000	1 5/8
6	5	2	1½	3	1¼	2½	17/32	4	½	6000	1 5/8
6	6	2	1½	3	1½	3	11/16	4	5/8	9000	2 3/8
8	4	3	1¼	2¾	1	2	17/32	6	½	6000	1 5/8
8	5	3	1¼	2¾	1¼	2½	17/32	6	½	6000	1 5/8
8	6	3	1¼	2¾	1½	3	11/16	6	5/8	9000	2 3/8
8	8	4	1¼	2¾	1¼	2¾	11/16	9	5/8	9000	2 3/8
10	4	3	1½	3½	1	2	17/32	6	½	6000	1 5/8
10	5	3	1½	3½	1¼	2½	11/16	6	5/8	9000	2 3/8
10	6	3	1½	3½	1½	3	11/16	6	5/8	9000	2 3/8
10	8	4	1½	3½	1¼	2¾	11/16	9	5/8	9000	2 3/8
10	10	4	1½	3½	1½	3½	11/16	9	5/8	9000	2 3/8

Figure 4-23: Guideline for implementing proper overlap joint between bus-bars

As shown in Figure 4-23, there are four cases of bus-bar joints discussed. The different sizes of holes that need to be drilled for the bolts and the recommended sizes of washers required for each case is also included in the figure.

4.3.3. Bus-bars for the Voltage Source Converter

Copper bus-bars have been used to make inter-connects for all the power components in the first prototype of the voltage source converter. Since copper bus-bars have been inserted into the half-bridge stack the copper bus-bars have been coated with a 5um tin coating. The tin has been electro-plated on the bare copper bus-bars to get a much even and uniform coating as compared to dipping the copper bus-bars in a tin bath. To reduce cost and for quick turn-around, in terms of stock and machining time, most of the bus-bars have been made from 3/8" x 4" copper bars. The holes are drilled on the bus-bars so that there are no surface imperfections that occur when the holes are punched using a hydraulic press. When the holes are punched the area around the hole does not remain level with the surface of the entire bus-bar. It is slightly bent downwards, assuming that the hydraulic press pushes the die downwards in the vertical direction.

The converter is mainly divided into xx components:

a. Half – Bridge stack
b. RCD clamp circuit arrangement
c. DC Capacitors
d. Snubber inductor
e. Resistor bank for the RCD clamp circuit.

Out of the five items listed above, the DC capacitors, resistor bank and snubber inductor are connected to the power converter using multiple parallel 4/0 cables to increase current carrying capacity. The usage of cables also allows them to be connected to the main power stage easily, as cables are more flexible. This allows more compact design and ease of assembly of the converter.

One of the main objectives of building high-power converters is to achieve maximum efficiency. However, even the most efficient of converters have to be economically feasible so that more than one prototype is ever built. The power converter has to be designed so that assembly is straight-forward and the foot-print is minimal along with minimum volume occupied. Using cables, to some extent, helps meet all of the above objectives. However, proper design precautions must be taken to ensure that no cable over-heats during the normal course of operation. Adding more cables in parallel often solves the over-heating problem, but this defeats the original purpose of using cables by increasing the volume/bulkiness of the power converter.

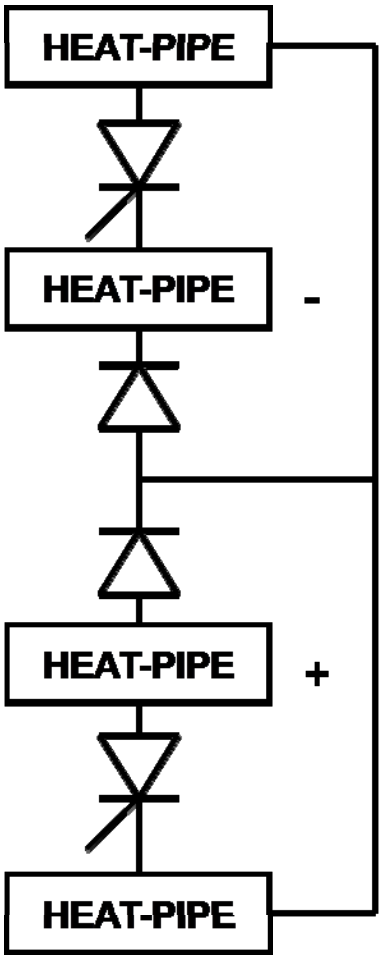


Figure 4-24: Arrangement of bus-bars for optimal stray inductance in half-bridge

The Figure 4-24 shows the most optimal way of arranging bus-bars to minimize the stray inductances associated with the half-bridge topology discussed in the earlier section. Since the stack is mechanically symmetrical along the x-axis, it will be most economical to design the bus-bars that would fit both the upper and lower sections of the stack. The bus-bars would have to be flipped to fit into both the sections. Copper is a very soft metal and is usually not recommended to be used in a 40kN stack with hockey-puck packaged devices. The copper bus-bars are therefore electroplated with tin to make the surface less elastic.

The Emitter Turn-Off (ETO) devices have been double-sided cooled by the 2.2 kW heat-pipes. The heat-pipes are isolated hence they can directly touch the anode and cathode of the ETO without any need of isolation materials. The direct metal to metal contact of the ETO device with the evaporator plates of the heat-pipes imposes a level tolerance on the upper and lower surfaces of the heat-pipe. The arrangement of an ETO device sandwiched by two heat-pipes is shown below.

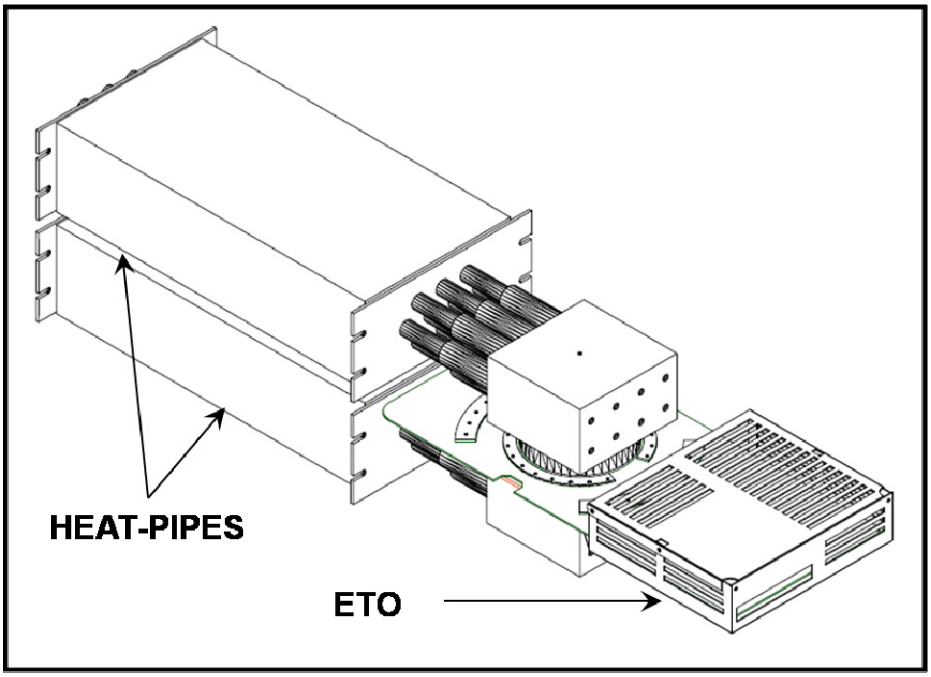


Figure 4-25: ETO with the heat-pipes

The anti-paralle diode of the stack will be placed over one of the heat-pipes. A interconnecting copper bus-bar will be required to complete the connection of the anode or cathode of the ETO device to the cathode or anode of the diode respectively. It depends on how the diode is chosen to be placed in the stack. A C-shaped bus-bar could serve the purpose of connecting the above mentioned terminals, however, it will be difficult to manufacture and assemble a C-shaped bus-bar in such a stack. The width of the heat-pipes and also the ETO and diode devices have a tolerance, hence the C-shaped bus-bar becomes impractical.

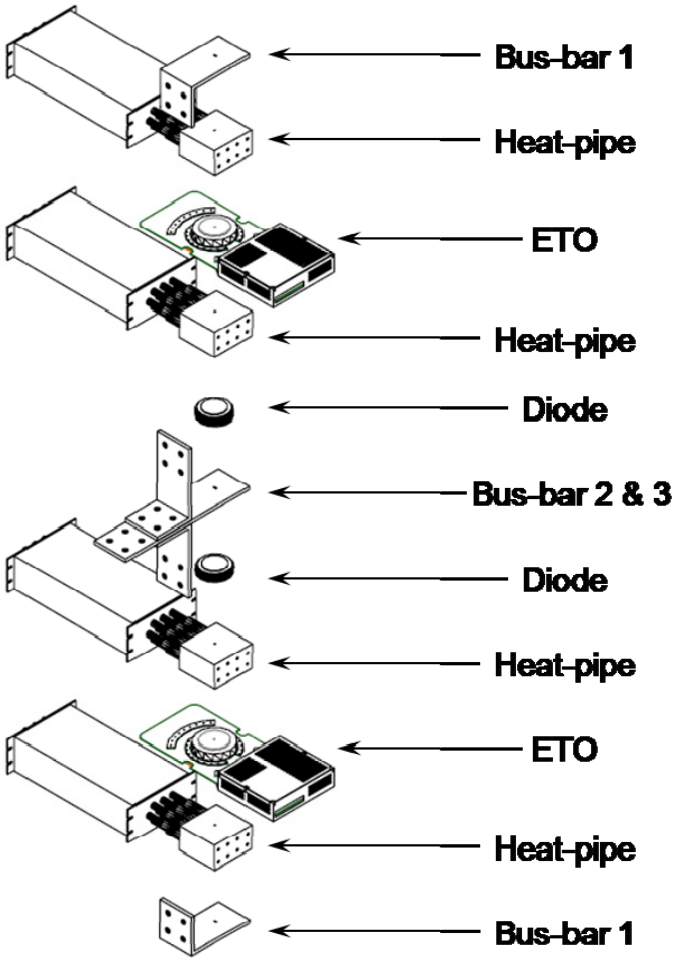


Figure 4-26: Exploded figure of components of the half-bridge circuit

The bus-bars have been split into L-shaped pieces so that the tolerances could be accounted for. Three pieces not form the C-shaped connection required for connecting the anti-parallel diode to the device. The bus-bars are connected together with four heavy gauge bolts per joint. The clamping force holding the bus-bars together is provided by belleville washers and hardened steel nuts. Steel is chosen for its elastic and load bearing properties. Other non-corrosive materials such as stainless steel may also be used, but they are an expensive solution and their use should be limited to large scale production only.

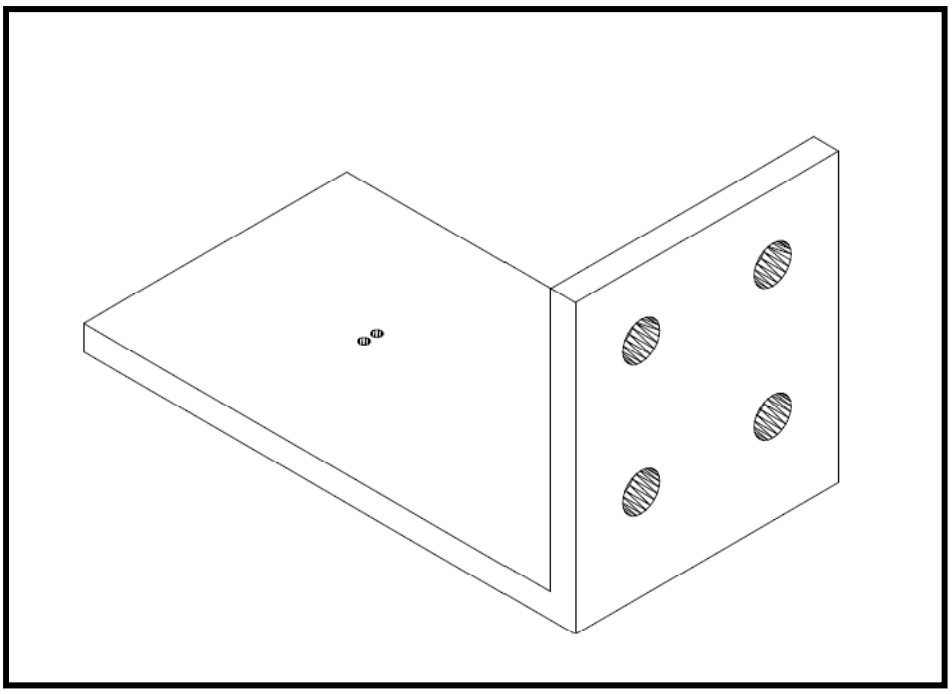


Figure 4-27: Isometric view of bus-bar 1

The Figure 4-27 shows the Bus-bar 1. It can be seen that there are two centering holes on the horizontal leg of the bus-bar so that it could be alinged both at the top and bottom of the stack. The center is slightly off because it is aligned with the center hole of the heat-pipe which is also slightly off-centered. The four large holes seen on the vertical leg of the bus-bar are meant for connection with Bus-bar 2.

The Figure 4-28 shows Bus-bar 2. This bus-bar is used for connecting bus-bar 1 and 3 together. Both the legs of the bus-bar have four holes each. This enables a good rigid connection with bus-bars 1 and 3 using four heavy gauge hardened steel nuts, bolts and belleville washers. Large fender washers are also used to increse the surface area over which the force of the belleville washers is spread.

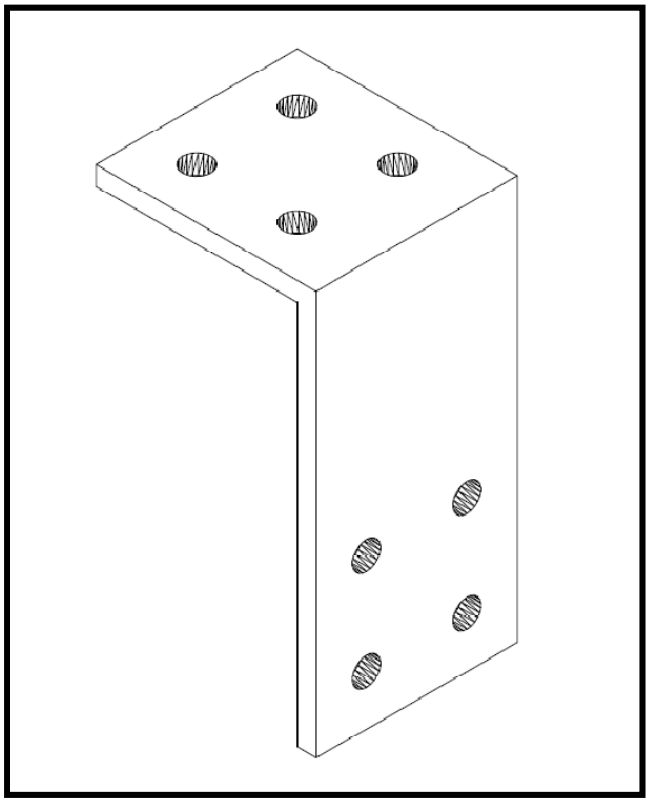


Figure 4-28: Isometric view of bus-bar 2

The Figure 4-29 shows Bus-bar 3. It serves two purposes; it acts as one of the AC connection terminals for the voltage source converter and also forms the connecting point for bus-bar 2. Longer bolts are required at the AC connection side of bus-bar 3 to connect both the Bus-bar 2 together.

Also shown in Figure 4-30, is Bus-bar 4. It is used to connec the DC bus terminals coming from the RCD clamp circuit to the half-bridge circuit. The Bus-bar 4 has to be isolated

because it carries high voltage. The isolation material used for the prototype is kapton tape. It would be better if the isolation material could be directly plated/coated chemically on the bus-bars. That would make the isolation more reliable and robust.

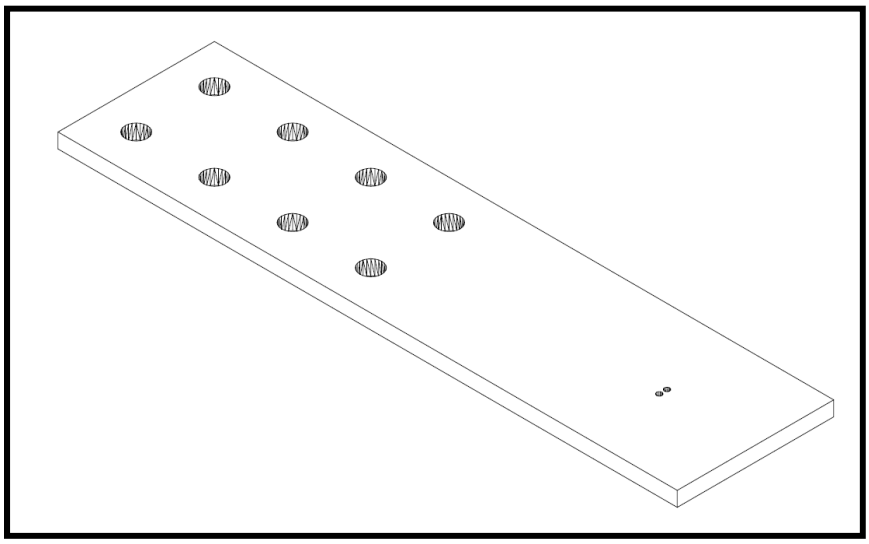


Figure 4-29: Isometric view of bus-bar 3

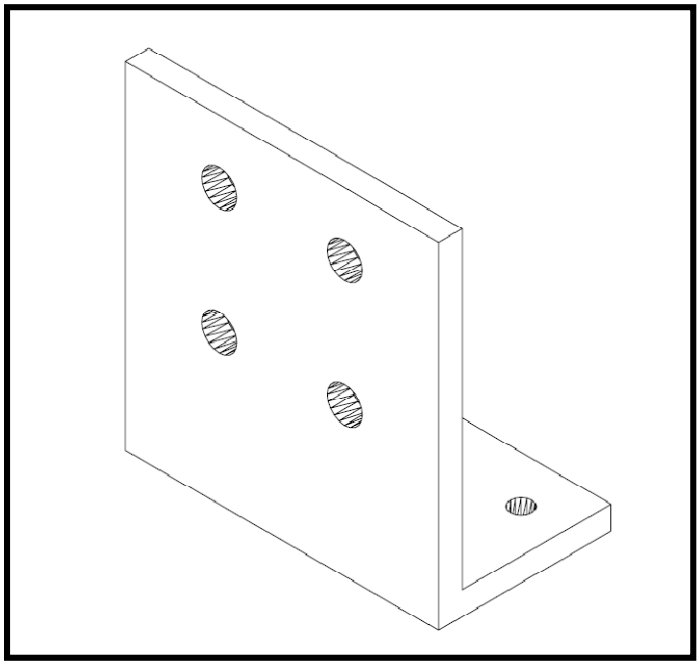


Figure 4-30: Isometric view of bus-bar 4

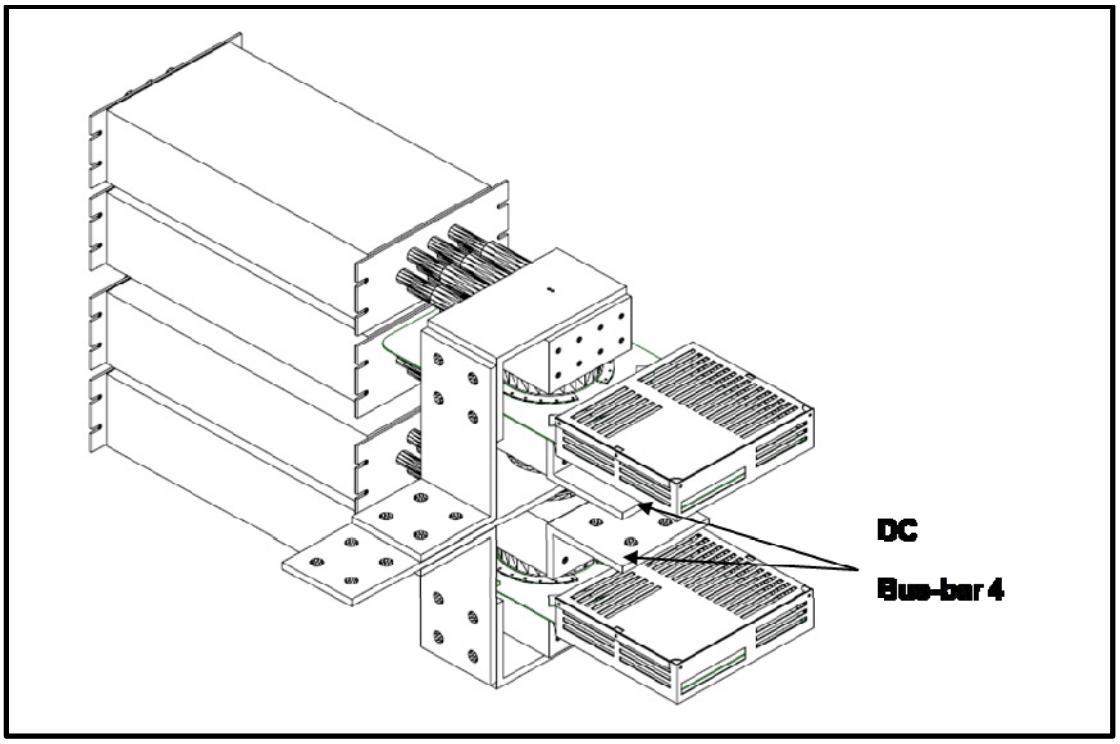


Figure 4-31: Arrangement of the half-bridge circuit

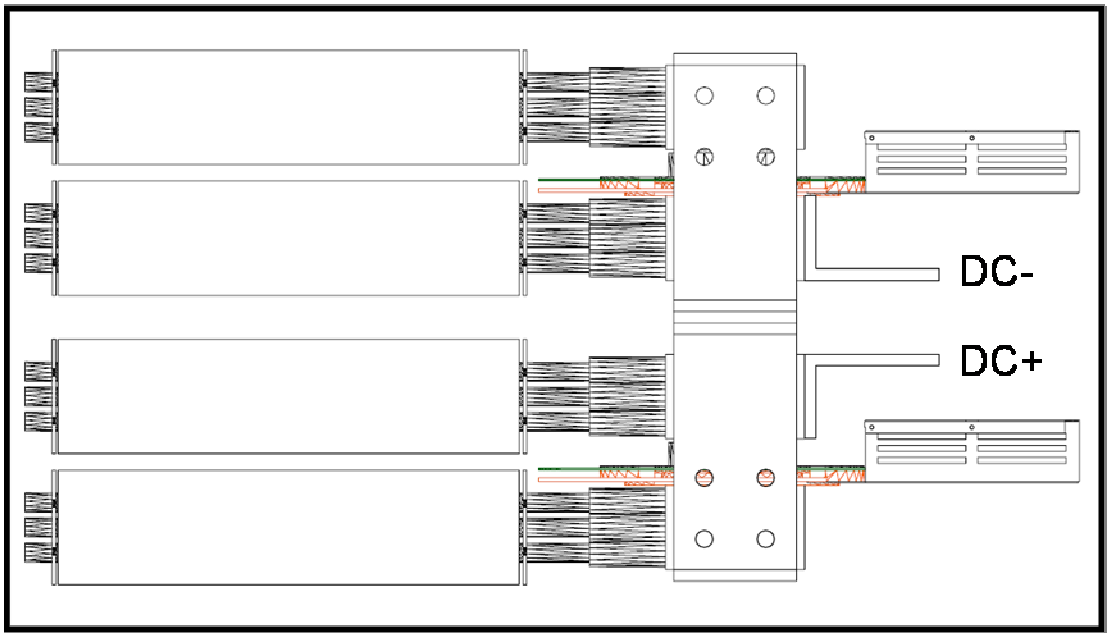


Figure 4-32: Right view of the half-bridge arrangement

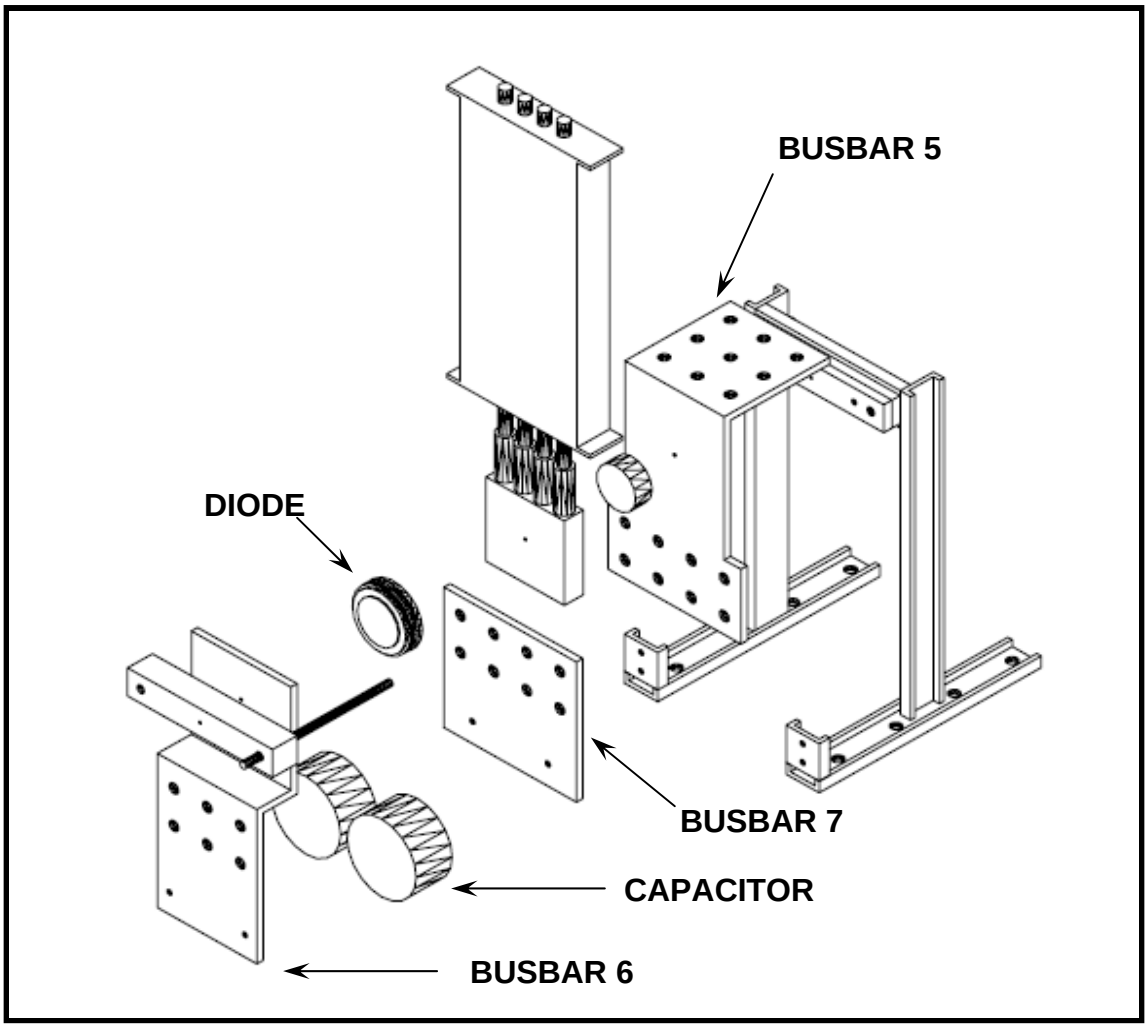


Figure 4-33: Exploded view of RCD clamp circuit

The Figure 4-33 shows the arrangement of the RCD clamp circuit. We can see the Bus-bars 5, 6 and 7 along with the clamp diode, clamp capacitor, 1 kW heat-pipe and the clamp support system. The exploded diagram is also used as the assembly reference diagram for the clamp circuit. It can be noticed that the bus-bars shown in Figure 4-33, do not have two centering holes like this in bus-bars 1, 2, 3 and 4. this is because the bus-bars 5, 6 and 7 do not need to be flipped and installed elsewhere.

Bus-bar 5 serves two purposes shown in Figure 4-34; first, it is used to connect the anode of the diode to the positive DC bus and second, it is used to connect one of the terminals of the

inductor to the positive DC bus. The leg of the bus-bar which has nine holes is used to connect the inductor. The leg which is wider is used to connect the DC bus from both the half-bridge circuits.

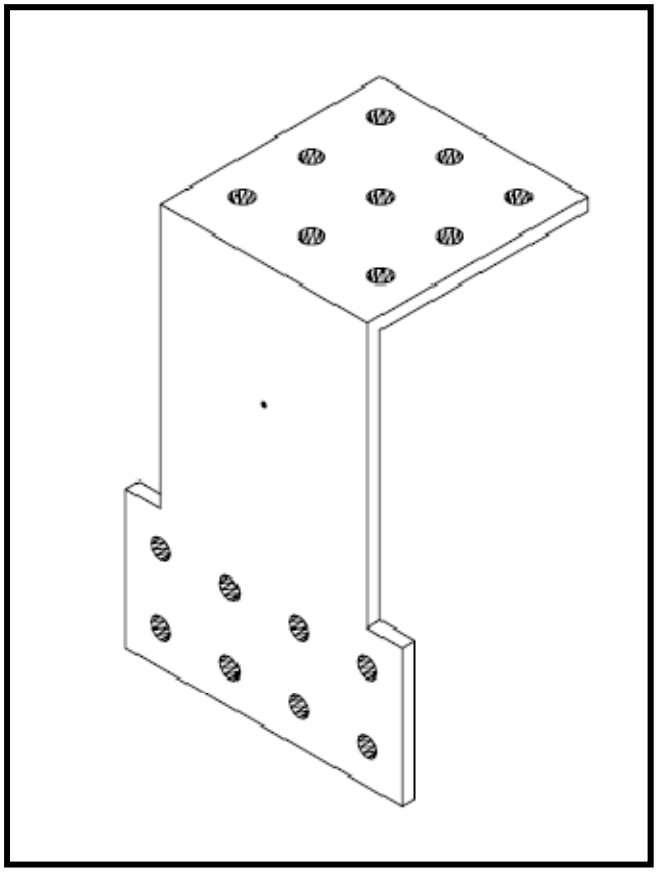


Figure 4-34: Isometric view of bus-bar 5

Bus-bar 6 shown in Figure 4-35, is used to connect the capacitors to the cathode of the diode. It is also used to connect one of the terminals from the resistor bank, thus completing the RCD clamp circuit, electrically.

Bus-bar 7 shown in Figure 4-36 is used to connect the clamp capacitors to the DC negative or the ground terminal of the voltage source converter.

Like the other bus-bars, the bus-bars 5, 6 and 7 also use high strenth steel nuts and bolts. Belleville spring washers are used to put a defined clamping force on the joints. Fender washers help spread that force over a larger area.

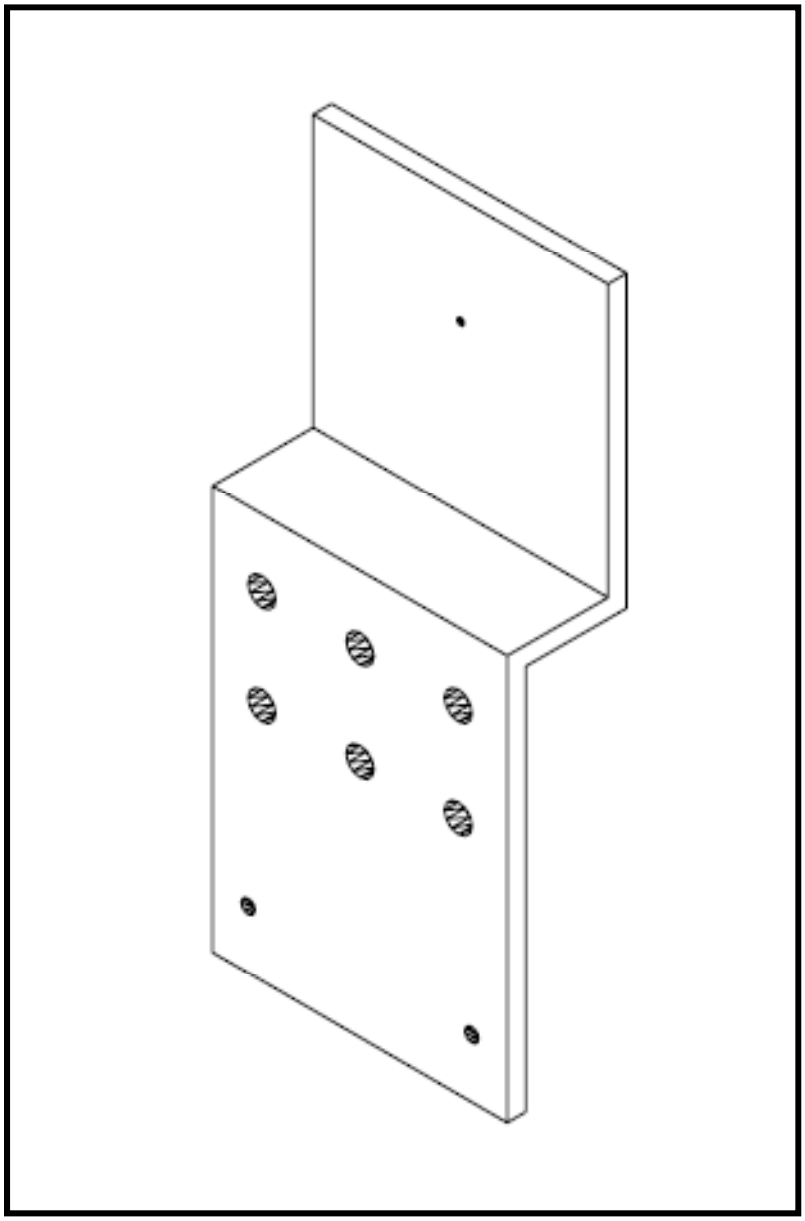


Figure 4-35: Isometric view of bus-bar 6

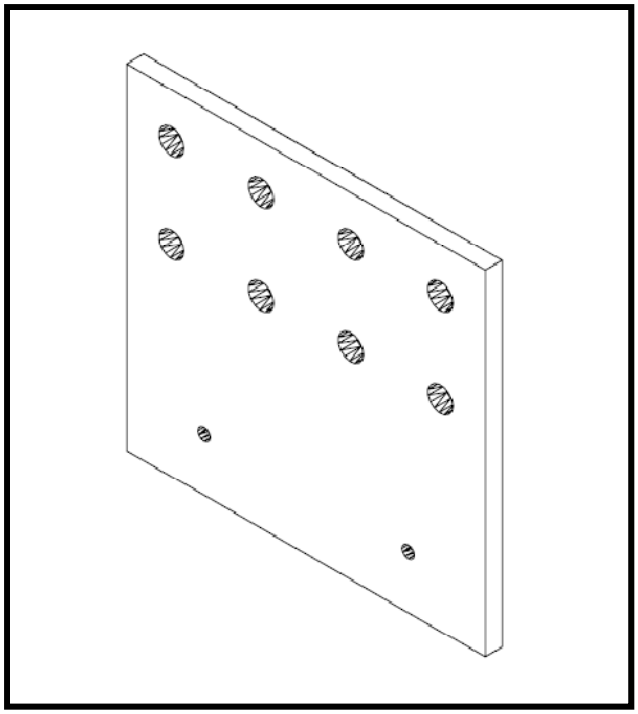


Figure 4-36: Isometric view of bus-bar 7

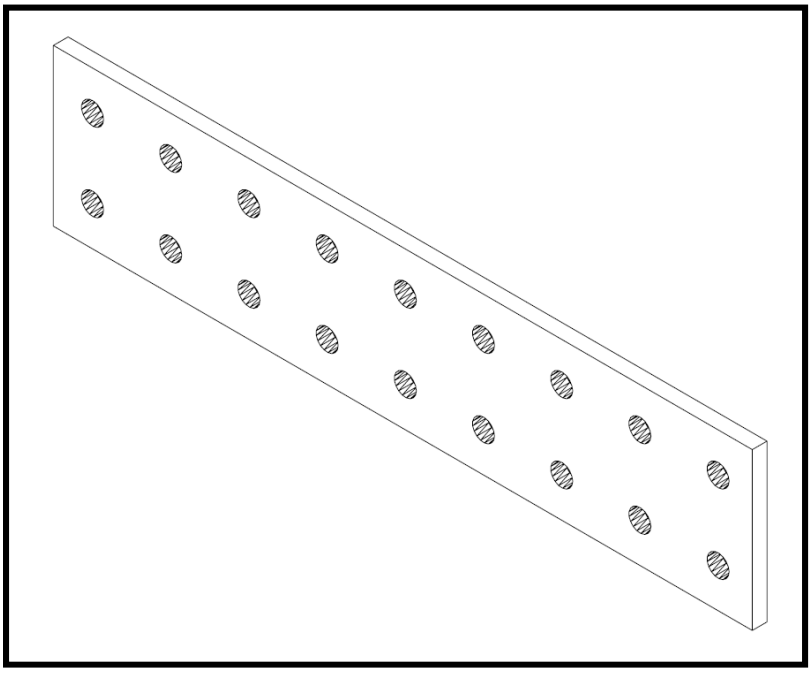


Figure 4-37: Isometric view of bus-bar 8

The final bus-bar, Bus-bar 8 is shown in the Figure 4-37 above. It is used to form both the positive and negative connections of the half-bridge sub-circuits to the clamp circuit. The positive bus is connected between bus-bar 5 and bus-bar 4, whereas the negative connection is between bus-bar 4 and bus-bar 7. These bus-bars are close to each other and carry high voltage on them. It therefore becomes essential to cover these bus-bars with kapton tape for isolation purposes. Several layers of kapton should be utilised in the prototype. In the final production a more permanent solution for isolation, such as coating with insulating polymers or electroplating with special chemicals will be better and more reliable in the extended periods of operation.

4.3.4. Discussion of the support for the H-bridge (12)

The half bridge consists of the switching devices, Emitter Turn-Off Thyristor, anti-parallel diodes, Heat-pipes and bus-bars. The stack is arranged and clamped together using a glass-epoxy clamp from ABB with a clamping force of 40kN. The arrangement of the stack is shown in the figure below.

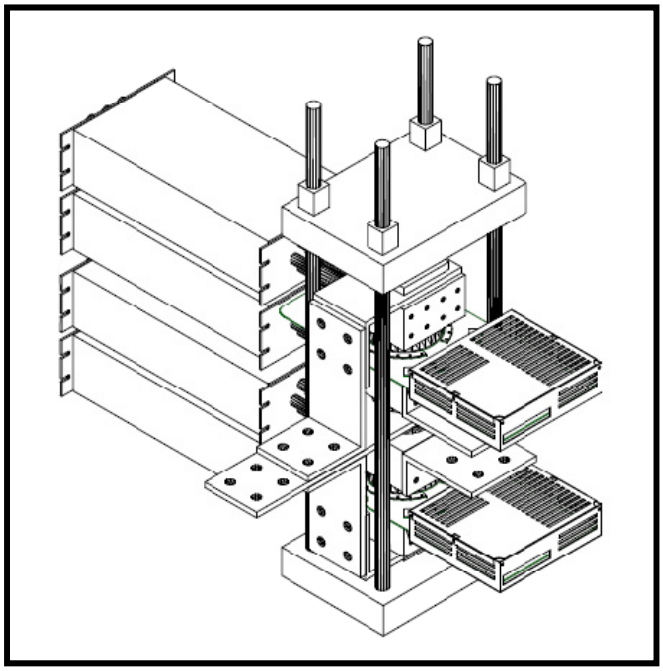


Figure 4-38: Half-bridge circuit clamped together with ABB glass-epoxy clamp

The orientation of the heat-pipes as shown in the figure above is horizontal; for proper operation of the heat-pipes their orientation should be vertical. Thus a method has to be devised to turn the stack by 90 degrees to keep the heat-pipes upright. Looking at the application notes supplied with the ABB clamp, it is found that the clamps have been designed to support devices in the vertical orientation only, as shown above. The vendors are unsure if the clamp could be horizontal at all. Design of a custom-made support for the clamps became necessary for the application and optimal performance of the heat-pipes. The designed support had to take a lot of weight, about 200 lbs. and be precise to avoid cracking or damaging the brittle epoxy clamp. An improperly designed support would twist the four poles of the clamp, causing uneven pressure distribution on the hockey-puck packaged semiconductor devices.

Various schemes were looked into for designing this support. It was obvious that one of the surfaces of the end-blocks of the clamp had to be used for support. The Figure 4-39 below shows the selected surface of the blocks.

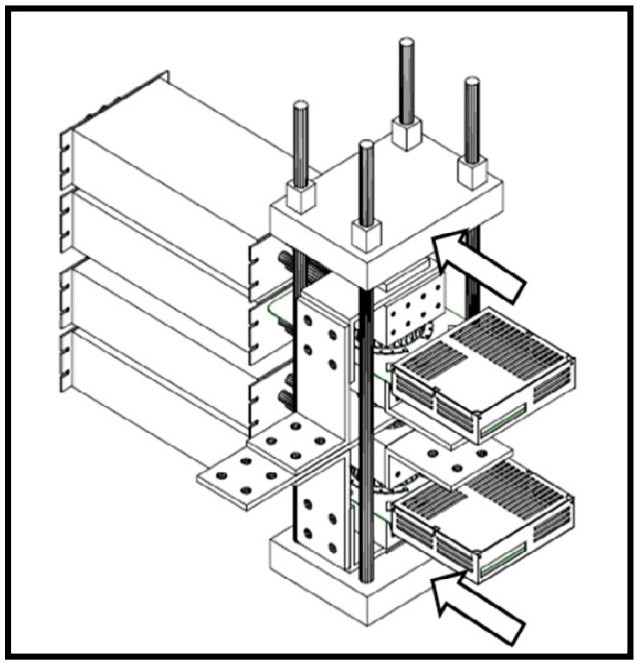


Figure 4-39: Pointing to surfaces selected for mounting on support

The support design was put through three iterations. The first support was designed out of ¼" steel tubing which had a cross-section of 2" x 2". The design was heavy and was estimated to need a lot of machine-time for manufacturing. In addition to the mentioned disadvantages, the support required high-precision cutting tools so that the welding joints were leveled. The support was meant to be bolted on the surfaces of the clamp as indicated in the diagram above. The bolted surface would then be elevated from the base to avoid the gate drive boards from touching the base.

The first and most crucial disadvantage of going with this is that the actual length of the stack varies because of the large 3mm tolerance that were specified when the clamp was under the 40kN force. The length of the total stack could vary by as much as 5 mm. Thus, if the support was rigid the 5mm tolerance could not be accounted for. The two elevated supports, which were to be fixed to the base-plate of the ABB clamp, had to be separated so that the tolerance could be accommodated in the design.

This lead to the second design iteration, where the two supports were separated, keeping the rest of the design same. Now, the basic problem of the tolerance was solved, however the problems associated with the weight and bulkiness of the support still existed.

The third design approach was based on a much simpler principle that is used in construction work in day-to-day life; the use of single/ double u-channel structural beams. The structural beams have sufficient load carrying capacity and do not buckle easily under stress. They are about half in size and weight as compared to the steel tubes. The precision tools that were required to get a level surface in case of a square pipe were not required for a u-channel. A simple grinder could be used to level surfaces for welding purposes.

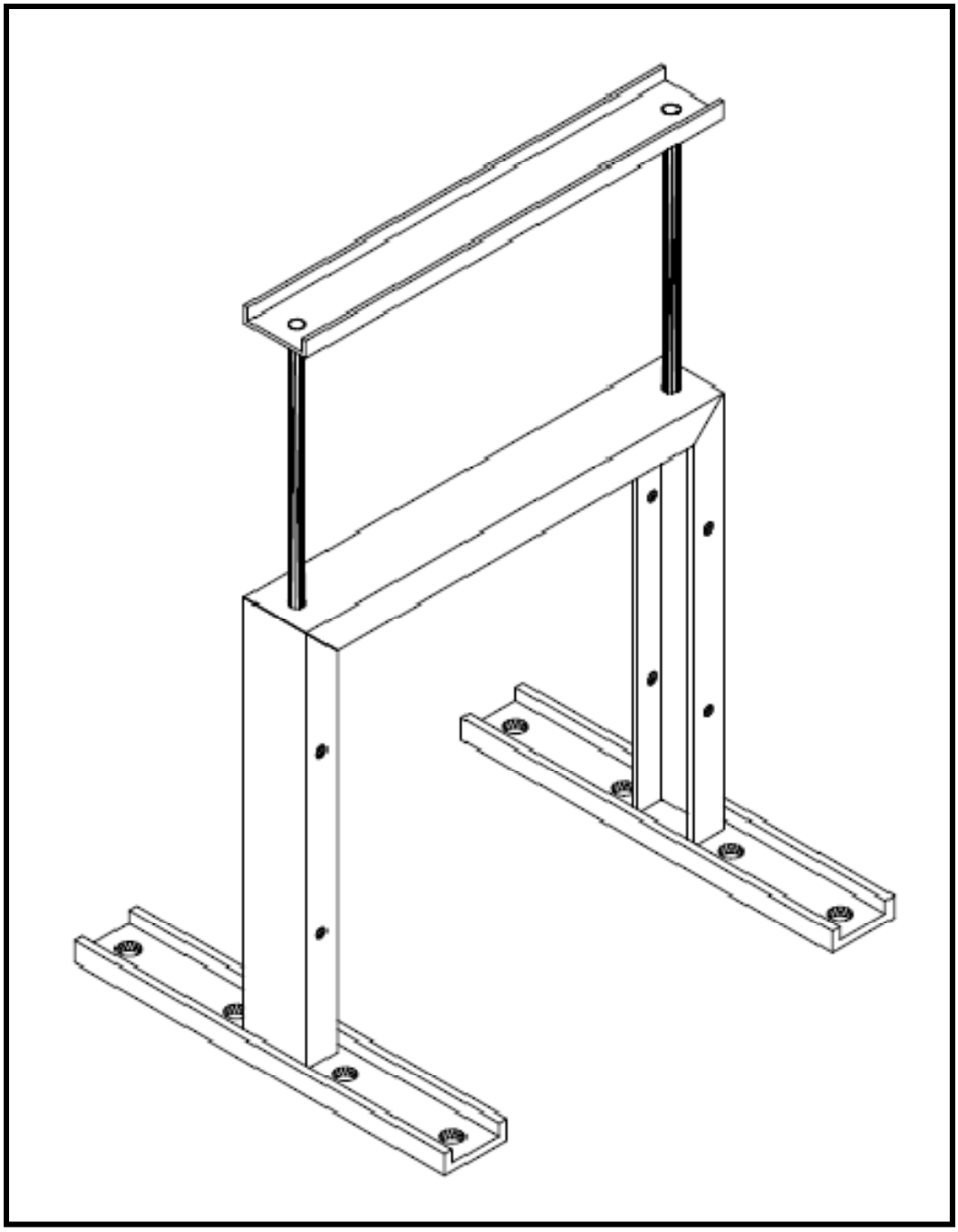


Figure 4-40: Half-bridge support structure

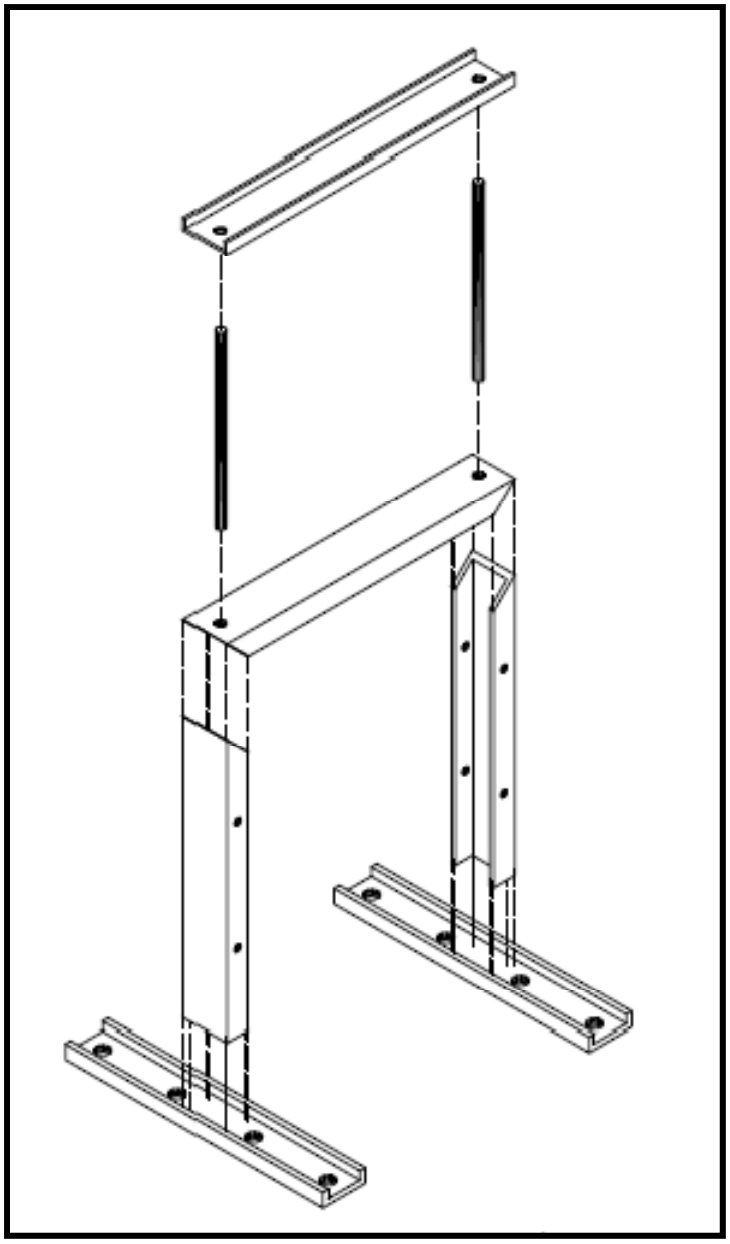


Figure 4-41: Assembly diagram of the support

The above diagram, Figure 4-41, shows the welding diagram, or an exploded assembly diagram of one of the two support legs.

The problem of supporting the structural weight of the H-Bridge was now partially solved; a more complex problem of rigidly holding the structure at one placed still had to be addressed.

The solution was as obvious as the earlier one; using a structural u-channel. A aluminium u-channel was used instead of a steel u-channel to save weight and processing cost. Also an added advantage of using aluminium wherever possible is its corrosion-resistant properties. The upper section of the Figure 4-40, shows this channel section.

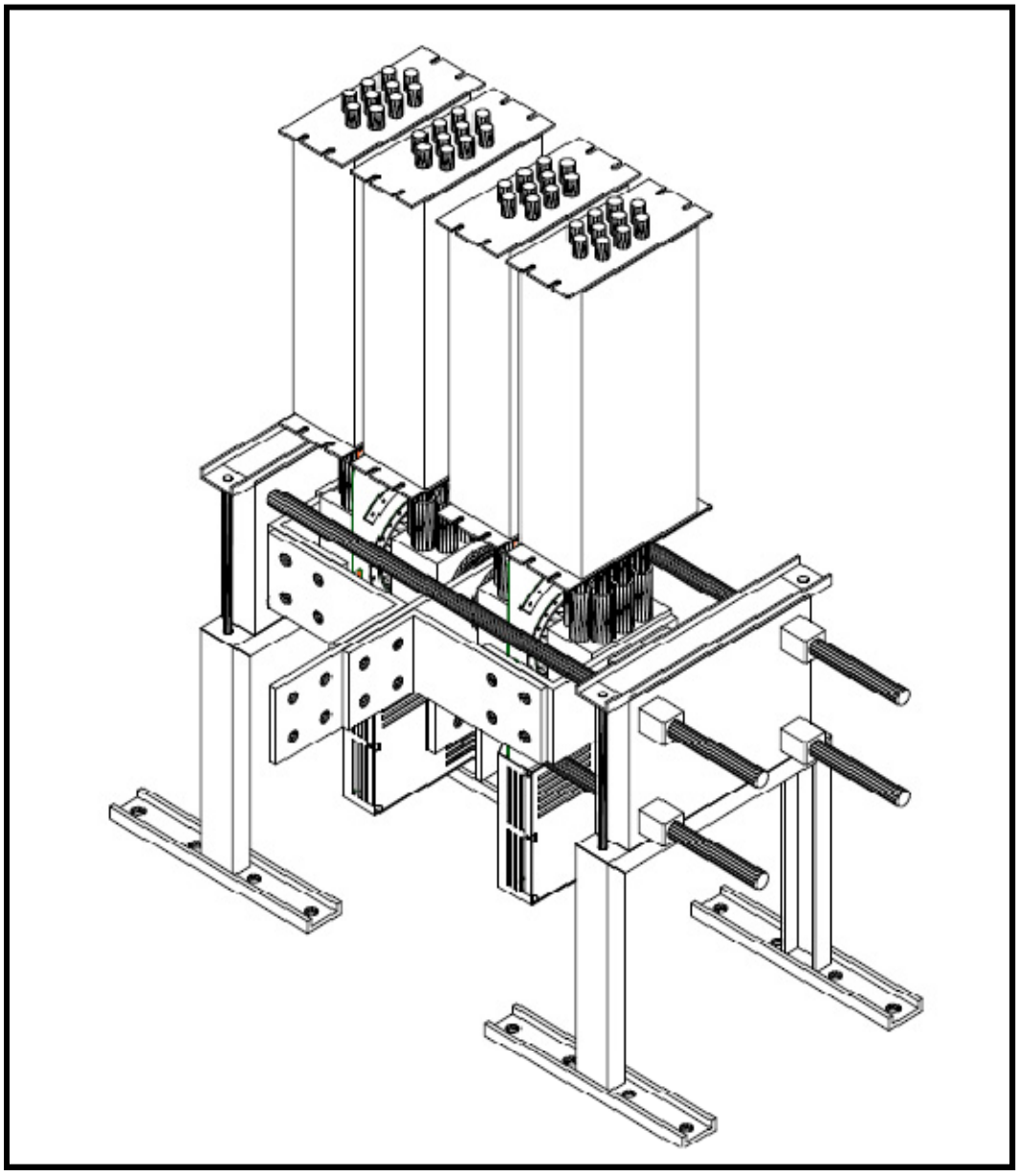


Figure 4-42: Half-bridge circuit on the support

The Figure 4-42 shows the h-bridge structure clamped and supported in a horizontal position using the designed support. The aluminium u-channel is used to hold the structure down and restrict any movement along the y-axis. The lateral movement was prevented by attaching a 1/8" thick glass-epoxy board to the support legs. It served the dual functions of preventing lateral movement and because the material chosen was an electrical-grade insulator, provided isolation between the high-voltage bus-bars and the metal support legs.

4.3.5. Support for the RCD Clamp circuit components:

The clamp circuit consists of a resistor, inductor, diodes and two low-inductance clamp capacitors. The circuit diagram is shown below in Figure 4-43.

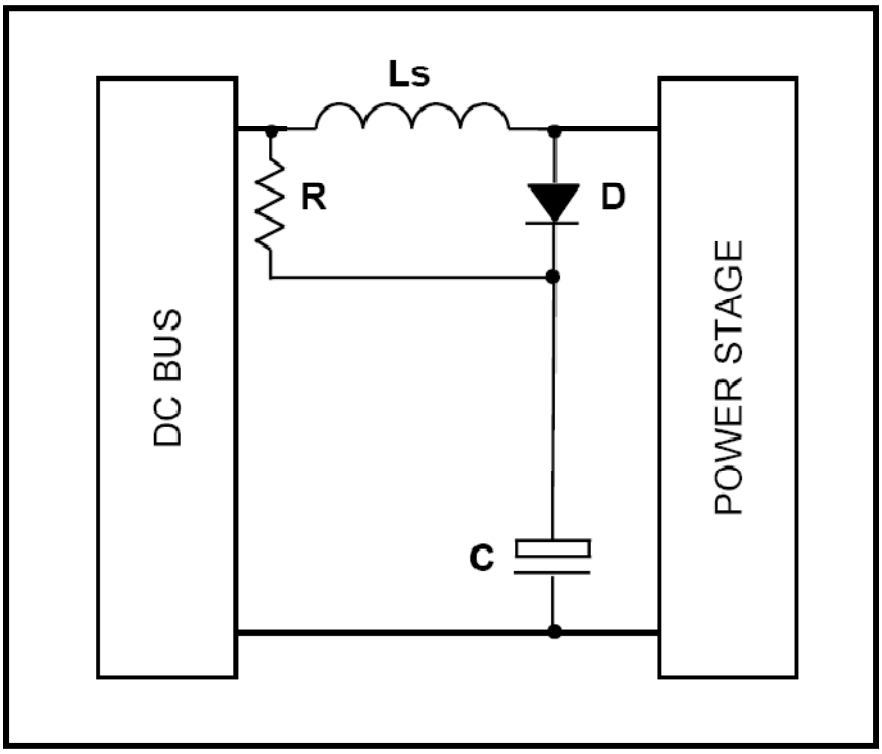


Figure 4-43: Electrical circuit of the RCD clamp

As mentioned before the clamp circuit is made up of resistor 'R', low-inductance clamp capacitor 'C', clamp diode 'D' and snubber inductor 'L'. We are using a hockey puck diode device and a 1.2kW heat-pipe for its thermal management. The clamp capacitor is

specifically packaged for clamp circuit applications and hence has a low series parasitic inductance/resistance. The resistors are the most heat-dissipating components and hence they are mechanically separated from the diode, heat-pipe and capacitor arrangement, however they are electrically connected using heavy gauge cables. Similarly, the iron-core inductor because of its sheer bulkiness is separated from the mechanical assembly and mounted behind the clamp circuit arrangement on a firm, rigid support. The inductor is electrically connected by bus-bars and cable arrangement.

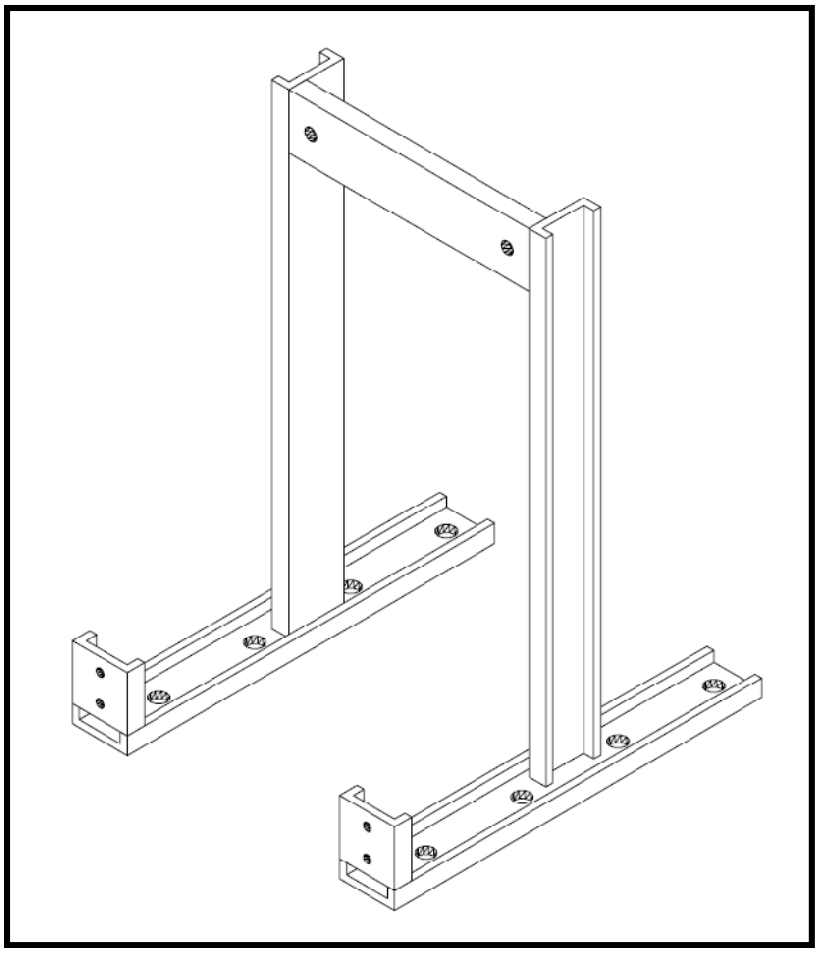


Figure 4-44: RCD clamp support structure

The support designed for the RCD clamp is shown in the Figure 4-44 above. The structure uses the same grade steel u-channel beams used to fabricate the supports for the H-Bridge. The support has similar four holes on the base channel to rigidly fix the support on a frame. Specially fabricated zinc-plates hardened bolts and nuts are used for fixing the support on to a frame. The upper section of the support has a lateral beam joining the two legs of the support and for holding the ABB diode clamp with the heat-pipe, in a horizontal position. The horizontal position is most optimal for thermal design considerations because this enables the heat-pipes to remain vertical, thus enabling maximum heat-energy transport to the ambient.

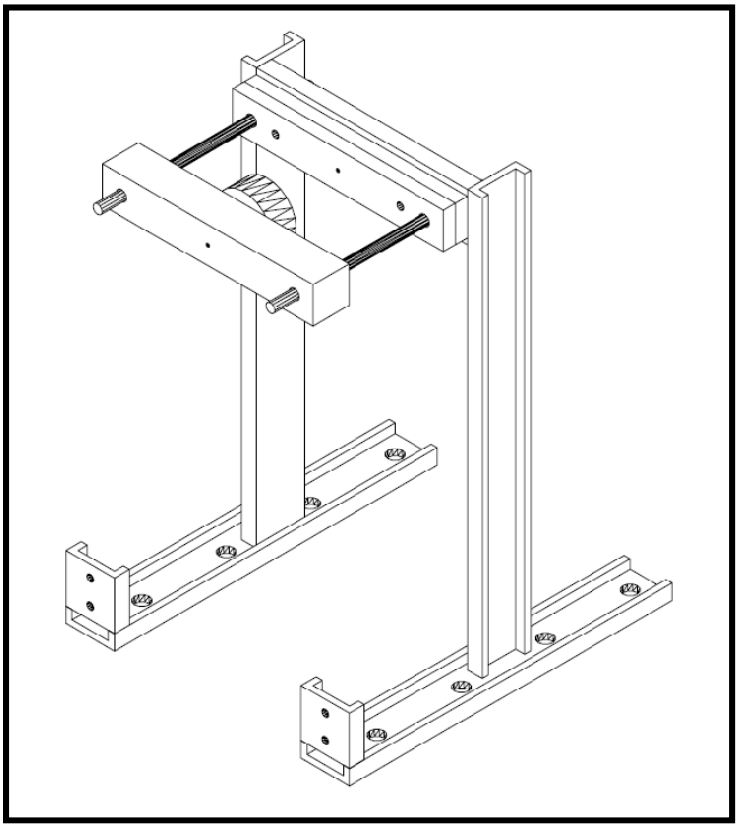


Figure 4-45: RCD support with diode clamp

The Figure 4-45 shows the arrangement of the ABB diode clamp with the support. The base of the ABB clamp is firmly attached to the support as shown in the figure, using right-hand

threaded steel rods. The steel rods serve the dual purpose of fixing the ABB clamp on the support as well as holding the devices in the clamp using a force of 40kN on them. Two smaller projections can also be seen at the base of the support. These projections have two holes each, so that the unsupported end of the ABB clamp could be supported either by some vertical beams or by some hardened epoxy board. Using an electrical grade board is recommended to enhance the isolation properties of the support. Usage of nylon/ epoxy nuts and bolts is also recommended for fixing any vertical structure to the projections and the ABB clamp for better isolation.

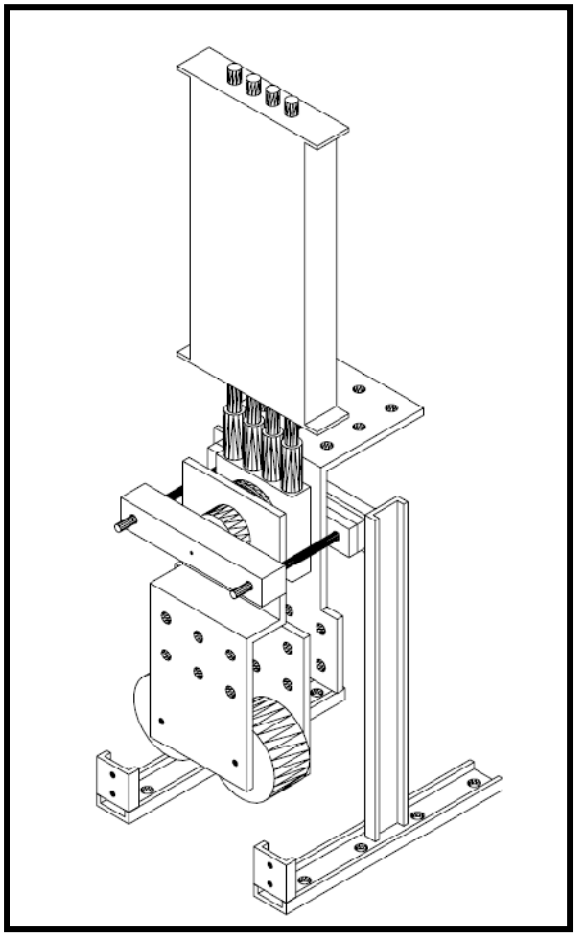


Figure 4-46: Clamp circuit arrangement

The Figure 4-46 shows the arrangement of the components in the clamp circuit. The components are put together with the ABB clamp and electrically connected with bus-bars. The arrangement also shows two clamp capacitors connected in parallel. They are oriented in a way such that the stray inductances (due to the bus-bars) in series with the capacitors are equalized for both the capacitors. This significantly affects the time-response of the clamp circuit. The bus-bar shown protruding at the back of the arrangement is meant for connecting the inductor; additional holes on the buses for the capacitor are for connecting the clamp resistor.

4.4. Interconnection of the major power components

The two main components comprising the power-stage have been discussed. Interconnection of these components finally gives us the H-Bridge power stage we have aimed to build.

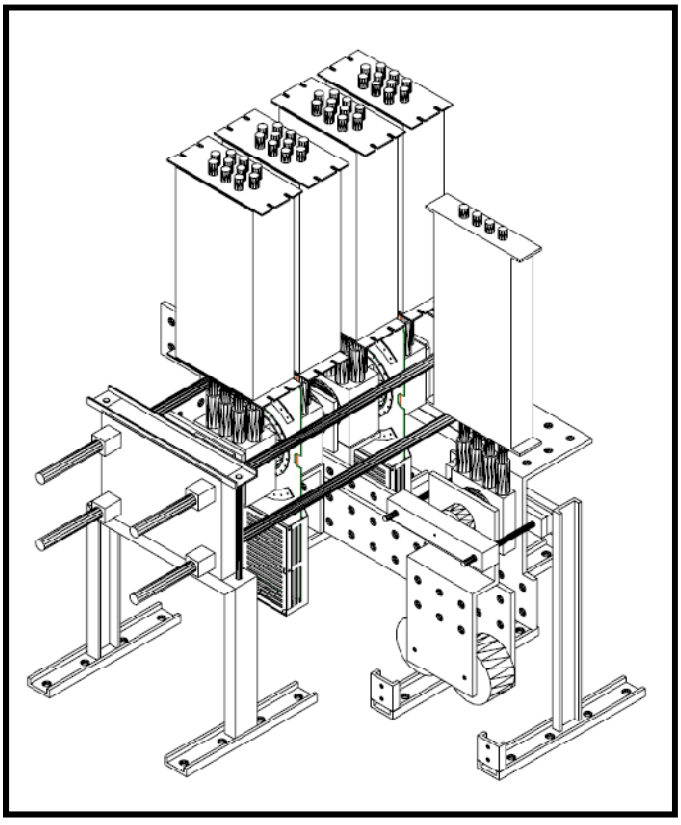


Figure 4-47: Clamp circuit with half-bridge

The Figure 4-47 shows the connection of the half-bridge setup with the RCD clamp circuit with two parallel DC bus-bars. The heat-pipes are vertically oriented as expected, for optimal thermal performance of the system. The interconnecting bus-bars between the two stages are intentionally kept parallel so as to minimize the loop inductance arising between the half-bridge and the RCD clamp circuit. The stray loop inductance leads to large voltage spikes on the DC bus during device turn-offs. The large voltage transients put the semiconductor devices under unnecessary voltage stress, occasionally leading to device failure.

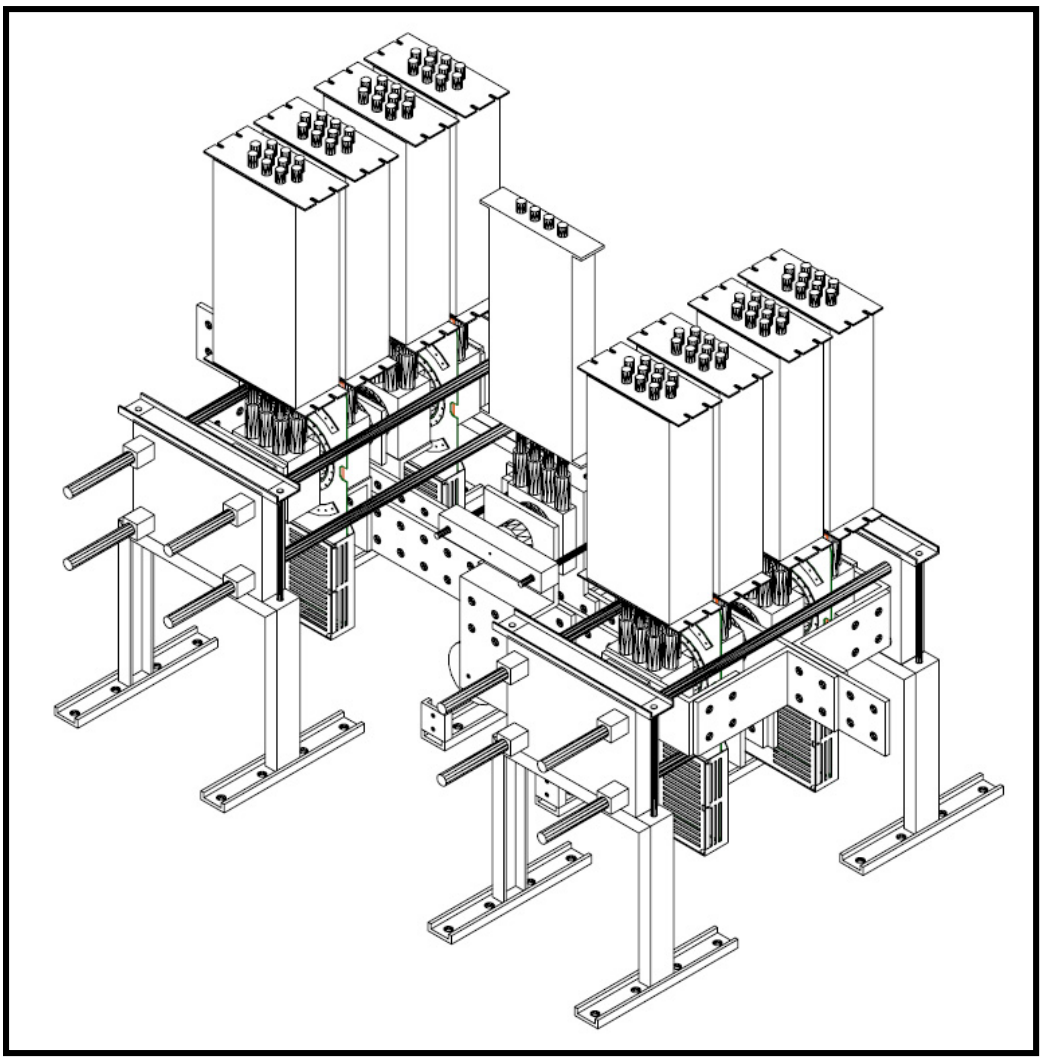


Figure 4-48: H-Bridge with clamp circuit

The Figure 4-48 shows the connection of the entire H-Bridge structure with the RCD clamp circuit. The interconnecting bus-bars between the three stages, two half-brides and the RCD clamp circuit must be identical in length and cross sectional area as much as possible, so that the electrical operation is balanced between the two phase legs of the H-Bridge. Three major components of the converter still need to be connected to the structure shown in Figure 4-43 to complete the power converter. They are the DC bus capacitors, snubber inductor and the clamp resistor array.

Two of the following possibilities were explored, assuming that the entire arrangement would be split in two levels and mounted on a frame with two shelves:

a. Keep the snubber inductor along with the large DC capacitors on the lower shelf and place the clamp resistor array with its thermal management behind the RCD clamp arrangement on the upper shelf.
b. Place the snubber inductor behind the RCD clamp circuit arrangement and keep the clamp resistor array on the lower shelf with the DC bus capacitors.

For option ‘a’, we have an advantage of keeping the resistor array mechanically close to the RCD clamp arrangement, so that there will be no need of long interconnecting cables between them. However there are two major disadvantages that can be easily seen form the Figure 4-49 and Figure 4-50 respectively. First, the resistor array along with its own heat-sinks has a very large foot-print which does not easily fit behind the RCD clamp arrangement. Second, the hot air coming from the heat-pipe used in the RCD clamp will directly flow into the heat-sinks of the resistor array. This will not only affect the thermal performance of the heat-sink, but also create more resistance for air to flow along this series path of the heat-pipe and the heat-sink. Option ‘a’ is not viable for the power converter design.

As for option ‘b’, the snubber with a small footprint easily fits behind the RCD clamp arrangement without increasing the overall footprint of the converter significantly. Since the resistor array will be dissipating about 5-6 kW of thermal energy, it will need a dedicated air

duct for supplying fresh air at the ambient temperature. This is easily possible when the resistor array is kept along with the DC bus capacitors on the lower shelf. These points are highlighted in Figure 4-51 and Figure 4-52 respectively.

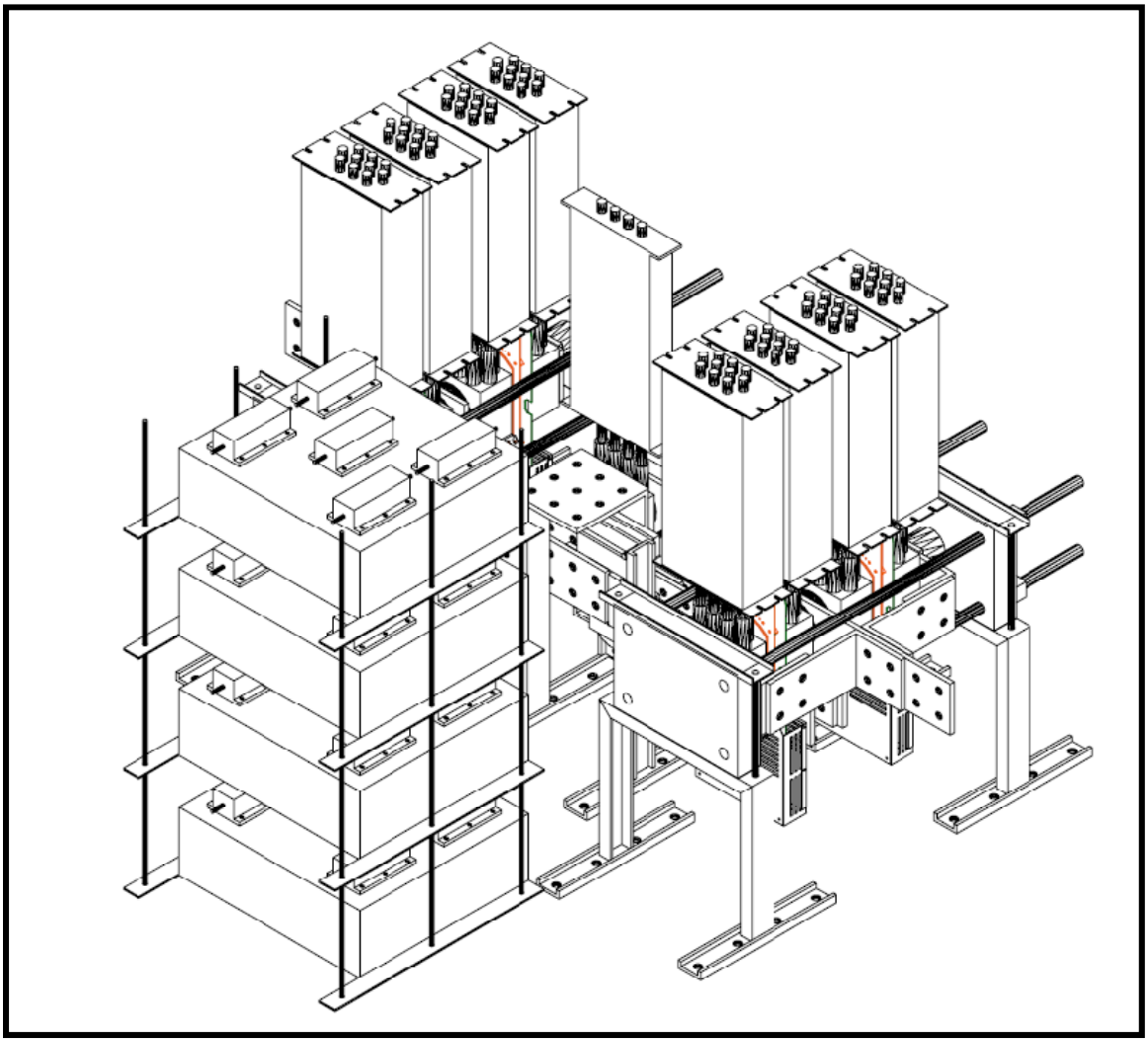


Figure 4-49: Isometric view of H bridge with clamp resistor

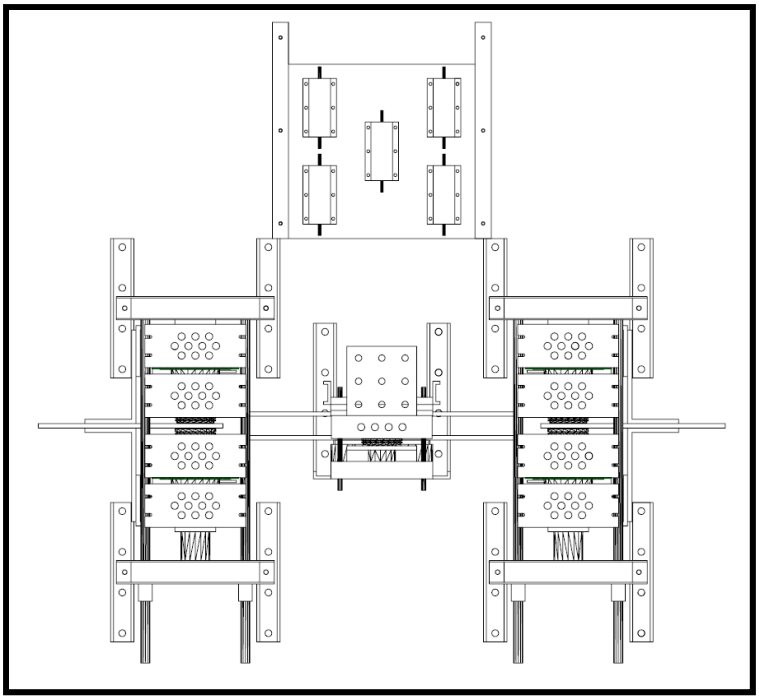


Figure 4-50: Top view of H-Bridge with clamp resistor

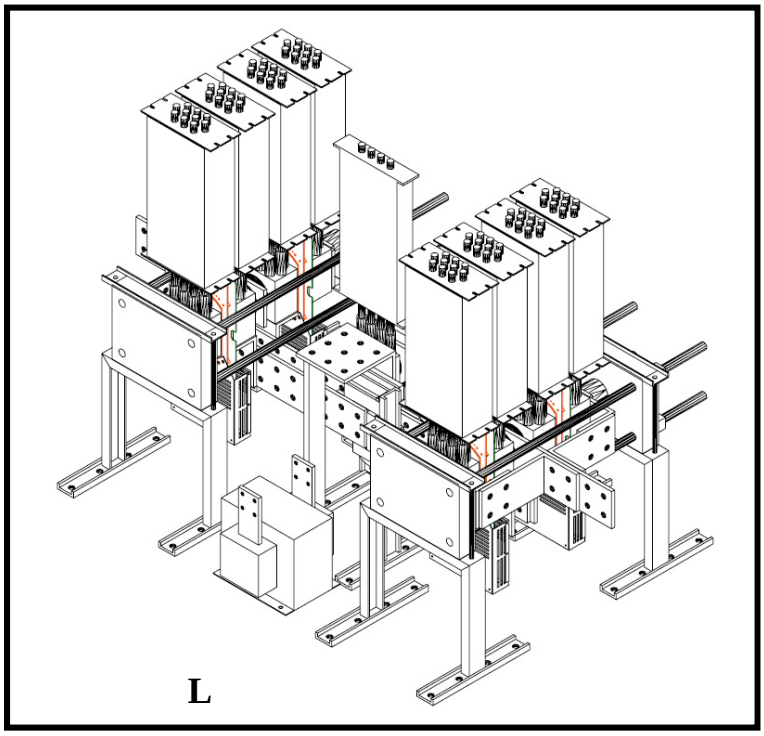


Figure 4-51: Isometric view of H-Bridge with snubber inductor

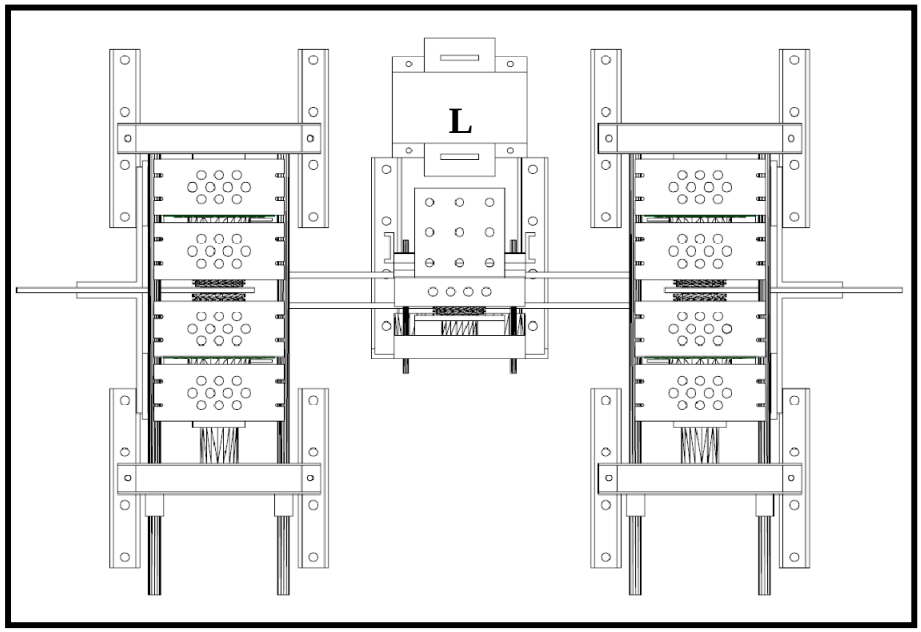


Figure 4-52: Top view of H-Bridge with snubber inductor

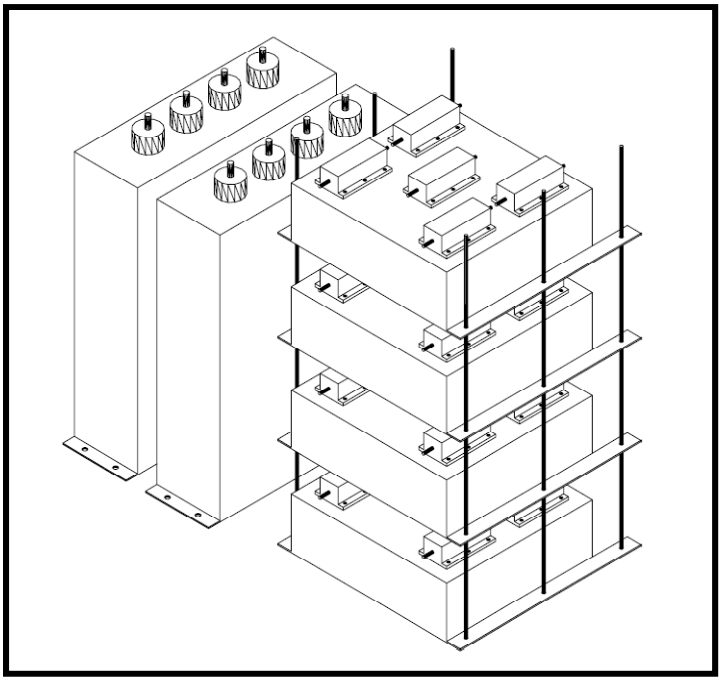


Figure 4-53: Clamp resistor stack arranged with the DC capacitors

The Figure 4-53 shows the arrangement of power components on the lower shelf of the two-tier cabinet. The DC Bus capacitors are to be connected in parallel, hence they are placed as close to each other as possible to reduce any stray inductance in between them. Such stray inductances between large value capacitors lead to oscillations on the DC bus during converter operation. Such oscillations can cause instability in control and unnecessary transients on the switching devices.

The Figure 4-53 also shows the resistor array, whose design has been discussed in detail in the thermal management chapter previously. It basically comprises of 20 resistors of 22 ohms each connected in parallel and mounted n four separate heat-sinks. The thermal resistance of the heat-sinks is sufficient to dissipate 6 kW of thermal energy during normal operation of the converter. The flow requirement of air on the heat-sinks is about 100 CFM.

4.5. Conclusion

The overall mechanical design of the H-Bridge building block has been explained in this chapter. A modular design approach has been undertaken while designing the support system and the bus-bars so that each individual component could be reused. Simple and quick assembly was also one of the important criteria influencing the design procedure (11). Design considerations that are required to minimize stray inductances and parasitic have been explained in depth with examples and experimental results. The theory of contact resistance arising from a contact between two metals has also been highlighted with experimental data. These fundamentals have been considered while designing the bus-bars and assembling them to obtain optimal system performance.

5. THERMAL MANAGEMENT DESIGN

5.1. Rationale

There are four modes of heat transfer; conduction, convection, radiation and phase-change. The latter of the above listed phenomenon is rarely known to be used in high-power converters for cooling purposes. But due to the increasingly complex water/ fluid cooled systems, there has been significant research effort put into phase-change heat transfer techniques. Starting off from smaller desktop cooling solutions to now available sophisticated kilowatt range heat-pipes, the phase-change heat-transfer techniques have grown both in complexity and functionality. They now replace water cooled systems in traction drives and high-power converters. As discussed in chapter three; heat-pipes have proven to be the best 'passive' air cooled heat energy dissipating medium. This chapter will continue with the discussion started in chapter three, and will focus more on the actual performance of the heat-pipes in a real world high-power converter application.

5.2. Organization of the chapter

The chapter will mainly discuss the performance characteristics of a phase-change based heat-pipe cooled system in a high power converter application. The thermal load on each heat-pipe was already established in chapter three; now the requirement of airflow for each heat-pipe based cooling device has to be established. A thorough investigation has to be done on air-movers, ducting systems and other related equipment to ensure that correct hardware is selected to meet the imposed requirements. For cooling the clamp resistor array, a simple aluminium bonded-fin heat-sink is selected. Since an array of such heat-sinks will be required to dissipate the heat load spread over a large number of resistors, proper attention has to be paid on the air-flow received by each of the heat-sinks. The chapter is concluded with a proposed thermal management system and its estimated cooling performance. The temperature rise on the system is calculated with an equivalent electrical model of the system.

5.3. Equivalent electrical circuit for heat-transfer

The definition of thermal resistance of any component, in simple terms, is an electrical representation of the thermal characteristics of the system. Thermal resistances can be used along with current sources representing thermal loads and voltage sources representing ambient temperatures to predict the temperature at each node of the representative circuit. Thermal capacitances can be added to the circuit to measure the rate of rise of temperature with respect to time. However, for this discussion, only thermal resistances will be considered.

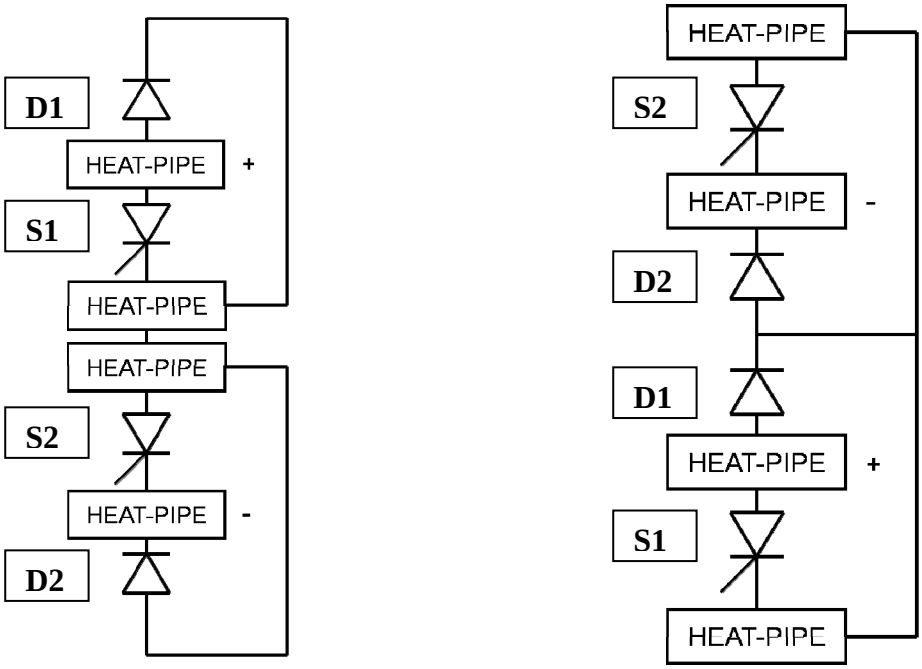


Figure 5-1: Two possible arrangements of devices in an H-Bridge Phase leg

Figure 5-1 shows two possible arrangements of devices in a phase leg of a H-Bridge converter. As per previous discussion in chapter four, the arrangement shown in Figure 5-1.ii is the most optimum arrangement in terms of parasitic inductances in the circuit. A detailed analysis with simulation has to be now performed on both the topologies to check which one

will be optimum in terms of thermal performance. Both the arrangements will be converted into electrical-equivalent models, to estimate junction temperature of the devices for that particular arrangement. A comparison of the device junction temperatures occurring in both the arrangements will then be compared to select the one with the least temperature profile. However, there has to be a trade-off made between the stray inductances and junction temperatures.

Let us first consider the thermal model for arrangement shown in Figure 5-1.i

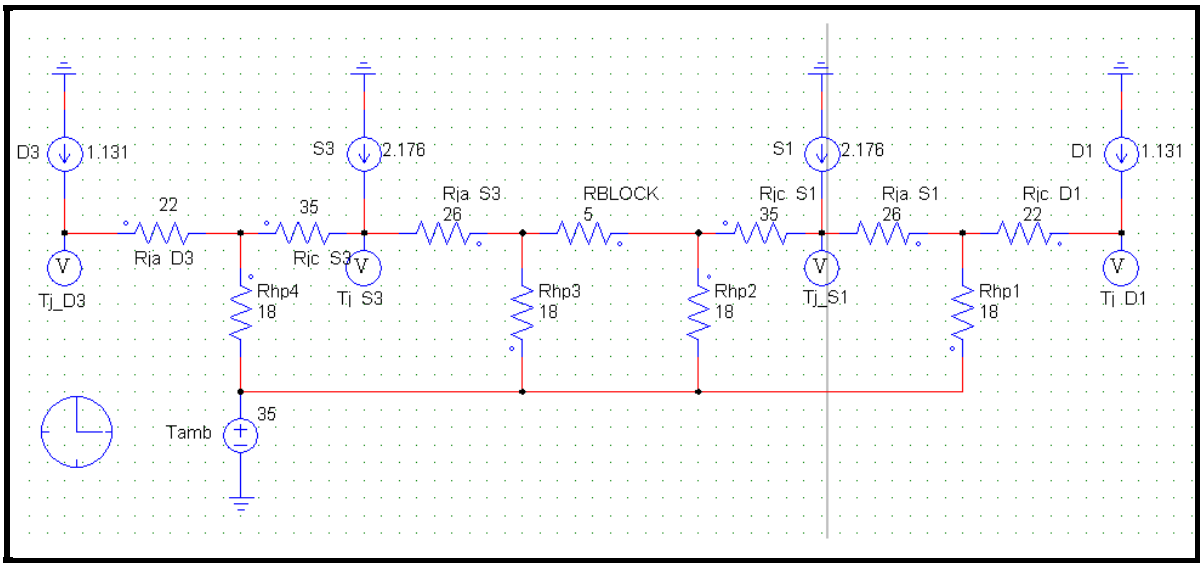


Figure 5-2: Electrical equivalent model for arrangement in Figure 5-1.i

In Figure 5-2, the resistances represent the thermal resistances of the devices; thermal resistances between the junction-case are denoted as R_{jc} and thermal resistances between junction-ambient are denoted as R_{ja}. The voltage source represents the ambient temperature of the enclosure. The current sources represent the heat-load on each device. The simulation is carried out and the junction temperatures of each semiconductor device are measured. The results are tabulated for both the capacitive and inductive modes of operation.

Table 5-1: Temperature profile of devices in capacitive/inductive mode (t_{amb} = 35 °C)

Devices	Capacitive (°C)	Inductive (°C)
S1	99.3	90.2
S2	99.3	90.2
S3	95.5	86.72
S4	95.5	86.72
D1	98.2	94.8
D2	98.2	94.8
D3	93.8	91.1
D4	93.8	91.1

Table 5-2: Temperature profile of devices in capacitive/inductive mode (t_{amb} = 55 °C)

Devices	Capacitive (°C)	Inductive (°C)
S1	124.3	115.2
S2	124.3	115.2
S3	120.5	111.7
S4	120.5	111.7
D1	123.2	119.7
D2	123.2	119.7
D3	118.8	116.1
D4	118.8	116.1

From the above tabulated results in Table 5-1 and Table 5-2 it can be clearly seen that there is non-uniformity in the distribution of temperature over all devices. This occurs mainly because of the single side cooling of the diode and the difference in the anode and cathode side thermal resistance of the ETO. The difference in thermal resistance has occurred because of the presence of a large area copper plate on the cathode side of the ETO. The temperature

range of the devices is well below the 125 °C limit for silicon based devices; there is sufficient room for 1.2 p.u. to 1.5 p.u. overload operation of the STATCOM in capacitive mode, for an ambient of 35 °C.

Simulations were also conducted for an ambient temperature of 55 °C. The average temperature of the switches is about 124 °C and the diode is 120 °C. The converter can still function correctly, but there will be no room for any overloads at that ambient temperature.

Let us now consider the thermal model for arrangement shown in Figure 5-1.ii

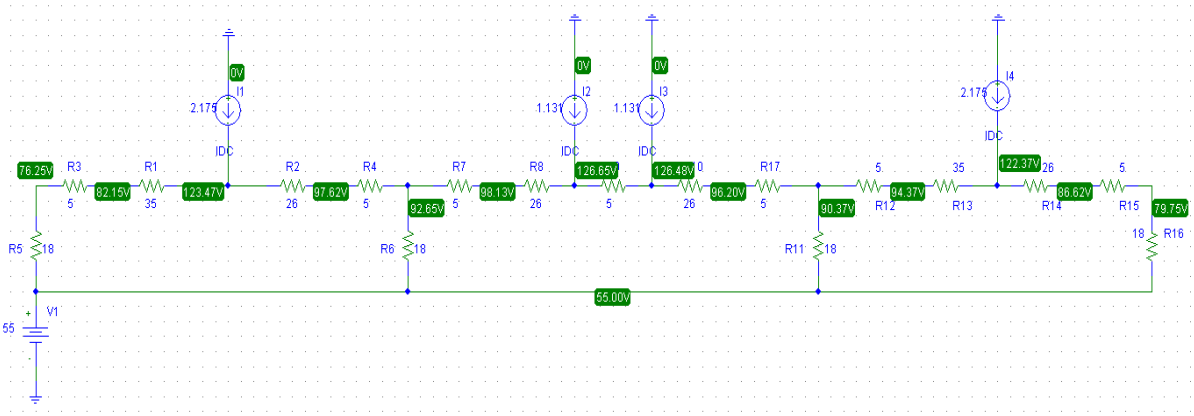


Figure 5-3: Electrical equivalent model for arrangement in Figure 5-1.ii

There is a certain advantage of having the diodes together instead of being at the extremes of the stack. The heat energy generated by the diodes can now be absorbed from both sides of the diode, thus improving thermal performance and better heat-load sharing between devices.

Table 5-3: Temperature profile of devices in capacitive/inductive mode (t_{amb} = 35 °C)

Devices	Capacitive (°C)	Inductive (°C)
S1	103.47	87.8
S2	103.47	87.8
S3	102.37	89.1
S4	102.37	89.1
D1	106.65	82.1
D2	106.65	82.1
D3	106.48	83.2
D4	106.48	83.2

Table 5-4: Temperature profile of devices in capacitive/inductive mode (t_{amb} = 55 °C)

Devices	Capacitive (°C)	Inductive (°C)
S1	123.47	112.8
S2	123.47	112.8
S3	122.37	114.1
S4	122.37	114.1
D1	126.65	107.2
D2	126.65	107.2
D3	126.48	108.2
D4	126.48	108.2

As compared to the temperatures in Table 5-1 and Table 5-2, the temperatures in and Table 5-4 are lower by about 3 to 4 degrees. This leaves some room for sustaining more overloads for longer times. It is also observed that the temperature differences between the devices have decreased to just 1 or 2 degrees, as compared to the 4 to 5 degrees between upper and lower devices of the stack. This leads to the fact that the temperature distribution has become more uniform. Thus it can be concluded that, arrangement of devices as shown in Figure 5-1.ii has dual advantages over other possible arrangements. The dual advantages can be listed as:

a. Minimal parasitic inductances, and
b. Lower junction temperatures; better temperature distribution

A thorough analysis, similar to the one discussed in this chapter should be performed to obtain optimal and efficient performance.

The results can also be summarized in the form of bar graphs. The uniformity of temperature distribution can be easily seen through bar-graphs.

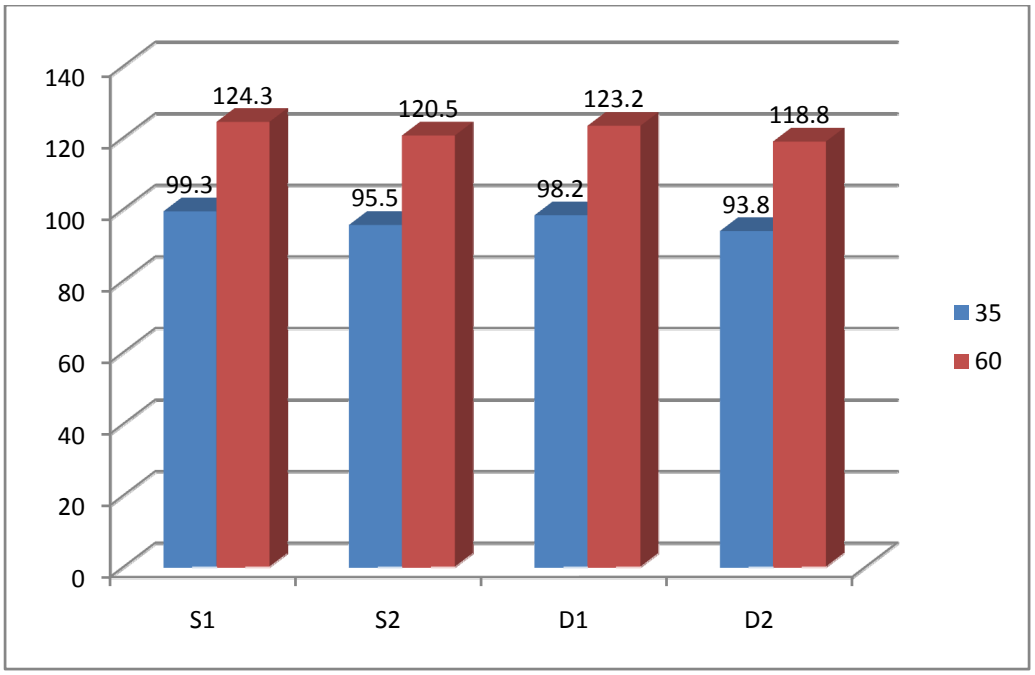


Figure 5-4: Summary of results for first arrangement

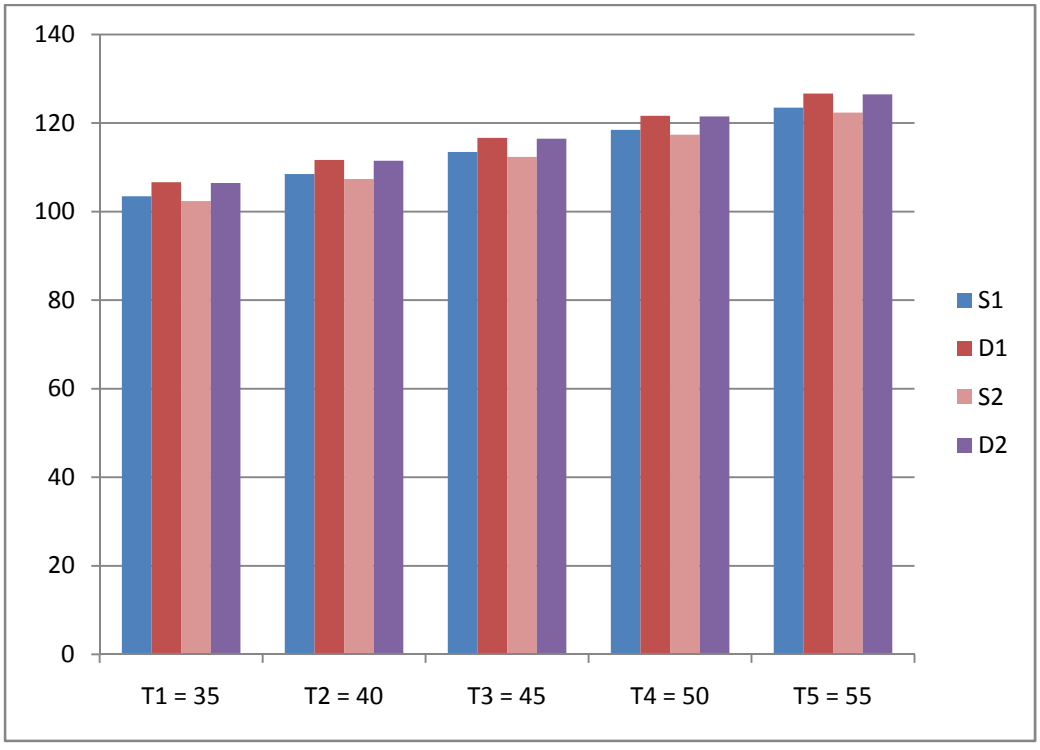


Figure 5-5: Summary of results for second arrangement

5.4. Air flow design

The effectiveness of any air cooled thermal management system greatly depends on the correct design of the air movement and distribution system. The process starts with calculation of the air-flow requirement for the individual heat dissipating components present in the enclosure (13). Once the air-flow requirement is calculated, a pressure drop analysis of the individual components is done to ensure that a correct air-mover is selected (14). This is again done using an electrical analogy of the airflow system where, the pressure drop across a component is analogical to a voltage, the air-flow is analogical to the current and the static-pressure head is analogical to the resistance value of the component. However, unlike the electrical definition of Ohm's Law, the resistance (static-head) is equal to the ratio of the pressure drop across the component to the square of air-flow through the component (15).

$$S = \frac{\Delta P}{CFM^2} \quad \text{..... Equation 5-1}$$

Here, ΔP denotes the pressure drop across the component

S denotes the static pressure head of the component

CFM denotes the air flow required through the component in cubic feet per minute

Another important formula that is used for estimation of air flow through the system is given by:

$$CFM = 1750 * \frac{W}{\Delta T} \quad \text{..... Equation 5-2}$$

Where, CFM again denotes the air flow through the system in cubic feet per minute

W denotes the heat load on the component in kilo-Watt

ΔT denotes the allowable maximum temperature rise on the system

The formula in Equation 5-2 is purely empirical and has been derived for use in the system under consideration only. Individual components now have to be examined to calculate their air-flow requirement for a given allowable temperature rise of the component.

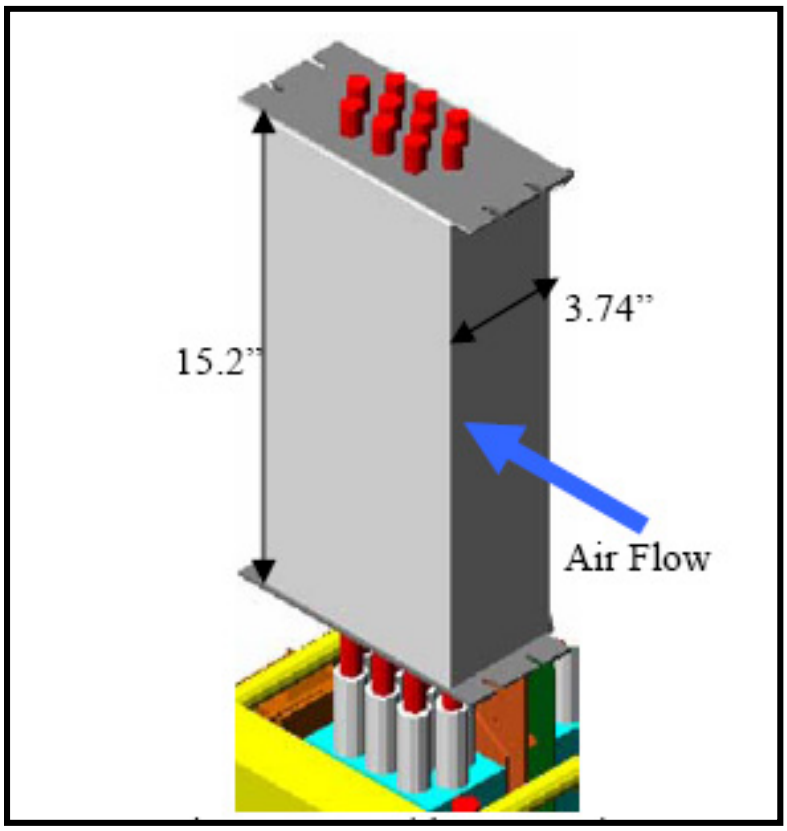


Figure 5-6: Analysis of the 2.2 kW Heat-Pipe

The heat-pipe shown in Figure 5-6 is the 2.2 kW heat-pipe used in the H-Bridge phase-leg to transport heat from the semiconductor devices to the ambient using phase change mechanism. The air flow through the fins of the heat-pipe specified by the vendor is 5 m/s in the direction of arrow shown in the figure. The dimensions of the cross section of the heat-pipe are calculated to obtain the area and together with the air flow velocity we get a volumetric sir flow number of 388.39 cubic feet per minute. Thus a minimum air-flow of 388 CFM is required for the heat-pipe to function to its full capacity.

Table 5-5: Air-flow requirement on the 2.2kW heat-pipe

Component	2.2 kW Heat-pipe
Minimum Air-flow (CFM)	388
Pressure drop (inch H2O)	0.315
Static pressure head (Ohms)	2.0879e-7
ΔT (°C)	9

The static pressure head listed in the table above is the electrical equivalent of the actual physical quantity.

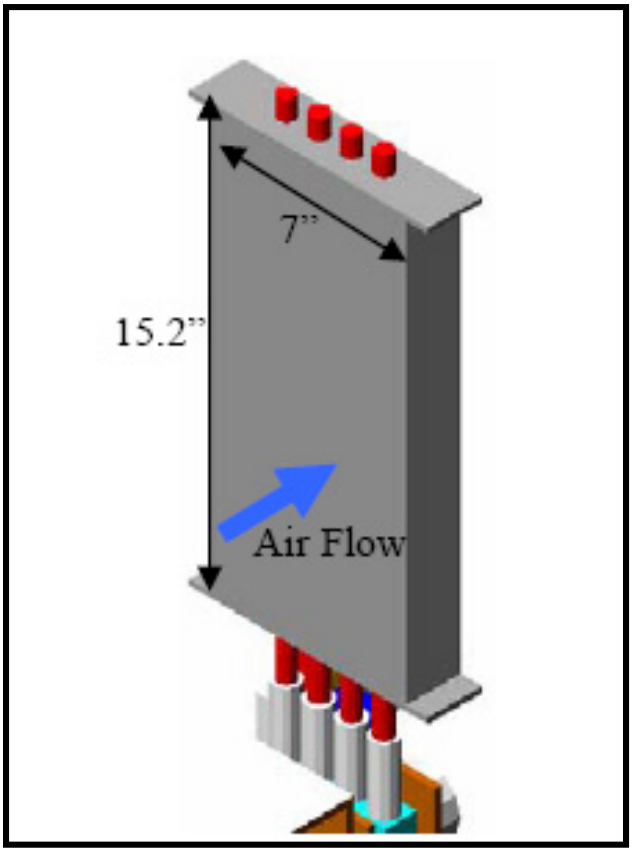


Figure 5-7: Analysis of the 1.2 kW Heat-Pipe

The heat-pipe shown in Figure 5-7 is the 1.2 kW heat-pipe used in the H-Bridge clamp circuit to transport heat from the semiconductor devices to the ambient using phase change mechanism. The air flow through the fins of the heat-pipe specified by the vendor is 5 m/s in the direction of arrow shown in the figure. The dimensions of the cross section of the heat-pipe are calculated to obtain the area and together with the air flow velocity we get a volumetric sir flow number of 736 cubic feet per minute. Thus a minimum air-flow of 736 CFM is required for the heat-pipe to function to its full capacity.

Table 5-6: Air-flow requirement on the 1.2kW heat-pipe

Component	1.2 kW Heat-pipe
Minimum Air-flow (CFM)	736
Pressure drop (inch H2O)	0.157
Static pressure head (Ohms)	2.908e-7
ΔT (°C)	2.4

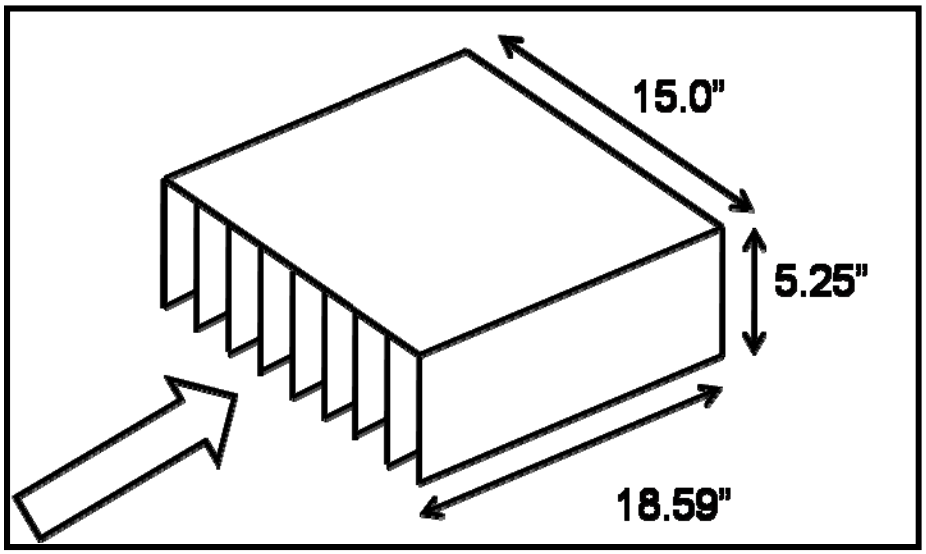


Figure 5-8: Heat-sink for the clamp resistor array

The heat-sink shown in Figure 5-8 is the 1.5 kW heat-sink used in the H-Bridge clamp circuit to transport heat from the resistor array to the ambient using conduction (heat-spreading) and convection (heat-transportation). The air flow through the fins of the heat-sink specified by the vendor is 100 CFM. Thus a minimum air-flow of 100 CFM is required for the heat-pipe to function to its full capacity. The pressure drop on the heat-sink is 11.25 inch in H2O. parameters such as the static pressure head, rise in temperature of the heat-sink and analogical resistance are calculated and listed in Table 5-6.

Table 5.6: Air-flow requirement on the 1.5kW heat-sink:

Component	1.2 kW Heat-sink
Minimum Air-flow (CFM)	100
Pressure drop (inch H2O)	11.25
Static pressure head (Ohms)	7.5e-5
ΔT (°C)	25.5

It can be seen that the numbers shown are aggressive. This is due to the fact that the heat-sink is big in size and boundaries of heat-transfer with conduction/ convection are pushed to the limit in this particular application.

A similar analysis has to be performed on the snubber inductor as well. But due to the lack of fins on the surface, a detailed analysis such as the ones done for the heat-pipes and heat-sink is not possible. Thus, an estimation of just the air-flow required for cooling the thermal load is performed.

Table 5-7: Inductor parameters

Component	Snubber inductor
Thermal load (Watts)	700
Air flow for ΔT of 2.5 °C (CFM)	525

Based on the above approximations a detailed equivalent electrical model is formed as shown in Figure 5-9 (13).

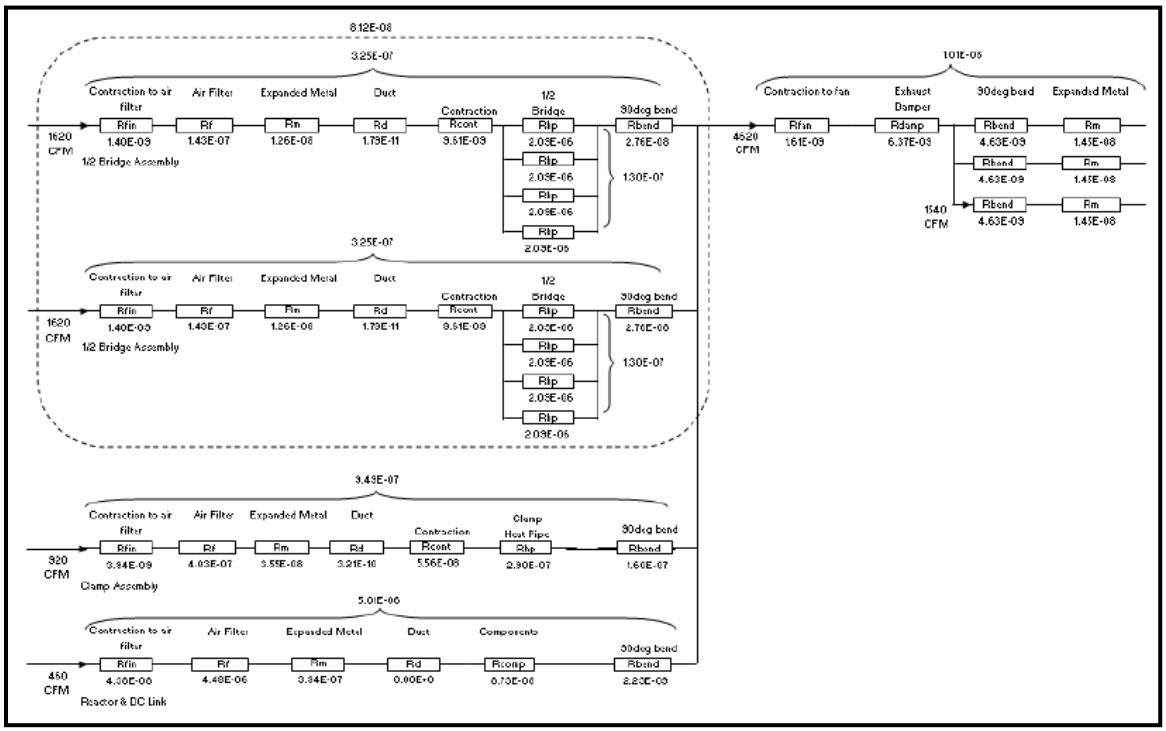


Figure 5-9: Air-flow electrical equivalent model for the system

Since, the model is excessively complex, it is simplified for quick analysis. A simplified version of the model is shown in Figure 5-10. The figure shown is an actual schematic used for simulation purposes.

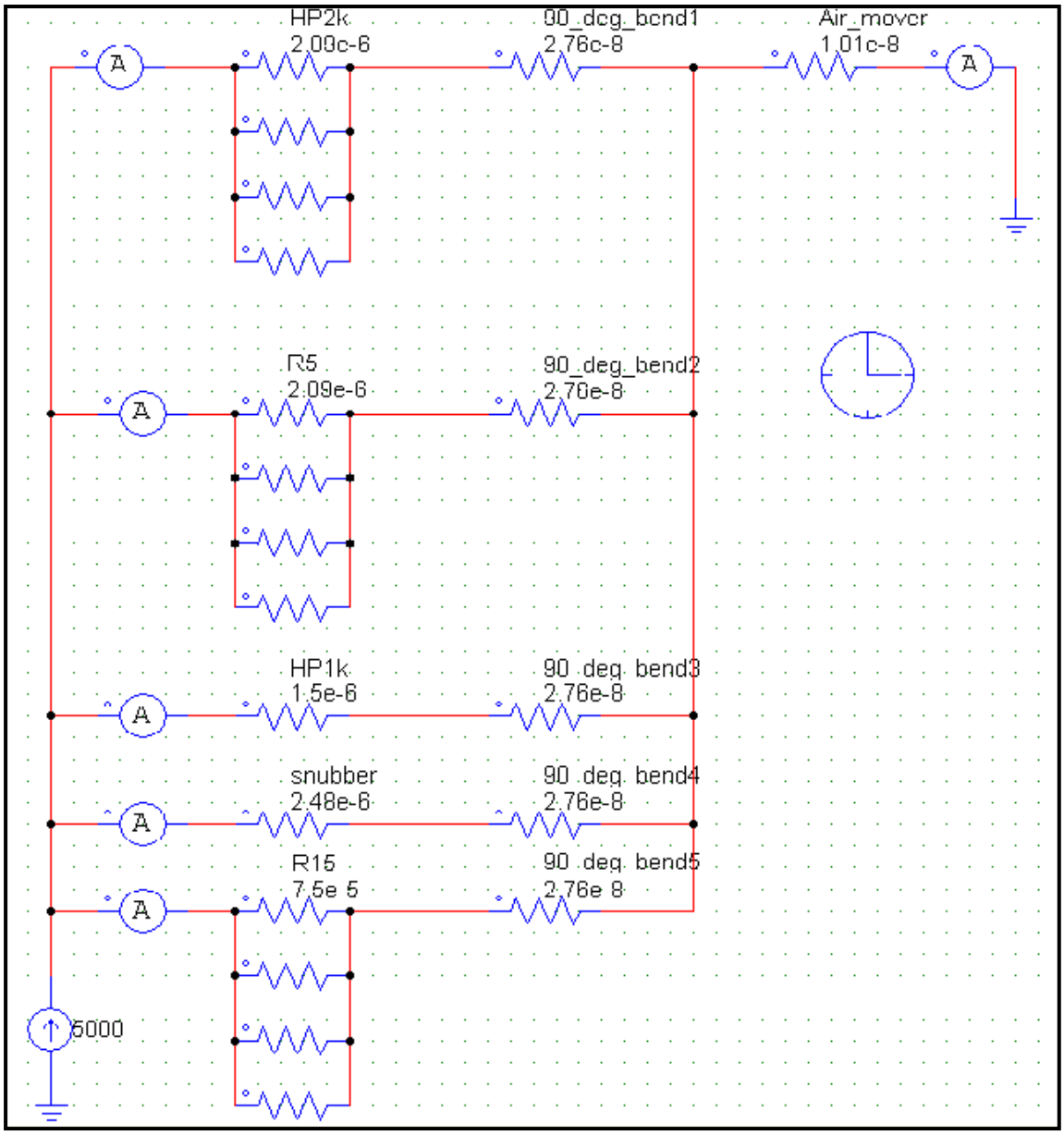


Figure 5-10: Simplified version of the model shown in Figure 5-9

The model shown above clearly shows the major components that have an influence on the system performance. The current meters present at various locations will give the measure of air flow through that path. The obtained values of airflow will then be compared with the

earlier tabulated values of air-flow requirement to check if the selected 5000 CFM air mover is sufficient to ensure optimal system performance.

Table 5-8: Obtained air-flow values as compared to the minimum required values

Component	Minimum Required (CFM)	Value from analysis (CFM)
2.2 kW heat-pipe	1552	1595
1.2 kW heat-pipe	736	978
Snubber	525	705
Resistor	100	125

It is clear from the above analysis that the required air-flow parameters have been met and the design is feasible.

5.5. Conclusion

From the detailed discussion on the thermal performance of the H-Bridge system, it can be concluded that the system thermal loads can be handled by the custom designed phase change agents and heat-sinks. The electrical equivalent models for obtaining both the junction temperatures of the devices and for obtaining the air-flow of the system gave near accurate results with reasonable margin for design. Complex physics based analysis, would have however given more accurate results. But the results obtained show with enough margin that an operational system can be made from the designed parameters.

6. Conclusions

6.1. Construction of ETO Light Converter

The design of the ETO Light converter has been through its main foundation steps – Electrical, Thermal and Mechanical. It is not essential that certain methodology be followed to construct the converter. The guidelines laid out in chapter 4 and chapter 5 must be followed to devise a plan for the converter's construction. The frame that supports the power converter has to be rigid enough to carry the weight of the converter and the passives and be able to sustain vibrations and shocks during the course of transportation. The framework should be reasonably mobile e.g. have coasters or have provisions for a forklift.

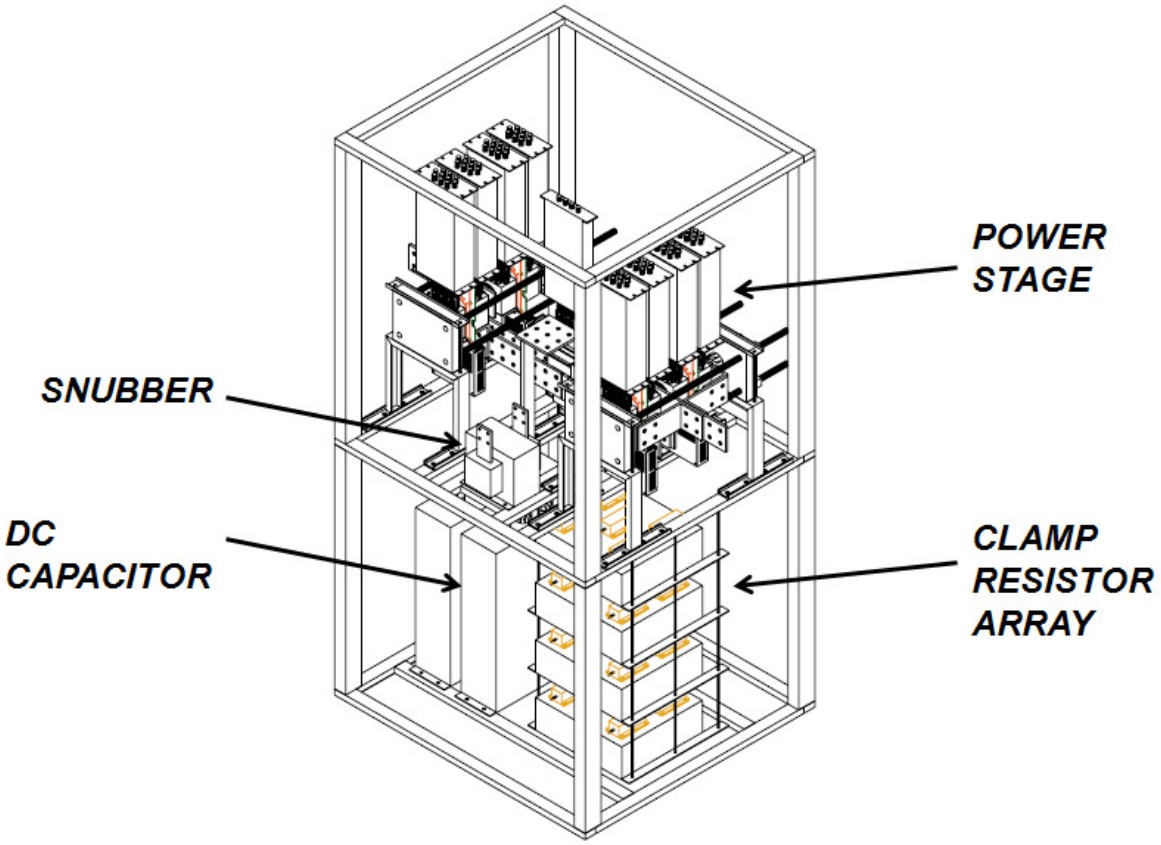


Figure 6-1: Framework for supporting the power-stage

Figure 6-1, shows the skeletal structure of the power converter with the framework, power-stage, snubber and the clamp-resistor array. As it can be clearly seen, the heaviest objects – the DC Capacitors and the clamp-resistor array with its thermal management are placed in the bottom section of the cabinet. The upper section of the cabinet/framework has the power stage and the snubber inductor; as per Figure 4-50 and Figure 4-52 the most optimal arrangement would be to have the power-stage and the snubber inductor together. This arrangement allows the upper and lower stages to have the same footprint, which is advisable as the two stages are to be stacked one top on the other, shown in Figure 6-1.

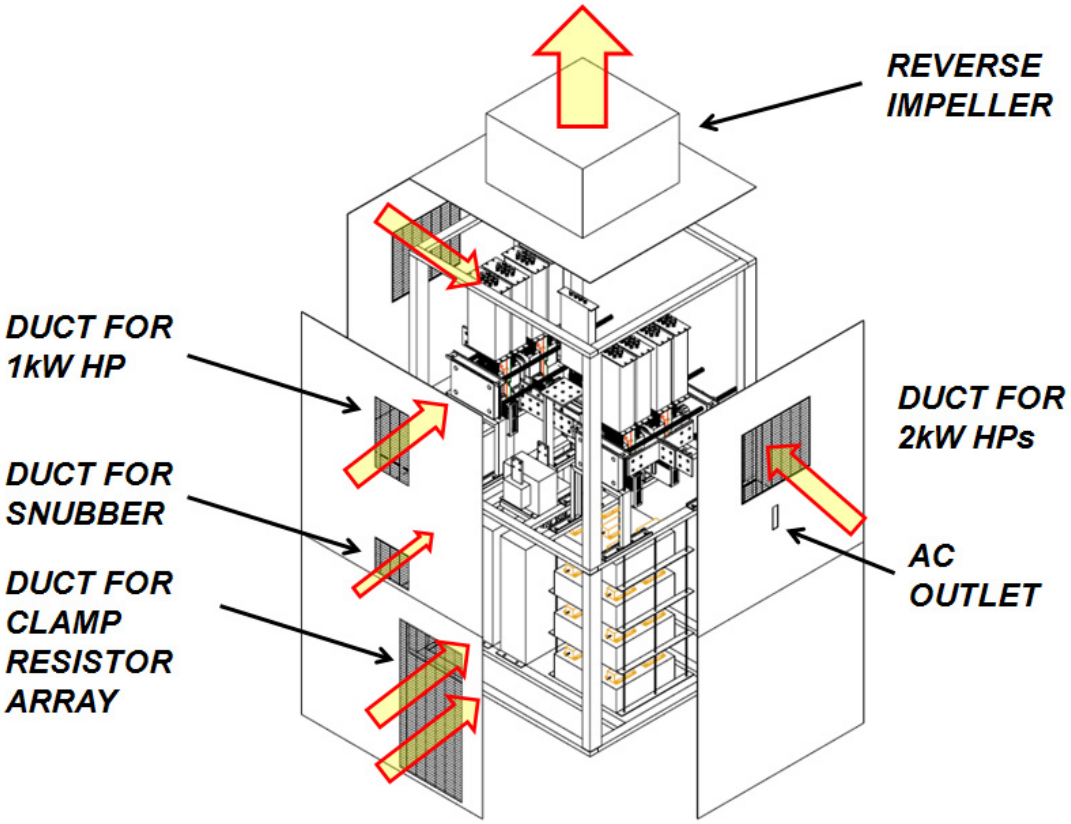


Figure 6-2: Air-flow scheme of the power converter

6.2. Thermal management

In terms of thermal management, the air-flow design is one of the most crucial aspects of the converter. Figure 6-1, shows the skeletal structure of the power converter; however, the Figure 6-2, shows the exploded view with the panels of the power converter, air flow

direction and air-inlets for the converter. The air-inlets have been specifically designed to meet the air-flow requirements, in terms of air-flow balancing and providing sufficient air through heat-generating components as discussed in Table 5-8. The top of the converter has room for accommodating two curved impellers. Actually, a single blower is required for the thermal management of the power converter; however, a second blower is added for the sake of redundancy. It can serve two purposes – first, it can be a true redundant blower and operate only when the primary air-mover fails; second, it can share the air-moving capacity with the first blower. This will allow the blowers to turn at a lower RPM, thus decreasing noise generated by the blowers.

6.3. Future work

Construction of an actual prototype is still pending. Building and testing the converter should be the primary task in the list of 'future tasks'. A simple test plan is required to test the basic functionality of the converter. It would involve a start-up control check to ensure that the semiconductor devices and all the sensors are functional. It is essential to check the sensors for correct functionality, offset and gain as these factors will affect the close loop control of the converter. The start-up check should also scan the gate drive boards and auxiliary power supplies to ensure correct operation. After all the start-up check sequences are complete the control would start gating the converter, incrementing the DC voltage gradually and monitoring the load current. A thermal-run test would ensure that all the components in the converter pass through the natal-failure period, mentioned in the bath-tub curve (16). Finally, a EMI compliance test would certify if the STATCOM meets all the

6.4. Conclusion

A new high power converter based on Emitter Turn-Off thyristors is proposed. The unique quality of this newly proposed converter is that the thermal management and heat-removal is done using custom designed heat-pipes. This feature completely eliminates a water circulation system, which forms a major part of power converters of similar rating. The isolation issues posed by circulating water in the system are avoided completely as isolated heat-pipes are used. The heat-pipes make the converter modular in terms of thermal

management. The bus-bars used in the converter have been optimized to have minimum stray inductance. This technique reduces the voltage stress on the devices, increasing the operational life of the converter. The interconnecting resistances of the bus-bars have been reduced using various techniques. Overall, the high power converter has been designed to meet the basic specifications and operate correctly.

Bibliography

1. **Tewari, Karan.** *Investigation of High Temperature Operature of Emitter Turn-Off Thyristor (ETO) and Electro Thermal Design of Heat-pipe based High Power Voltage Source Converter using ETO.* s.l. : North Carolina State University, 2006.

2. **Chen, Bin.** *Development and Application of the Light Triggered Emitter Turn-Off (LT-ETO) Thyristor.* s.l. : North Carolina State University, 2007.

3. *Electro-Thermal Design of a Heat Pipe Based High Power Voltage Source Converter Using Emitter Turn-Off Thyristor.* **K. Tewari, S.R. Doss, Bin Chen, A.Q. Huang, S. Bhattacharya.** s.l. : Industry Applications Conference, 2006. 41st IAS Annual Meeting. Conference Record of the 2006 IEEE, 2006. 10.1109/IAS.2006.256615.

4. **IEEE.** *IEEE Recommended Practices and Requirement for Harmonic Control in Electrical Power Systems.* s.l. : IEEE, 1992. IEEE-519-92.

5. *An Optimal Combination modulation Strategy for a Seven-level Cascade Multilevel Converter based STATCOM* . **Yu Liu, Zhong Du, Alex Q. Huang and Subhashish Bhattacharya.** s.l. : Industry Applications Conference, 2006. 41st IAS Annual Meeting. Conference Record of the 2006 IEEE, 2006. 10.1109/IAS.2006.256769 .

6. **Zhou, Xigen.** *Electrical, magnetic, thermal Modelling and Analysis of a 5000A Solid State Switch module and its Application as a DC Circuit Breaker.* s.l. : Virginia Tech, 2005.

7. *High frequency operation of a megawatt voltage source inverter equipped with ETOs.* **K.Motto, Yuxin Li, Zhenxue Xu, A.Q. Huang,.** s.l. : Applied Power Electronics Conference and Exposition, 2001. APEC 2001. Sixteenth Annual IEEE, 2001. 10.1109/APEC.2001.912478.

8. *Introducing the emitter turn-off thyristor (ETO).* **Yuxin Li, Huang A.Q., Lee F.C.** s.l. : Industry Applications Conference, 1998. Thirty-Third IAS Annual Meeting. The 1998 IEEE, 1998. 10.1109/IAS.1998.730246.

9. **ABB.** *Device Datashhet of 5SDF 10H4520.* s.l. : ABB.

10. **Wikipedia.** Thermal Conductivity. *www.wikipedia.com.* [Online] http://en.wikipedia.org/wiki/Thermal_conductivity.

11. **Aluminium Company of America.** Electrical Conductor Handbook.

12. **Curtis Wright - Jonathan Kunkle, Derek Danzen, J. Franklin Roach, Kevin B. Huges.** *Evaluation of Condon Wind Farm STATCOM Design: Interim Report.* 2008.

13. **Curtis Wright - Jonathan Kunkle.** *Air Flow Analysis and Suggestions, Rev A.*

14. **Azar, Kaveh.** *Thermal Measurements in Electronics Cooling.*

15. **Ellison, Gordon N.** *Thermal Computations for Electronic Equipment.*

16. **Wikipedia.** Bathtub curve. *www.wikipedia.com.* [Online] [Cited: November 14, 2008.] http://en.wikipedia.org/wiki/Bathtub_curve.